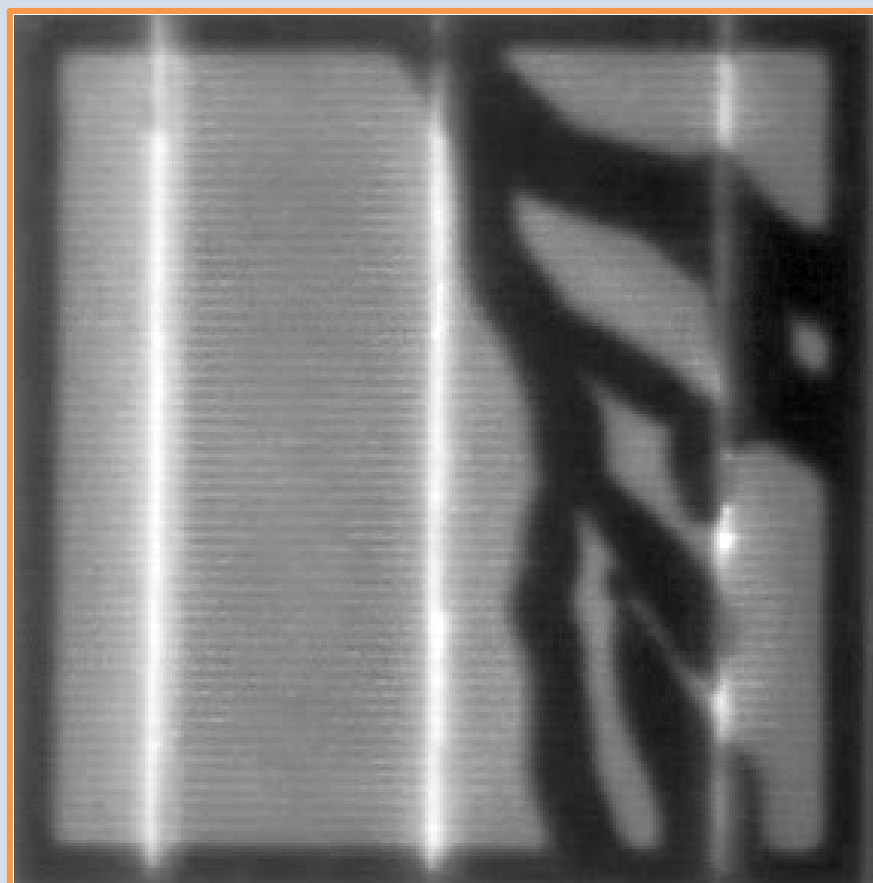




Review of Failures of Photovoltaic Modules



PVPS

PHOTOVOLTAIC
POWER SYSTEMS
PROGRAMME

Report IEA-PVPS T13-01:2014

*Ultraviolet fluorescence image of a cracked solar cell in a photovoltaic module.
Courtesy of Marc Köntges, Institute for Solar Energy Research Hamelin.*

INTERNATIONAL ENERGY AGENCY
PHOTOVOLTAIC POWER SYSTEMS PROGRAMME

Performance and Reliability of Photovoltaic Systems

Subtask 3.2: Review of Failures of Photovoltaic Modules

IEA PVPS Task 13
External final report IEA-PVPS
March 2014

ISBN 978-3-906042-16-9

Primary authors:

Marc Köntges,
Institute for Solar Energy Research Hamelin, Emmerthal, Germany

Sarah Kurtz, Corinne Packard,
National Renewable Energy Laboratory, Golden, CO, USA

Ulrike Jahn,
TÜV Rheinland Energie und Umwelt GmbH, Cologne, Germany

Karl A. Berger,
Austrian Institute of Technology GmbH, Energy Department, Vienna, Austria

Kazuhiko Kato,
National Institute of Advanced Industrial Science and Technology, Tsukuba, Japan

Thomas Friesen,
SUPSI ISAAC, Canobbio, Switzerland

Haitao Liu,
Institute of Electrical Engineering, Chinese Academy of Sciences, Beijing, China

Mike Van Iseghem,
Electricité de France, EDF R&D, Moret-sur-Loing, France

Contributing authors:

John Wohlgemuth, David Miller, Michael Kempe, Peter Hacke
National Renewable Energy Laboratory, Golden, CO, USA

Florian Reil, Nicolas Bogdanski, Werner Herrmann
TÜV Rheinland Energie und Umwelt GmbH, Cologne, Germany

Claudia Buerhop-Lutz
The Bavarian Centre for Applied Energy Research, Würzburg, Germany

Guillaume Razongles
Institut National de l'Energie Solaire, INES-CEA, Le Bourget-du-Lac, France

Gabi Friesen,
SUPSI ISAAC, Canobbio, Switzerland

This report is supported by
Austrian Federal Ministry for Transport, Innovation and Technology (BMVIT) under
FFG contract No. 828105,

Chinese Academy of Sciences (CAS),

German Federal Ministry for Economic Affairs and Energy under Contract
No.0325194A&C (BMWi),

Supported by:



on the basis of a decision
by the German Bundestag

Swiss Federal Office of Energy (SFOE)

and

U.S. Department of Energy under Contract No. DE-AC36-08-GO28308 with the
National Renewable Energy Laboratory (NREL)

Table of Contents

1 Foreword	1
2 Executive summary	2
3 Introduction	4
4 Definitions	10
4.1 Definition of a PV module failure.....	10
4.2 PV module failures excluded by definition	10
4.3 Important PV module failures due to external causes.....	12
4.3.1 Clamping	12
4.3.2 Transport and installation	13
4.3.3 Quick connector failure	14
4.3.4 Lightning.....	14
4.3 Definition of safety failure and safety categories.....	16
4.4 Definition of power loss failure and power loss categories	17
4.5 Definition of a defect.....	18
4.6 Definition of PV module parts	18
5 Basics of measurement methods used to identify failures.....	20
5.1 Visual inspection.....	20
5.1.1 Visual inspection in accordance with IEC PV standards	21
5.1.2 Documentation of visual failures in the field	23
5.2 <i>I-V</i> curve	26
5.2.1 Introduction of the important <i>I-V</i> curve parameters	26
5.2.2 Series resistance and shunt resistance.....	27
5.2.3 Accuracy.....	28
5.2.4 Effect of failures on the <i>I-V</i> curve	29
5.3 Thermography	33
5.3.1 Thermography under steady state conditions	33
5.3.2 Pulse thermography	36
5.3.3 Lock-in thermography	37
5.4 Electroluminescence.....	41
5.5 UV fluorescence	47
5.6 Signal transmission method.....	49
6 Failures of PV modules	53
6.1 Review of failures found in all PV modules	55
6.1.1 Delamination	55
6.1.2 Back sheet adhesion loss.....	56

6.1.3 Junction box failure	58
6.1.4 Frame breakage.....	58
6.2 Review of failures found in silicon wafer-based PV modules.....	61
6.2.1 EVA discolouration	61
6.2.2 Cell cracks.....	62
6.2.3 Snail tracks.....	67
6.2.4 Burn marks.....	71
6.2.5 Potential induced degradation.....	73
6.2.6 Disconnected cell and string interconnect ribbons	82
6.2.7 Defective bypass diode	85
6.3 Review of failures found in thin-film modules.....	88
6.3.1 Micro arcs at glued connectors	88
6.3.2 Shunt hot spots	89
6.4 Review of specific failures found in CdTe thin-film PV modules.....	92
6.4.1 Front glass breakage	93
6.4.2 Back contact degradation.....	94
7 Adapting testing methods to failure mechanism for PV modules.....	96
7.1 Mechanical loads caused by transport.....	96
7.1.1 Determination of resonance frequencies of single PV modules	97
7.1.2 Transport and environmental testing of silicon wafer-based PV modules in a shipping stack	97
7.1.3 Transport testing of single silicon wafer-based PV modules	99
7.2 Mechanical loads caused by snow	104
7.3 Testing for UV degradation of PV modules	106
7.3.1 UV preconditioning for PV modules	107
7.3.2 Performance degradation of PV modules	108
7.4 Ammonia Testing	110
7.4.1 Tests performed on crystalline Si glass/foil PV modules	112
7.4.2 Tests performed on non-glass modules.....	113
7.5 Testing for potential induced degradation of crystalline silicon PV modules .	114
7.6 Extended IEC testing in the lab.....	116
7.6.1 Test results from extended testing.....	118
7.6.2 Accelerated testing and field experience.....	121
8 Conclusions.....	123
ANNEX A: Module condition checklist	127

1 Foreword

The International Energy Agency (IEA), founded in November 1974, is an autonomous body within the framework of the Organization for Economic Co-operation and Development (OECD) which carries out a comprehensive programme of energy co-operation among its member countries. The European Union also participates in the work of the IEA. Collaboration in research, development and demonstration of new technologies has been an important part of the Agency's Programme.

The IEA Photovoltaic Power Systems Programme (PVPS) is one of the collaborative R&D Agreements established within the IEA. Since 1993, the PVPS participants have been conducting a variety of joint projects in the application of photovoltaic conversion of solar energy into electricity.

The mission of the IEA PVPS programme is: To enhance the international collaborative efforts which facilitate the role of photovoltaic solar energy as a cornerstone in the transition to sustainable energy systems.

The underlying assumption is that the market for PV systems is rapidly expanding to significant penetrations in grid-connected markets in an increasing number of countries, connected to both the distribution network and the central transmission network.

This strong market expansion requires the availability of and access to reliable information on the performance and sustainability of PV systems, technical and design guidelines, planning methods, financing, etc., to be shared with the various actors. In particular, the high penetration of PV into main grids requires the development of new grid and PV inverter management strategies, greater focus on solar forecasting and storage, as well as investigations of the economic and technological impact on the whole energy system. New PV business models need to be developed, as the decentralised character of photovoltaics shifts the responsibility for energy generation more into the hands of private owners, municipalities, cities and regions.

The overall programme is headed by an Executive Committee composed of representatives from each participating country and organisation, while the management of individual research projects (Tasks) is the responsibility of Operating Agents. By late 2013, fourteen Tasks were established within the PVPS programme, of which six are currently operational.

The overall objective of Task 13 is to improve the reliability of photovoltaic systems and subsystems by collecting, analysing and disseminating information on their technical performance and failures, providing a basis for their assessment, and developing practical recommendations for sizing purposes.

The current members of the IEA PVPS Task 13 include:

Australia, Austria, Belgium, China, EPIA, France, Germany, Israel, Italy, Japan, Malaysia, Netherlands, Norway, Spain, Sweden, Switzerland, Turkey and the United States of America.

This report concentrates on the detailed description of PV module failures, their origin, statistics, relevance for module power and safety, follow-upfailures, their detection and testing for these failures. The report mainly focuses on wafer-based PV modules. Thin-film PV modules are also covered, but due to the small market share of these types of PV modules reliable data is often missing. The author team also focuses on types of PV module failures which are not specific for one special manufacturer and have a broader relevance.

The editors of the document are Marc Köntges, Institute for Solar Energy Research Hamlin, Emmerthal, Germany (DEU) and Ulrike Jahn, TÜV Rheinland Energie und Umwelt GmbH, Cologne, Germany (DEU).

The report expresses, as nearly as possible, the international consensus of opinion of the Task 13 experts on the subject dealt with. Further information on the activities and results of the Task can be found at: <http://www.iea-pvps.org>.

2 Executive summary

One key factor of reducing the costs of photovoltaic systems is to increase the reliability and the service life time of the PV modules. Today's statistics show degradation rates of the rated power for crystalline silicon PV modules of 0.8%/year [Jordan11]. To increase the reliability and the service life of PV modules one has to understand the challenges involved. For this reason, the international Task 13 expert team has summarized the literature as well as their knowledge and personal experiences on actual failures of PV modules.

The target audience of this work is PV module designers, PV industry, engineering lines, test equipment developers, testing companies, technological research laboratories, standardisation committees, as well as national and regional planning authorities.

In the first part, this document reports on the measurement methods which allow the identification and analysis of PV module failures. Currently, a great number of methods are available to characterise PV module failures outdoors and in labs. As well as using *I-V* characteristics as a diagnostic tool, we explain image based methods and visual inspection. For each method we explain the basis, indicate current best practice, and explain how to interpret the images. Three thermography methods are explained: thermography under steady state conditions, pulse thermography and lock-in thermography. The most commonly used of these methods is thermography under steady state conditions. Furthermore electroluminescence methods have become an increasingly popular standard lab approach for detecting failures in PV modules.

A less common but easier to use method is UV fluorescence. This method can be used to detect module failures similar to those detected with thermography and electroluminescence techniques; however, the PV modules must be sited outdoors for at least one and a half years for the method to be effective. For visual documentation of module conditions in the field, we set up a standard which is now accepted and used by all authors documenting such tests. This standard format allows the documentation of visible module failures in standardised way and makes the data accessible for statistical evaluation. Furthermore we introduce a signal transition method for the detection of defective circuits in installed PV modules. All methods are linked to the PV module failures which are able to be found with these methods.

In the second part, the most common failures of PV modules are described in detail. In particular these failures are: delamination, back sheet adhesion loss, junction box failure, frame breakage, EVA discolouration, cell cracks, snail tracks, burn marks, potential induced degradation, disconnected cell and string interconnect ribbons, defective bypass diodes; and special failures of thin-film modules, such as micro arcs at glued connectors, shunt hot spots, front glass breakage, and back contact degradation. Where possible, the origin of the failure is explained. A reference to the characterisation method is given to identify the failure. If available, statistics of the failure type in the field and from accelerating aging tests are shown. For each failure, a description of safety issues and the influence on the power loss is given, including typical follow-up failure modes.

In the third part, new test methods are proposed for detection of PV module failures in the field. A special focus is made on mechanical tests because many problems have arisen in the last few years from the mechanical loading of modules. These mechanical loads occur during transportation and from snow loads on modules mounted on an incline. Furthermore, testing for UV degradation of PV modules, ammonia corrosion (sometimes found in roofs of stock breeding buildings) and potential induced degradation are described. The latter method caused some controversy within the international standardization committee until the finalization of this report because many alternative suggestions from different countries were proposed. The test methods are explained in detail, linked to failure descriptions and the results are compared to real failure occurrences, where possible.

During a past Task 13 project phase, we recognised that the topic “3.2 Characterising and Classifying Failures of PV Modules” is an important on-going subject in the field of PV research. The current review of failure mechanisms shows that the origin and the power loss associated with some important PV module failures is not yet clear (e.g. snail tracks and cell cracks). There are also still some questions as to how best to test for some types of failure (e.g. potential induced degradation and cell cracks). Furthermore, despite the fact that a defective bypass diode or cell interconnect ribbon in a PV module may possibly lead to a fire, very little work has been done to detect these defects in an easy and reliable way once installed in a PV system. However, there are research groups currently working on those topics in order to overcome these challenges. Therefore, it is planned to continue our in-depth review of failures of photovoltaic modules in an extension of the TASK 13 project.

References

[Jordan11] D. C. Jordan and S. R. Kurtz, Photovoltaic Degradation Rates - an Analytical Review, *Prog. Photovolt: Res. Appl.* **21** (12–29) (2011) doi: 10.1002/pip.1182

3 Introduction

Typically failures of products are divided into the following three categories: Infant-failures, midlife-failures, and wear-out-failures. Figure 3.1 shows examples for these three types of failures for PV modules. Besides these module failures many PV modules show a light-induced power degradation (LID) right after installation. The LID is a failure type which occurs anyhow and the rated power printed on the PV module is usually adjusted by the expected standardized saturated power loss due to this failure. LID is defined as no failure in this document as long as the saturated power loss is equal or less than expected.

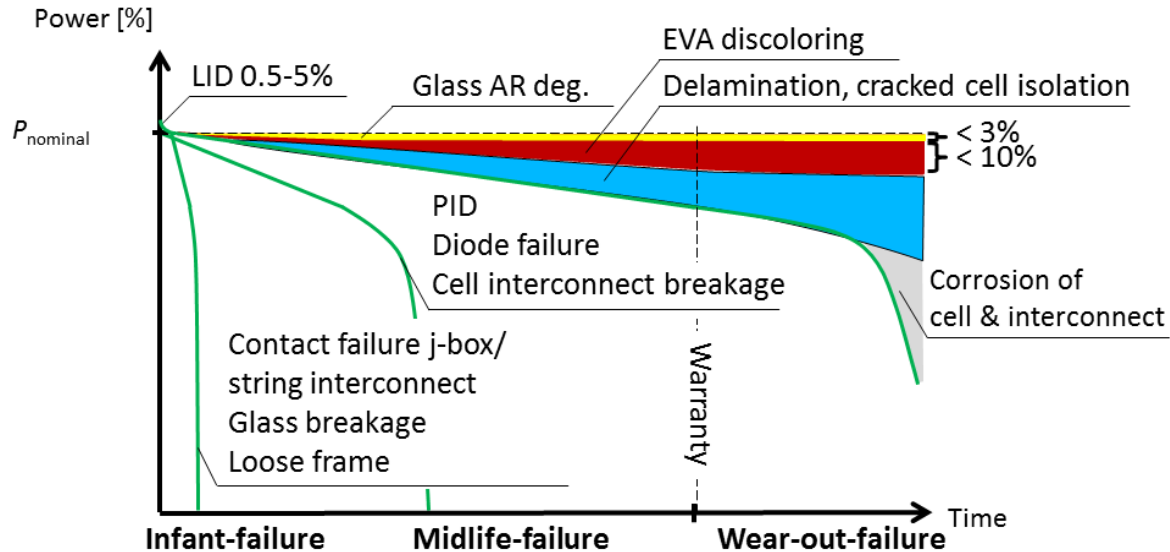


Fig. 3.1: Three typical failure scenarios for wafer-based crystalline photovoltaic modules are shown. Definition of the used abbreviations: LID – light-induced degradation, PID – potential induced degradation, EVA – ethylene vinyl acetate, j-box – junction box.

Infant-mortality failures occur in the beginning of the working life of a PV module. Flawed PV modules fail quickly and dramatically impact the costs of the module manufacturer and the installer because they are responsible for these failures. Figure 3.2 shows the distribution of the failure types at the start of the working life given by a German distributor. Due to transportation damages 5% of all failure cases occur. The most important failures in the field are j-box failure, glass breakage, defective cell interconnect, loose frame, and delamination. Unfortunately the other defects of the statistics are not well defined.

Failures occurring in the midlife of PV modules are described in a study of DeGraaff [DeGraaff11]. Figure 3.3 shows the failure distribution of PV modules that have been in the field for 8 years. Two percent of the PV modules are predicted not meet the manufacturer's warranty after 11-12 years of operation. This study shows a quite high rate of defect interconnections in the module and failures due to PV module glass breakage. The relative failure rate of j-box and cables (12%), burn marks on cells (10%), and encapsulant failure (9%) are comparable high.

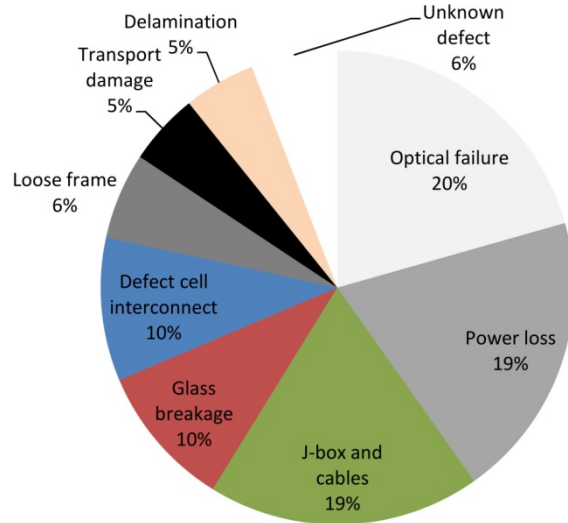


Fig. 3.2: Failure rates due to customer complaints in the first two years after delivery. The rate is given relative to the total number of failures. The PV modules are delivered by a German distributor in the years 2006-2010 [redrawn from Richter11]. The statistic is based on a total volume of approximately 2 million delivered PV modules. Categories not found in other module failure statistics are drawn in grey scale.

Most of the PV modules go through the wear out scenario. This scenario is the base for the best case yield analysis and determines therewith the cost efficiency of well operating PV modules.

Wear out failures occur at the end of the working lifetime of PV modules. They determine the maximum working life of a PV module. The working life of a PV module ends if a safety problem occurs or the PV module power drops under a certain level, which is typically defined between 80% and 70% of the initial power rating. Figure 3.4 shows the defect rate of some special PV module types after 15 years of operation and more [Schulze12]. The predominant PV module failures are delamination, cell part isolation due to cell cracks, and discolouring of the laminate. However, all these failures lead to a power loss between 0% and 20%, in the mean 10%. Nearly all of these PV modules meet the manufacturer's power warranty.

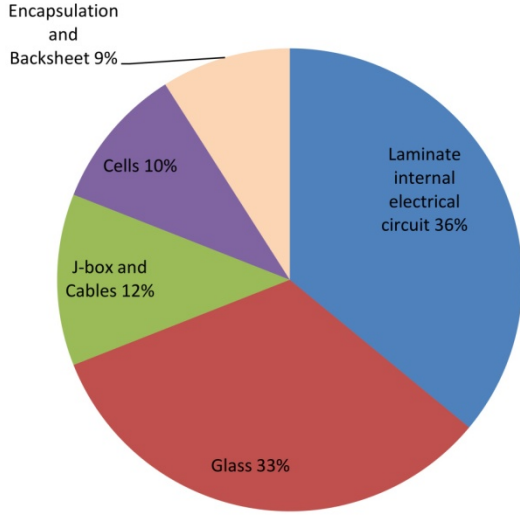


Fig. 3.3: Field study of PV module failures found for various PV modules of 21 manufacturers installed in the field for 8 years [redrawn from DeGraaff11]. The rate is given relative to the total number of failures. Approximately 2% of the entire fleet are predicted to fail after 11-12 years (do not meet the manufacturer's warranty).

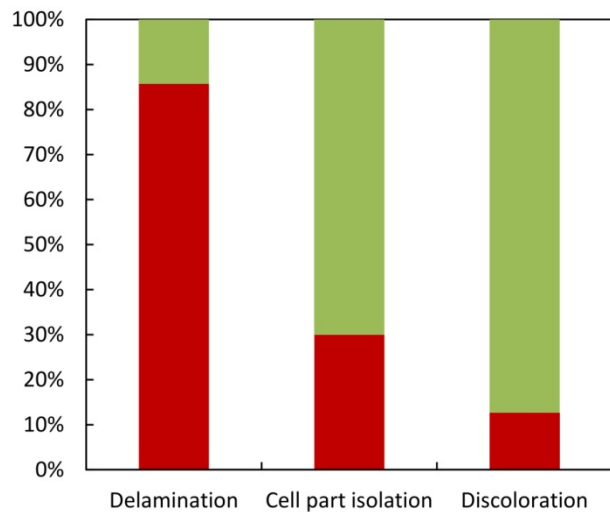


Fig. 3.4: Failures occurring in a fleet of 272 PV modules of 3 different manufacturers after more than 15 years of operation [redrawn from Schulze12]. Each PV module may be affected by more than one failure type. The red and green colours indicate the percentage of modules having or not having a specific failure respectively. Each PV module may show more than one failure type.

However, these PV modules used in the study of Schulze are not representative of today's PV modules. On the one hand the lamination material being responsible for the delamination and discolouration are not used in today's PV modules anymore. On the other hand in former times the manufacturers had no possibility to check the cells for cracking, the cells, and cell metallisation have been much thicker than today and the cell and module sizes deviate strongly from today's PV modules. These facts very much affect the cell part isolation of cells in a PV module. However, the knowledge of the most important long-term degradation mechanisms helps us to look at the most important factors to produce long-term stable PV modules. So it is imperative to understand the degradation mechanisms to enable failure specific tests.

Type approval certifications according to the standards IEC 61215 and IEC 61646 have gained industry acceptance in the past 15 years as a quality label for PV modules [IEC61215], [IEC61646]. Nowadays it is required for most national and international funding programmes. IEC 61215 for crystalline PV modules and IEC 61646 for thin-film PV modules are type approval standards and aim to identify the weaknesses of a product responsible for "infant failure". They are not test procedures to determine the working lifetime of a product. These standards do however include several accelerated stress tests derived from real outdoor stresses.

TÜV Rheinland has analysed a total of 2000 certification projects conducted at the Cologne Solar Testing Centre over the past ten years. A certification project may cover several variants of the same module type because manufacturers often exchange and attain qualifications for a variety of materials. These are based on the design certifications in accordance with IEC 61215, IEC 61646, and the safety

qualification in accordance with IEC 61730 [IEC61730]. A long-term trend can be clearly identified here as shown in Fig. 3.5. While 54% of all projects were still failing the IEC qualification certifications in 2002, by 2007 this had risen to 67% for the new thin-film modules and 29% for the new crystalline photovoltaic modules. In 2007/2008 many thin-film start-ups entered the PV market and contributed to these failure rates, possibly because they used the test labs to speed their screening of new product designs. Similarly, this high failure rate may be attributed to the large number of new module manufacturers on the market originating from Asia in particular, again, possibly because they had not fully tested their products before attempting certification. By 2012, the rate of failed IEC projects for both technologies had dropped to 10%. The experts ascribe this not only to the fact that manufacturers have learned to better fulfil the IEC standards when constructing new module types but also to the on-going developments of the market.

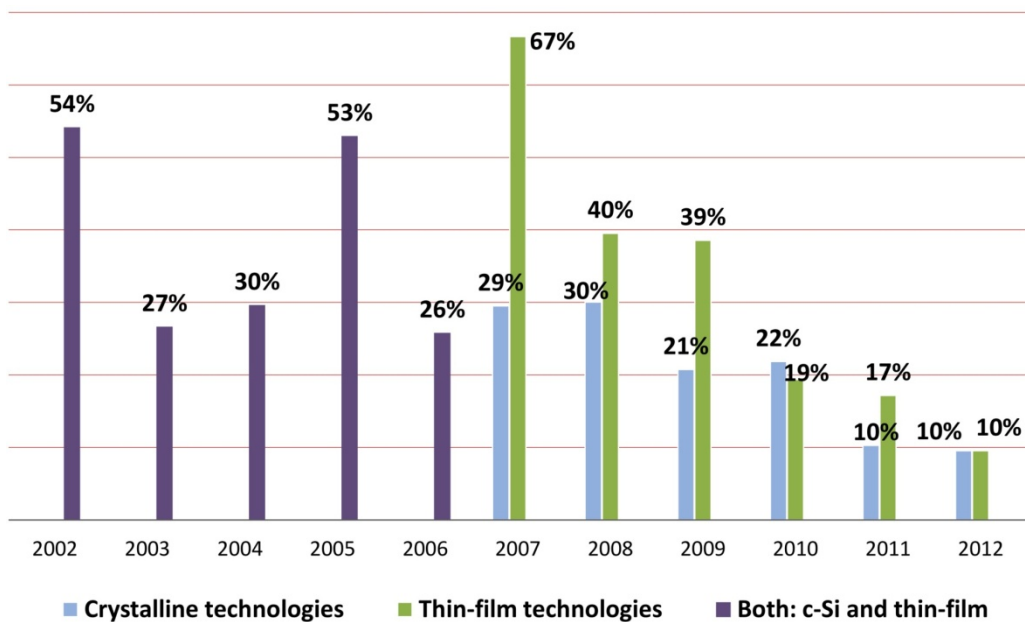


Fig. 3.5: Failure rates of 2000 certification projects for IEC 61215 and IEC 61646 type approval tests for the years 2002 to 2012. The given figures are the annual percentages of IEC projects with at least 1 module test failure compared to the sum of all conducted IEC projects. Since 2007 figures of crystalline and thin-film technologies are shown separately.

The distribution of failed tests as shown in Fig. 3.6 indicates parallels between crystalline modules (1740 projects) and thin-film modules (370 projects analysed): Of those projects in which tests were failed between 2006 and June 2013, 49% of all crystalline module tests (inner ring) and 43% of all thin-film module tests (outer ring) failed during the four test series in the climate chamber of the TÜV Rheinland test laboratory (marked in blue colours in Fig. 3.6), which include 200 cycles thermal cycling test (TCT200), damp heat test (DHT), humidity freeze test (HFT), and 50 cycles thermal cycling test (TCT50). The climate chamber tests are a good indication of the longevity to be expected, the quality of the materials, and the workmanship of the products. However, it is also notable that 11% (crystalline) and 12% (thin-film) of failures occurred during the required initial measurements, that is, before any stress tests had actually been carried out. These modules failed, for example, because the

information on the name plate did not meet requirements or because they already exhibited damage by visual inspection. Tests comprising <3% of failures each are summarized under “All other tests (<3%)” in Fig. 3.6.

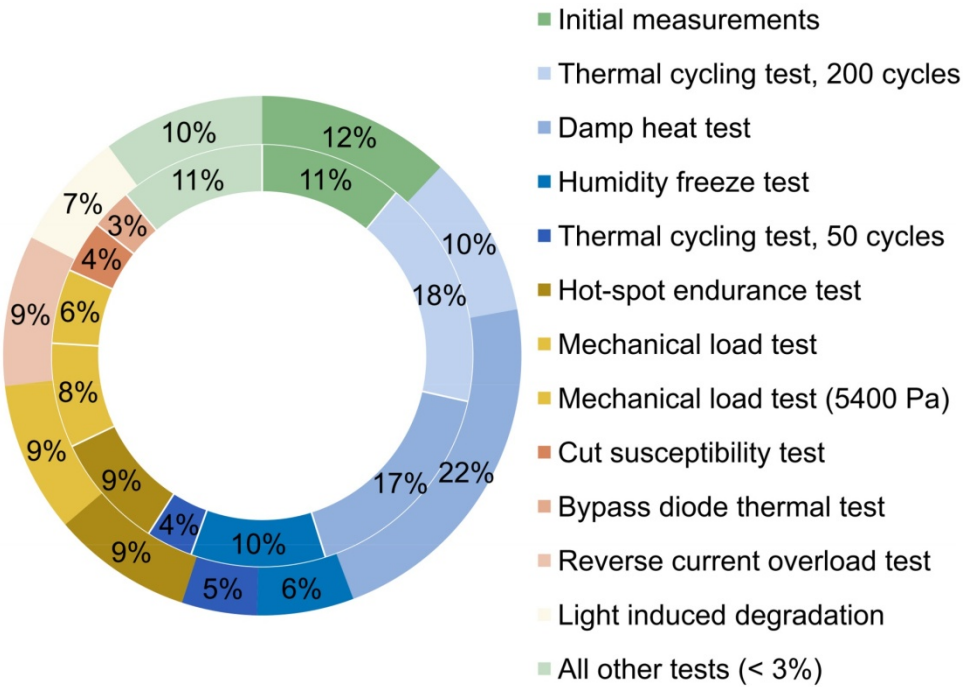


Fig. 3.6: Distribution of failed tests of 1740 IEC projects for crystalline PV modules (inner ring) and of 370 IEC projects for thin-film PV modules (outer ring) between 2006 until June 2013. A test is considered a failure, if one or more PV modules will not pass the specific test. One certification project may contribute to one or several test failures.

The most critical tests for crystalline PV modules are the temperature cycling test 200 (18 %), damp heat test (17%), initial measurements (11 %), humidity freeze test (10%), hot-spot endurance test (9%), and mechanical load test (8%). During the temperature cycles (TCT200) test the solder connection of wafer-based PV modules are stressed; therefore we found a higher proportion of TCT failed modules among crystalline technologies. The TCT200 failure distribution over time dropped from 25% in 2006 to 11% in 2011. Most significant for the quality of lamination to protect the solar cells from humidity ingress is the DHT. The DHT proved critical for crystalline PV module throughout time ranging from 21% (maximum) in 2007 to 13% (minimum) in 2009.

The most critical tests for thin-film modules are damp heat test (22%), initial measurements (12%), temperature cycling test 200 (10%), mechanical load test (9%), reverse current overload test (9%), and hot spot endurance test (9%). However, comparing the two periods 2007 to 2009 vs. 2010 to 2012, for the thin-film PV modules, the key tests with high failure rates are clearly improving: damp heat test (44% in 2007 vs. 11% in 2011), hot-spot endurance test (16% in 2008 vs. 6% in 2011). More or less as for the c-Si modules, the glass quality is the main reason for failures in the mechanical load test. More manufacturers are seeking to have even higher maximum overload protection rate, which leads to the high failure rate of reverse current overload test.

The failure rates for the most critical damp heat test seem to decline during recent years. Many manufacturers have on-site climate/environmental chambers for the pre-testing of new products or new material extension, which is a highly effective way of failure prevention. Furthermore, the improvement of the lamination process and a better protection of module edges, for example, cover bands being introduced, are also key factors for reducing the failure rate of thin-film modules after the damp heat test.

The aim of this document is to review detection, analysis and new tests for failures in PV modules. The document is structured into four parts. The first part (chapter 4) gives definitions about failures in PV modules and defines PV module parts. The second part (chapter 5) reports the basics of the most important and new measurement methods which are used to identify and analyse failures in PV modules. In the third part (chapter 6) failures of PV modules are described in detail, statistics of the failure, the origin of the failure, and a classification of the failure and if possible the dependencies of the failure from time, temperature, humidity, and other parameters are given. In the fourth part (chapter 7) new test methods are presented which test for specific PV module failures which are not yet included in existing standards.

References

- [DeGraaff11] D. DeGraaff, R. Lacerda, Z. Campeau, Degradation Mechanisms in Si Module Technologies Observed in the Field; Their Analysis and Statistics, Presentation at PV Module Reliability Workshop, NREL, Denver, Golden, USA, (2011) http://www1.eere.energy.gov/solar/pdfs/pvmrw2011_01_plen_degraaff.pdf
- [IEC61215] International Electrotechnical Commission (IEC) 61215: 2nd edn, 2005. Crystalline silicon terrestrial photovoltaic (PV) modules – Design qualification and type approval, Edition 2, 2005-04
- [IEC61646] International Electrotechnical Commission (IEC) 61646: 2nd edn, 2008. Thin-film terrestrial photovoltaic (PV) modules – Design qualification and type approval, Edition 2.0, 2008-05
- [IEC61730] International Electrotechnical Commission (IEC) 61730-2: Photovoltaic (PV) module safety qualification – Part 2: Requirements for testing, Edition 1.0 2004-10
- [Richter11] A. Richter, Schadensbilder nach Wareneingang und im Reklamationsfall, 8. Workshop "Photovoltaik-Modultechnik", 24/25. November 2011, TÜV Rheinland, Köln
- [Schulze12] K. Schulze, M. Groh, M. Nieß, C. Vodermayer, G. Wotruba und G. Becker, Untersuchung von Alterungseffekten bei monokristallinen PV-Modulen mit mehr als 15 Betriebsjahren durch Elektrolumineszenz- und Leistungsmessung, Proceedings of 28. Symposium Photovoltaische Solarenergie, (OTTI, Staffelstein, Germany, 2012)

4 Definitions

4.1 Definition of a PV module failure

A PV module failure is an effect that (1) degrades the module power which is not reversed by normal operation or (2) creates a safety issue. A purely cosmetic issue which does not have the consequences of (1) or (2) is not considered as a PV module failure. A PV module failure is relevant for the warranty when it occurs under conditions the module normally experiences.

A problem that is caused by mishandling or by the local environment is not considered to be a “failure” in this report. Here we give some examples. On the one hand, soiling of the module or a failure due to lightning are not considered to be PV module failures. The soiling problem has to be handled by the operator and the lightning is a force majeure which the module is not designed for. On the other hand, defects due to heavy snow load are considered as module failure if the module is specified for heavy snow load. To clarify the spirit of the definition, we give examples in the next chapters which we define as no module failure although they may lead to power loss or safety issues.

4.2 PV module failures excluded by definition

There may be module defects which originate directly from its production. These defects may be the reason for some modules not performing as well as possible, but as long as the defect is not relevant to safety and the power rating on the label takes account of the power loss caused by imperfect production, this defect is no module failure if the defect does not accelerate power loss or cause safety issues in the future. Moderate crystal defects in multicrystalline solar cells or striation rings in monocrystalline solar cells are examples.

Furthermore, there are production-induced features that may appear to a layperson as a failure. These are also no failures. For instance, Fig. 4.2.1 shows brown marks at the edges of solar cells in a PV module. These marks originate from the solar cell carrier during the deposition of the anti-reflection coating and are not considered to be PV module failures.

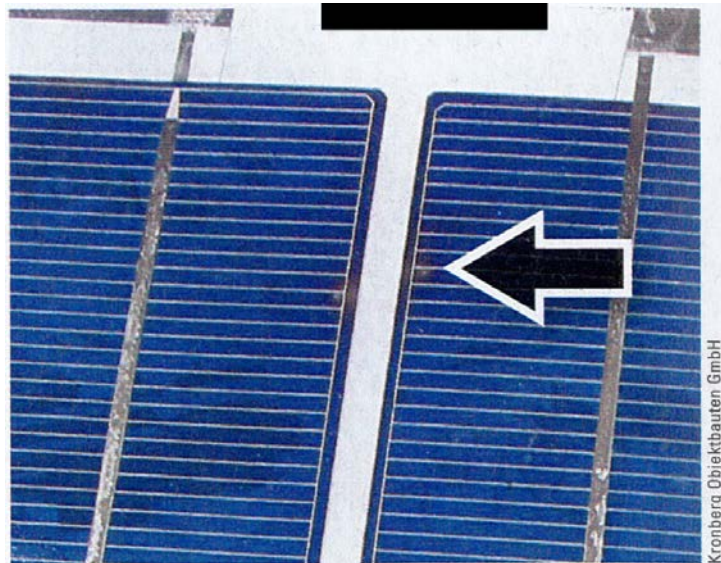


Fig. 4.2.1: Brown marks at the edge of the solar cell are no failure.

Other typical effects that change the module power and are not considered as PV module failures are described in the following.

Light-induced power degradation in crystalline silicon modules due to the well-known boron-oxygen complex [Bothe06] is defined as no module failure, because the manufacturer has to take this effect into account for the power rating of the PV module as it is defined in standard EN 50380 [EN 50380]. It is a PV module failure if the manufacturer has not taken this effect into account for the power rating.

Amorphous silicon (a-Si)-based modules are subject to a light-induced initial degradation, which may account for a loss of power of up to 10-30% within the first months of outdoor exposure [Shah10]. A part of this degradation can be temporarily recovered by thermal annealing during the warm months of the year. The two counteracting effects, light-induced degradation and thermal-induced recovery, lead to a seasonal variation in performance of 0-15% around an average value, which depends on the module technology, local climatic conditions and type of integration [Fanni11, Skoczek11].

The observed degradation is due to the well-known Staebler-Wronski effect (SWE) [Shah10, Gostein11] studied since its discovery in 1977 [Staebler77]. Even if still not fully understood, the effect is reported to be associated with light-induced defect centres that lower the carrier lifetime, which can be partially reversed by thermal annealing at high temperatures. Single-junction modules with thicker intrinsic layers are more affected compared to technologies with thinner i-layers such as amorphous silicon multi-junction modules and micromorph (microcrystalline/amorphous) modules are even less affected. The higher the degradation rate is, the greater is also the potential recovery. Figure 4.2.2 shows an example of a first-generation single-junction amorphous silicon PV system, where one of two strings has been insulated to demonstrate the thermal-annealing effect.

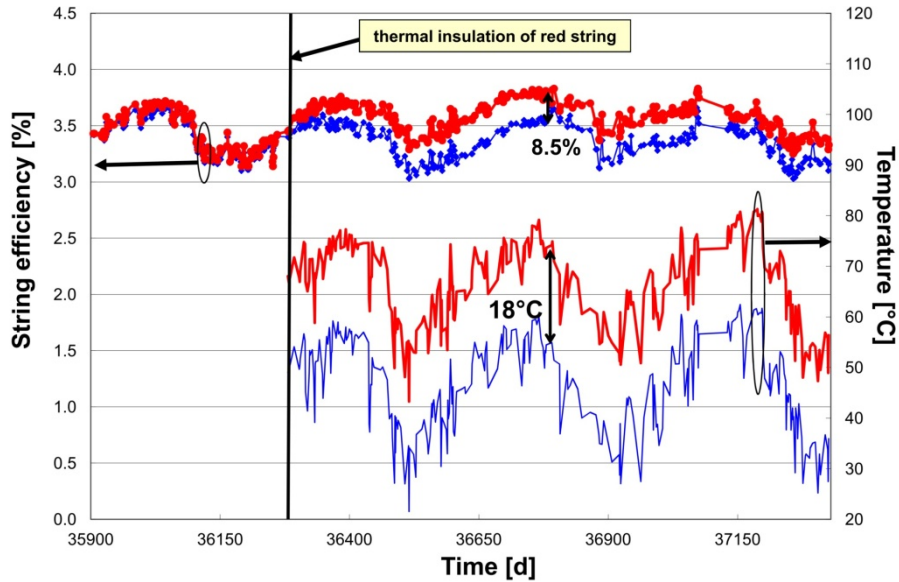


Fig. 4.2.2: Comparison of a ventilated string (blue lines) and a back-insulated string (red lines) of single-junction amorphous silicon PV modules.

The observed instability results in the requirement for stabilisation before determining the power of an amorphous silicon module by measuring the *I-V* curve, see chapter 5.2. The stabilizstion has to be performed according to the light soaking procedure described in [IEC61646]. For amorphous silicon modules light soaking mainly influences the fill factor (and consequently the module power), to a minor extent the short-circuit current of a module and even less the open-circuit voltage. Both initial and stabilised powers have to be stated on the datasheet and nameplate as defined in the standard EN 50380 [EN 50380].

The change in power due to the SWE effect is here considered not to be a PV module failure as long as the stabilised power of the PV module given by the manufacturer is higher than or equal to the measured stabilized value.

4.3 Important PV module failures due to external causes

Some failures are typically difficult to define as a PV module failure or as a failure of the contractor, of the installer or the system designer or even for other reasons. Examples of these types of failures are discussed in this chapter.

4.3.1 Clamping

A relatively often seen failure in the field is glass breakage of frameless PV modules caused by the clamps. In Fig. 4.3.1 two examples from the field are shown.

Glass/glass modules are more sensitive to glass breakage. The origin of the failure is, on the one hand, at the planning and installation stage either (a) poor clamp

geometry for the module, e.g. sharp edges, (b) too short and too narrow clamps [Dietrich08] or (c) the positions of the clamps on the module not being chosen in accordance with the manufacturer's manual. The second origin, which induces glass breakage could be excessively-tightened screws during the mounting phase or badly-positioned clamps [Urban09].

Glass breakage leads to loss of performance in time due to cell and electrical circuit corrosion caused by the penetration of oxygen and water vapour into the PV module. Major problems caused by glass breakage are electrical safety issues. Firstly, the insulation of the modules is no longer guaranteed, in particular in wet conditions. Secondly, glass breakage causes hot spots, which lead to overheating of the module.

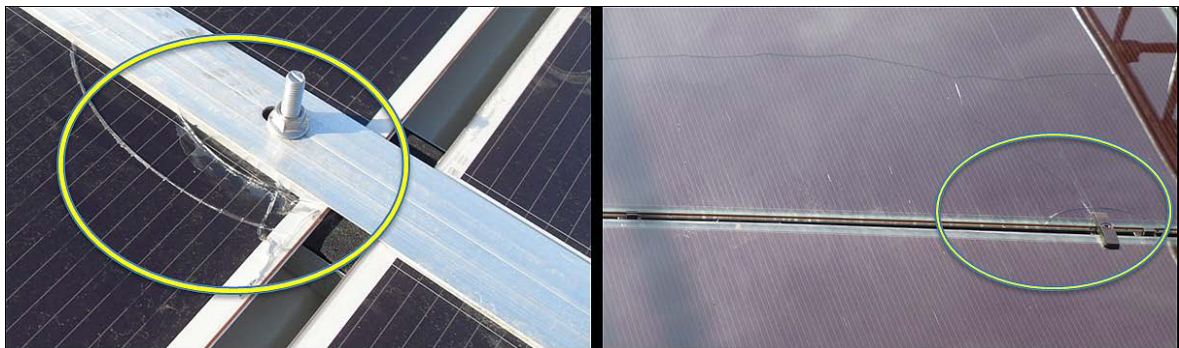


Fig. 4.3.1: Left figure shows glass breakage caused by too tight screws and the right figure a PV module that broke due to poor clamp design.

4.3.2 Transport and installation

Transport [Reil10, Koentges11] and installation [Olschok12] are the first critical stages in a PV module's life. The glass cover of some PV modules may break or cells in the laminate may break due to vibrations and shocks. In the former case it is easy to attribute the glass breakage to the transportation or installation. This is clearly no PV module failure. However, the cause of cell breakage is much more difficult to decide. Visually it cannot be seen and in many cases it cannot be detected by a power rating of the PV module directly after occurrence of the cell breakage. Only an electroluminescence image (chapter 5.4) or a lock-in thermography image (chapter 5.3.3) can reveal the damage. Some typical situations leading to cell cracks but not necessarily to glass breakage are:

1. A PV module falling over.
2. An insufficiently rigid pallet touching the lowest PV module in the stack during transportation.
3. Too tight transport corners in the transport stack. During de-stacking of the top module of the stack the second uppermost module is also lifted and suddenly drops down.
4. Someone steps on the PV module.
5. Even in well-designed transport containers, the cells of PV modules may crack during "normal" transport.

This damage may have the consequences described in chapter 6.2.1. It is especially difficult to decide who is responsible in case no. 5. Currently there is no definition of

what a PV module must be able to withstand during transport. For this reason, chapter 7.1 discusses how to test PV modules for transportation.

4.3.3 Quick connector failure

The quick connector electrically connects solar modules to each other, to fuse boxes, to extension cables, combiner boxes and to the inverter. This element is very important for the safety and reliable power generation of the system. However, there is very little literature on the reliability of quick connectors available in the PV community. Low-voltage DC connectors as a special kind of contact pair are also frequently discussed in respect of (electric vehicle) automotive as well as PV applications. Electrical contacts in general are considered at electrical contact conferences [Schoepf12] with several contributions concerning PV systems. For a brief introduction to the subject, see publications by Rieder [Rieder00, Rieder01].

In most cases problems caused by the quick connector are not considered a PV module failure. Typical failures are caused by using not exactly fitting quick connectors of different types or inaccurately crimped quick connectors to connect PV modules to extension cables, the fuse box, combiner box or the inverter at the installation site.

Ill-fitting or not well-crimped quick connectors may cause a total power loss in a whole string. In even worse cases, they can cause electric arcs and thus fires. In many cases, the quick connectors are much closer to flammable material such as wooden roof beams or heat-insulation materials than the PV module laminate. A statistical review of fire sources in 75 PV systems, which caught fire, shows that the chance of the quick connector causing the fire (29%) is nearly as high as for the rest of the module (34%) or other parts of the PV system (37%) [Schmidt13].

Despite the safety relevance of quick connectors there is, as yet, no standardised quick connector. Quite the reverse - there are many very similar-looking and even apparently fitting quick connectors on the market, which must not be combined.

Currently, only a draft version of an international PV connector standard [IEC62852] exists, while a European standard for PV connectors, EN 50521 [EN50521], has been available since 2008, based on the more general IEC 61984 [IEC61984].

4.3.4 Lightning

A defective bypass diode caused by a lightning strike is caused by an external source, for which the module is not designed. However, this effect has often been found and may cause subsequent safety failures, but the PV module is not the source of the failure. Typical induced defects caused by a lightning strike are open-circuit bypass diodes or a mechanically broken PV module directly hit by the lightning strike. Both defect types may cause hot spots as subsequent failures.

References

- [Bothe06] K. Bothe, J. Schmidt, Electronically activated boron-oxygen-related recombination centers in crystalline silicon, *Journal of Applied Physics* **99** (2006), p. 013701
- [Dietrich08] S. Dietrich, M. Pander, M. Ebert, J. Bagdan, Mechanical Assessment of large photovoltaic modules by test and finite element analysis, Proc. 23rd EUPVSEC (WIP, Valencia, Spain, 2008), p. 2889-2892
- [EN 50380] European Standard (EN) 50380: Datasheet and nameplate information for photovoltaic modules, 2003-09
- [EN5021] EN 50521:2008 + A1:2012: Connectors for photovoltaic systems - Safety requirements and tests, CENELEC, 2013-02
- [Fanni11] L. Fanni, A. Virtuani, D. Chianese, A detailed analysis of gains and losses of a fully-integrated flat roof amorphous silicon photovoltaic plant, *Solar Energy* **85** (2011), pp. 2360–2373
- [Gostein11] M. Gostein, L. Dunn, Light soaking effects on photovoltaic modules: Overview and literature review, Proc. 37th IEEE PVSC (IEEE, Seattle, USA, 2011), pp. 003126–003131
- [IEC 61646] IEC 61646 Ed2.0: Thin-film terrestrial photovoltaic (PV) modules - Design qualification and type approval. English & French version - 81p. IEC 2008-05
- [IEC62852] IEC62852 Ed.1.0: Connectors for DC-application in photovoltaic systems – Safety requirements and tests. Draft version 82/707/NP. 40p. IEC 2012
- [IEC6984] IEC 61984 Ed. 2.0 Connectors - Safety requirements and tests. English & French, 91p. IEC 2008-10
- [Koentges11] M. Köntges, S. Kajari-Schröder, I. Kunze, U. Jahn, Crack statistic of crystalline silicon photovoltaic modules, Proc. 20th EUPVSEC (WIP, Hamburg, Germany, 2011), pp. 3290-3294
- [Olschok12] C. Olschok, M. Pfeifer, M. Zech, M. Schmid, M. Zehner, G. Becker, Untersuchung von Handhabungsfehlern bei der Montage und Installation von PV Modulen, Proc. 27. Symposium Photovoltaische Solarenergie (OTI, Bad Staffelstein, Germany, 2012), p. 202
- [Reil10] F. Reil, J. Althaus, W. Vaaßen, W. Herrmann, K. Strohkendl, The Effect of Transportation Impacts and Dynamic Load Tests on the Mechanical and Electrical Behaviour of Crystalline PV Modules, Proc. 25th EUPVSEC (WIP, Valencia, Spain, 2010), pp. 3989 – 3992
- [Schoepf12] Thomas Schöpf (ed.): Electrical Contacts 1953 to 2012. Proceedings of the IEEE HOLM Conference on Electrical Contacts (1953-2012) - International Conference on Electrical Contracts (1961-2012) - Albert Keil-Kontaktseminar (1972-2011). ISBN 978-3-8007-3459-7, 97 conference proc. on DVD app. 4500p. VDE-Verlag 2012
- [Rieder00] Werner Rieder, Electrical Contacts. An Introduction to their Physics and Applications. ISBN-13: 9780780396395. IEEE 2001 - 90 pages, [Rieder01] Werner

Rieder, Elektrische Kontakte: Eine Einführung in ihre Physik und Technik. ISBN-13: 9783800725427. VDE Verlag GmbH, 2000 - 56 pages

[Schmidt13] H. Schmidt, F. Reil, Begrüßung zum 2. Workshop „PV-Brandschutz“, Zweiter Brandschutz-Workshop, Freiburg, Germany, 24.01.2013 (http://www.pv-brandsicherheit.de/fileadmin/WS_24-01-13/01_Schmidt_Begr%C3%BC%C3%9Fung.pdf)

[Shah10] A. Shah, W. Beyer, Thin-film Silicon Solar Cells. Shah A (ed.), EPFL Press, 2010, pp. 30-35

[Skoczek11] A. Skoczek, A. Virtuani, T. Cebecauer, D. Chianese, Energy yield prediction of amorphous silicon PV modules using full time data series of irradiance and temperature for different geographical locations, Proc. 26th EUPVSEC (WIP, Hamburg, Germany, 2011), pp. 3248–3252

[Staebler77] D. L. Staebler, C. R. Wronski, Reversible conductivity changes in discharge-produced a-Si, *Applied Physics Letters* **31**, (1977), pp. 292-294

[Urban09] H. Urban, Befestigungstechniken von Dünnschichtmodulen, Fifth User Forum Thin Film Photovoltaics (Würzburg, Germany, January 2009)

4.3 Definition of safety failure and safety categories

A safety failure is a failure that may endanger somebody who is applying or working with PV modules or simply passing the PV modules. The safety categories categorise the failure type for the safety of the PV system. In Tab. 4.3.1 three classes are defined. These classes are useful to assess the action needed to be taken if the failure occurs.

Tab. 4.3.1: List of safety categories.

Safety category	Description
A	Failure has no effect on safety.
B(f,e,m)	Failure may cause fire (f), failure may cause electrical shock (e), failure may cause physical danger (m), if a follow-up failure and/or a second failure occurs.
C(f,e,m)	Failure causes direct safety problem (definition of f,e,m see B).

However, the action needed after a safety failure has occurred depends on the application of the PV modules. For example, the criticality of electrical shocks depends on the application class the PV module is used for. The application classes are defined in IEC 61730-1 [IEC 61730-1]. E.g. a C(e) safety classification means a damaged PV module may cause an electrical danger for that application class.

Also, the physical danger resulting from a failure may lead to different courses of action, for example if a mechanical defect occurs in a PV module installed overhead or in a PV module installed in a field surrounded by a fence, to which only skilled

people have access. In the former case, a PV module of a B(m) or C(m) safety category should be immediately replaced, but in the latter case, the module may sometimes remain in place.

References

[IEC 61730-1] International Electrotechnical Commission (IEC) 61730-1: Photovoltaic (PV) module safety qualification - Part 1: Requirements for construction, 2004-10-14

4.4 Definition of power loss failure and power loss categories

If the module power P_m measured in accordance with IEC 60904 [IEC 60904] plus the total uncertainty of the measurement ΔP_m is lower than the power printed on the module label P_l minus the tolerance stated on the label ΔP_l a power loss failure occurs:

$$P_m + \Delta P_m < P_l - \Delta P_l . \quad (4.4.1)$$

The reverse definition is given in the standard IEC 61853-1 [IEC 61853-1] for the case of no power loss. The power loss categories describe how the power loss evolves from the initial power value to a time in the service life of a PV module. In most cases this discrepancy between the reference values may lead to inconsistent results, because the power printed on the PV module label may substantially deviate from the initial PV module power.

However, each definition is useful for its application area.

1. Legal application: power loss failure uses the power printed on the PV module label as reference value.
2. Technical application: the power loss category uses the initial power as a reference value.

The power loss categories given in Tab. 4.4.1 allow the assessment of the impact of the failure over time.

Tab. 4.4.1: Definition of power loss categories.

Power loss category	Description
A	Power loss below detection limit <3%
B	Exponential-shaped power loss degradation over time
C	Linear-shaped power loss degradation over time
D	Power loss degradation saturates over time
E	Degradation in steps over time
F	Miscellaneous degradation types over time

An appendix to the power loss category adds information regarding the dependency of the power loss. The possible appendixes are explained in Tab. 4.4.2. The following example describes a linear power loss with time $C(t,h,u)$. The power loss for this example increases with temperature, humidity, and UV irradiation.

Tab. 4.4.2: List of possible dependencies of the power loss.

Appendix letter	Power loss increases with
t	Temperature
v	Voltage
i	Current
h	Humidity
m	Mechanical load
u	UV irradiation
tc	Thermal cycling
s	Shading

References

[IEC 60904] International Electrotechnical Commission (IEC) 60904: Photovoltaic devices, 2006

[IEC 61853-1] International Electrotechnical Commission (IEC) 61853-1: Photovoltaic (PV) module performance testing and energy rating - Part 1: Irradiance and temperature performance measurements and power rating, 2011

4.5 Definition of a defect

A defect is everything in a PV module that is not as it is expected to be. A defect may imply a PV module failure or not. A defect is a much broader term than a failure. A defect does not necessarily result in a safety or power loss for a PV module but specifies a part of a PV module that is different from a perfect PV module.

4.6 Definition of PV module parts

Terms for PV module components and different levels of electrical interconnects, in particular, are sometimes used ambiguously or interchangeably, leading to confusion. In the following section, definitions are provided for several module parts to ensure clarity in reference to component-specific defects and failures. Definitions are not provided for module components that are unambiguous (i.e. frame, junction box, encapsulant, etc.) in the interest of brevity or already given in IEC/TS 61836 [IEC61836].

A ‘cell’ is defined as the smallest piece of semiconductor, having a voltage associated with a single junction. In a polycrystalline or monocrystalline silicon module, each cell consists of a single piece of silicon. In a thin-film module, semiconductor material is deposited over a large area, with cells defined by scribing through the material to produce electrically-insulated regions. A ‘string’ of cells represents a set of cells, usually 10 or 12 cells in a wafer-based module or approximately 60-100 cells in a thin-film module, that are electrically connected in series. Two or more strings of cells are sometimes connected in parallel with a bypass diode, creating an electrically independent ‘sub-module’, the function of which is isolated from any cells or strings not in the sub-module.

Up to four levels of metallisation and electrical interconnects are considered. ‘Gridlines’ (interchangeably referred to as ‘fingers’) make up the finest level of metallisation directly on the cells and consist of an array of lines <0.4 mm thick. Current from the gridlines is collected in the ‘busbars’, which are also directly on the cell. Figure 4.6.1 shows a schematic of gridlines and busbars on a mono- or polycrystalline silicon cell.

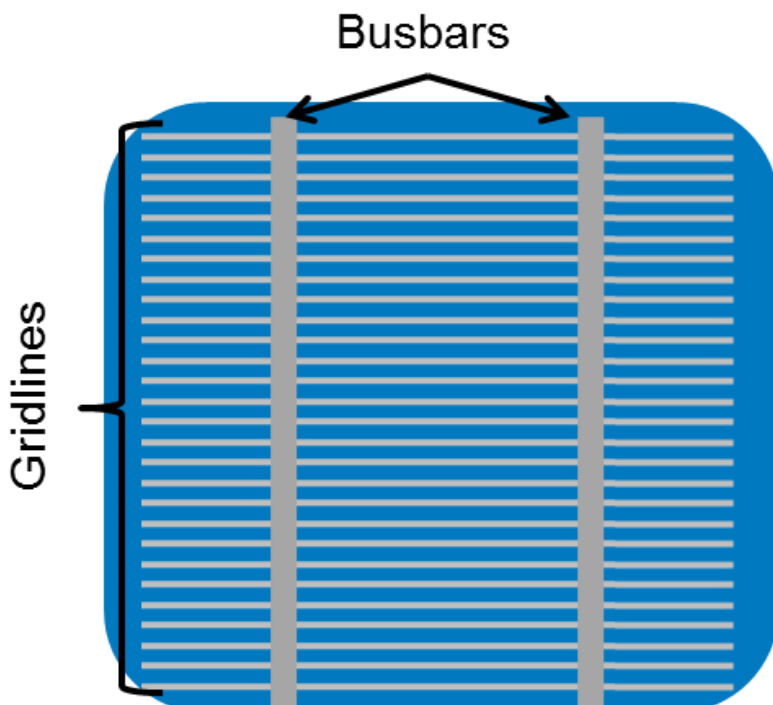


Fig. 4.6.1: Metallisation on a silicon cell consists of gridlines and busbars.

Cells wired in series are connected to form a string by the ‘cell interconnect ribbon’. It should be noted that the cell interconnect ribbon often obscures inspection of the busbars on silicon cells because it directly overlaps them. Multiple strings are connected via the ‘string interconnect’, which is usually located near the edge of the module and may be obscured by the module frame or cover layers. Figure 4.6.2 shows a schematic illustrating cell interconnect ribbons and a string interconnect. The arrangement of metallization and/or interconnects may be less standardized in thin-film modules than that of mono- and polycrystalline silicon modules. In the case of thin-film modules, all four levels of metallisation and electrical interconnects may not be necessary; the naming convention for these modules follows the function of the particular interconnect level described above.

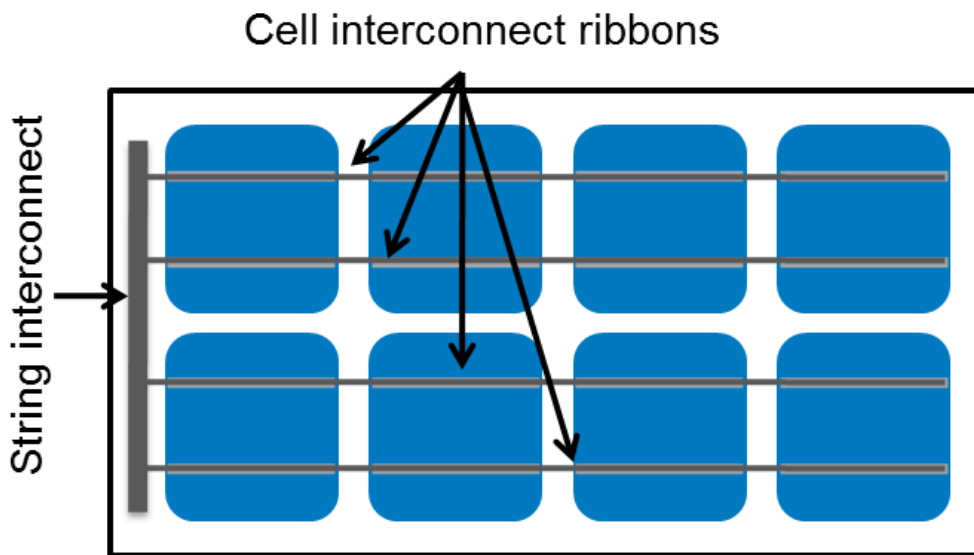


Fig. 4.6.2: Cells are electrically connected into strings via cell interconnect ribbons and the string interconnect connects multiple strings of cells.

References

[IEC61836] IEC/TS 61836 Ed. 2.0 2007-12, Solar photovoltaic energy systems - Terms, definitions and symbols

5 Basics of measurement methods used to identify failures

In this chapter the setup, best practice and the interpretation of the most important measurement methods are described. At the end of each chapter a list of failures are given which may be identified by the introduced measurement method.

5.1 Visual inspection

The most effective and quickest method to find failures and defects in a PV module is the visual inspection. For the sake of completeness we introduce the visual inspection of new modules being tested in standard tests as described in the standards [IEC61215, IEC61646]. This visual inspection method is not well applicable to weathered PV modules. Therefore we introduce an international harmonized “Documentation of visual failures in the field” to collect data from visually inspected modules in a uniform way. This allows defect and failure collection in a way being applicable for statistical evaluations from various experts and countries.

5.1.1 Visual inspection in accordance with IEC PV standards

Visual inspection of a PV module is performed before and after the module has been subjected to environmental, electrical, or mechanical stress testing in the laboratory. Stress tests are usually used to evaluate module designs in the pre-phase of production, production quality, and lifetime of the modules. The most common stress tests are: thermal cycling, humidity-freeze cycling, damp heat exposure, UV irradiation, mechanical loading, hail impact, outdoor exposure, and thermal stress.

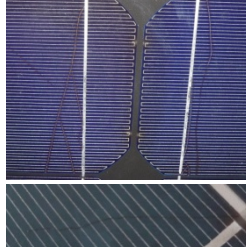
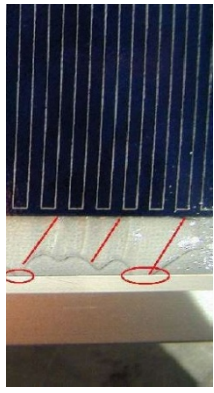
To approach the visual inspection of the PV module it can be divided in its parts and each PV module part is inspected and documented separately with the relative defects. The IEC 61215 and 61646 standards [IEC61215, IEC61646] require an illumination of more than 1000 lux during the visual inspection and only defects detectable with the bare eye are considered. The defects conditions are listed in the IEC 61215, 61646 standards in chap. 10.1.1 as shown in Tab. 5.1.1.

Table 5.1.1: Typical failures found during IEC 61215, 61646 visual inspection.

PV module component	PV module failures
Front of PV module	Bubbles, delamination, yellowing, browning,
PV Cells	Broken cell, cracked cell, discolored anti reflection
Cell metallization / cell and	Burned, oxidized
Frame	Bend, broken, scratched, misaligned
Back of module	Delaminated, bubbles, yellowing, scratches, burn
Junction box	Loose, oxidation, corrosion
Wires – connectors	Detachment, brittle, exposed electrical parts

It is a good laboratory practice to record all visible defects – even if judged irrelevant - because in case of worsened defects during testing sequences the documentation is complete and allows the follow up. For a good documentation the following rules should be taken into account. The photo should be taken without light or flash reflection and mirror image. The position and the dimension of each defect should be documented. Clear terms and definition should be used to describe the defect. Standardization, at least in the same laboratory, for the defect description is desirable to minimize interpretation errors caused by individual judgment. In clause 7 of the IEC 61215 and 61646 standards the major visual defects which cause the failure (not passed) in the design qualification of the PV module are defined and described in Tab. 5.1.2.

Tab 5.1.2: Visual defects as defined in clause 7 of the IEC 61215 [IEC61215] and IEC 61646 [IEC61646]. The failures are described in detail in the chapter referenced in column named “chapter”. The codes used in column “Safety” and “Power” are defined in chapter 4.3 and 4.4.

Chapter	Type	Safety	Power	Image
--	Bent or misaligned external surfaces, substrates, frames, and junction boxes to the extent that the installation and/or operation of the module would be impaired Module wire touching the diode with the risk of arcs- operation is compromised Cell fragment laminated in the module, operation could be impaired	B(m,e) B(f) B	A A A	
6.2.2, 6.2.3	Crack in cell - a propagation which could remove more than 10% of the cell area from the electrical circuit	A	D	
6.1.1	Bubbles or delaminations forming a continuous path between any part of the electrical circuit and the edge of the module.	C(e)	D/E	 [Zamini07]
--	Loss of mechanical integrity, to the extent that the operation or the installation of the module would be impaired	B(e,m)	A	

5.1.2 Documentation of visual failures in the field

Visual inspection is a powerful tool to identify causes of failures of PV modules or to identify problems that could cause failures in the future. Sometimes changes that lead to aesthetic concerns are considered failure even if the module is functioning well. Many changes in performance are invisible and need to be studied with more sophisticated tools, but the visual inspection is quite effective for identifying hot spots (burn marks), delamination, encapsulant yellowing, back sheet blistering, junction box failure, and many others.

The simplicity of visual inspections allows the possibility of collecting data very widely. Here we attempt to regularize the collection of this data by developing an inspection checklist for the evaluation of visually observable defects in fielded PV modules. A checklist harmonised by the Task 13 group for module conditions can be found in Annex A. This checklist is used for collecting visual failures in this report. We recommend this checklist as an international standard for visual inspection in the field. Table 5.1.3 gives a list and a gallery of failures which are detectable by visual inspection.

Tab. 5.1.3: List of failures detectable by visual inspection in the field. The failures are described in detail in the chapter referenced in column named “chapter”. The codes used in column “Safety” and “Power” are defined in chapter 4.3 and 4.4.

Chapter	Type	Safety	Power	Image
6.2.4	Burn marks at the backsheet, heating along a busbar	B(f,e,m)	D/E	
6.2.4	Burn marks at the front, discolouration of the encapsulant associated with overheating along the metallic interconnections	B(f,e,m)	D/E	 Detailed description: This image shows a close-up of a solar module's front surface. A prominent dark, horizontal band of discoloration runs across the center, labeled 'Dark Discoloration on String Interconnect'. To the right, a vertical line labeled 'Gridline' is visible. A red arrow points to a specific area where the discoloration meets a cell interconnect ribbon, labeled 'Cell Interconnect Ribbon'.
6.1.1	Delamination of a multicrystalline Si module	B(e)	D/E	

6.1.1	Delamination of c-Si module	B(e)	<u>D/E</u>	
-	Electrochemical corrosion of a thin-film module and associated delamination	B(e)	<u>D/E</u>	
6.4.1	Thin-film glass breakage	B(e)	<u>D/E</u>	
6.2.1	Slightly browned EVA in the center of the cell, but bleaching occurs in the parts of the EVA that have access to atmospheric oxygen and/or that are close enough to the edge that the acetic acid diffuses out of the cell	A	<u>C</u>	
6.2.1	A single cell will brown much faster than the others when it is hotter than the others.	B(f)	<u>D</u>	

6.2.1, 6.2.2	Browned EVA on top of a cell with two cracks in a cell. Photobleaching takes also place along cell cracks therefore the crack is visible. The browning takes several year to appear. This may not be mistaken for Snail tracks.	B(f)	C	 [Schulze13]
6.2.3	Snail Track is a discolouration of the silver paste used for the gridlines on the cells. The discolouration appears along cell cracks. This may not be mistaken for photobleaching of EVA along cell cracks.	B(f)	C	
6.1.2	Delamination of backsheets	B/C(e)	D	

Visual defects like bent or misaligned external surfaces, frames or junction boxes may lead to failures in the field. Otherwise defects like cracked cells have a high probability to cause follow-upfailures of the modules with power loss or safety issues. Other defects like delamination or small cell-frame distances can cause safety failures, because the insulation is not guaranteed.

References

[IEC61215] International Electrotechnical Commission (IEC) 61215: 2nd edn, 2005. Crystalline silicon terrestrial photovoltaic modules - Design qualification and type approval.

[IEC61646] International Electrotechnical Commission (IEC) 61646: 2nd edn, 2008. Thin-film terrestrial photovoltaic modules - Design qualification and type approval.

[Schulze13] K. Schulze, M. Groh, M. Nieß, C. Vodermayer, G. Wotruba und G. Becker, Untersuchung von Alterungseffekten bei monokristallinen PV-Modulen mit mehr als 15 Betriebsjahren durch Elektrolumineszenz- und Leistungsmessung, Proc. 28. Symposium Photovoltaische Solarenergie (OTI, Staffelstein, Germany, 2013)

[Zamini07] S. Zamini, S. Mau, T. Krametz: "IEC 61215 - Erfahrungen aus 4 Jahren Prüftätigkeit." TÜV Modulworkshop, (TÜV, Cologne, Germany) 2007

5.2 *I-V* curve

Measurements of module *I-V* characteristic determine short-circuit current, open-circuit voltage, and other parameters. A typical module *I-V* measurement system consists of a natural or artificial simulated light source, a test bench to illuminate the module under test, module temperature control, monitoring facility, and a data acquisition system to measure the current-voltage curve when the voltage across the module or current through the module is varied with an external electronic load or power supply.

Under natural sunlight condition, a portable *I-V* tracer is often used for measuring module *I-V* curves, but probably not under standard test conditions (STC, 1000 W/m², 25°C, AM 1.5G reference spectrum of IEC 60904-3 [IEC60904-3]). Usually, a pyranometer or sunlight irradiance sensor is used as a reference solar device for rating global irradiance. For comparison, e.g. with data sheet values at STC, it is then necessary to correct the measured *I-V* curves, see IEC 60891 [IEC60891].

Under simulated light irradiance conditions, a reference cell or reference module which has identical or similar spectral response characteristics to the module under test is often used as a reference solar device to measure the irradiance of the light source. As the environment of measurement is much easier to control, the test parameters (I_{sc} , V_{oc} , P_{max} , temperature) can be translated to STC more accurately. To meet the requirements and characteristics of different PV technologies, the simulated light source (or sun simulator) is a steady state type or pulse type (flash type) simulator. The pulse simulator can be further divided into single pulsed and multi pulse light source. Different artificial simulated light sources can be used for adapting different PV technologies. For instance, the high capacity PV modules need much longer pulse time or a steady state simulator to evaluate module *I-V* characteristic accurately. The typical duration of light pulses for solar simulators usually varies between 1 ms to 20 ms with different profiles. These time intervals are too short for a proper characterization of some high-efficiency PV modules like heterojunction (HIT) or floating emitter cells (SUNPOWER cells). The cells of these PV modules have a high charge carrier life time and therefore a quite high diffusion capacity which leads to long test durations of 50 ms or more. The long-pulse or steady-state simulators would be more suitable for these modules. The specific procedures and requirements of high efficiency module *I-V* characteristics measurement are described by Mau, Virtuani, and Herman [Mau05, Virt08, Herman12]. Furthermore thin-film PV modules show several metastable states, which make it challenging to define a standardised PV module power for each technique. Procedures to measure the PV module power of metastable thin-film modules are described by Silverman [Silverman14].

5.2.1 Introduction of the important *I-V* curve parameters

From the *I-V* curve some key parameters can be extracted to access the quality of the PV module. The *I-V* curve of an illuminated PV module has the shape shown in Figure 5.2.1.

The open-circuit voltage (V_{oc}) is the maximum voltage available from a PV module and occurs at zero current. The short-circuit current (I_{sc}) is the current through the module when the voltage across the cell is zero. The maximum power (P_{max}) is defined as a point on the I - V curve of a PV module under illumination, where the product of current (I_{mpp}) and voltage (V_{mpp}) is maximal. The fill factor (FF) is essentially a measure of the quality of the solar cell or PV module. It is the ratio which compares the maximum power of the PV module to the virtual power (P_T) that would result if V_{mpp} would be the open-circuit voltage and I_{mpp} would be the short-circuit current. The fill factor can be interpreted graphically as the ratio of the rectangular areas depicted in Fig. 5.2.1.

From these parameters optical influences (I_{sc}), cell degradation and shunting (V_{oc}), and series resistance or inhomogeneity effects (FF) can be assessed.

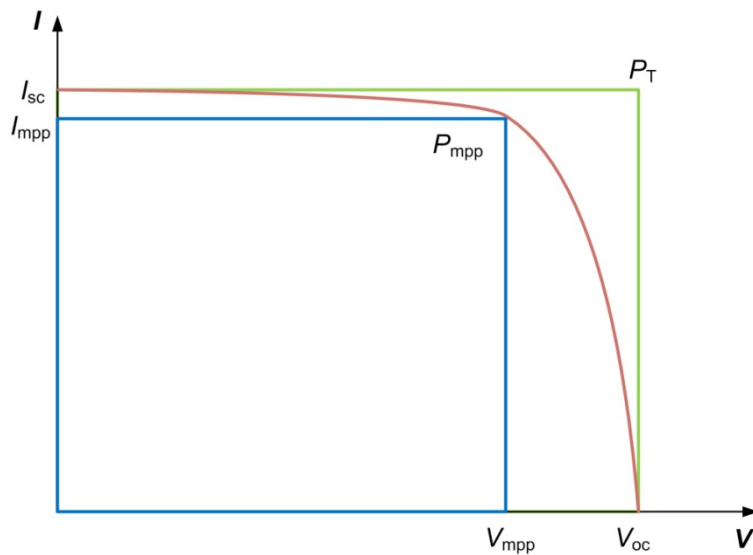


Fig. 5.2.1: The figure shows a schematic I - V curve of an illuminated PV module and the most important parameters: short circuit current I_{sc} , open-circuit voltage V_{oc} , the maximum power point P_{mpp} , the current and voltage belonging to the maximum power point I_{mpp} and V_{mpp} , and the virtual power point P_T .

5.2.2 Series resistance and shunt resistance

In order to understand more about the I - V characteristic of PV modules, it is necessary to define the slopes at each of the intercepts. These slopes will be denominated numbers with units of resistance. They are called series resistance (R_s) and shunt resistance (R_{sh}). These resistances are defined as depicted in Fig. 5.2.2.

The series resistance is a lumped parameter. All series resistances of the solar cells and interconnects affect this parameter. So it may be used to access the effect of series resistances in the PV module. However for the production of a PV module various cells with various I - V characteristics are used. The difference in I - V characteristics also affects the lumped parameter R_s in a PV module. So a high

series resistance may be caused by the addition of series resistances in the module or caused by a mismatch of the individual cell characteristics.

The shunt resistance illustrates a shunt path for the current flow bypassing the active solar cell. If the shunt resistance of a cell is low, the shunt path shows higher leakage currents. A change of shunt resistance in single solar cells is not detected by the shunt resistance of the module because all the other cells block the additional current from the cell. Only in the very unlikely case that all cells have a low shunt resistance will the shunt resistance of the PV module also be low. In all other cases shunts of single cell affect the Fill Factor of the module and not the shunt resistance. The shunt resistance also influences short-circuit current and open-circuit voltage (V_{oc}) of $I-V$ characteristics of cells especially when a hot-spot endurance phenomenon occurs.

It should be noticed that the interpretation of R_s and R_{sh} as shunt and series resistance only apply if all solar cells in the module are quite comparable. In many practical cases the value of R_s and R_{sh} is just a lumped parameter which can be obtained from the $I-V$ curve slope at I_{sc} and V_{oc} . In some cases, for analyzing the behavior of the PV module it is necessary to give the R_s and R_{sh} parameters physical meanings.

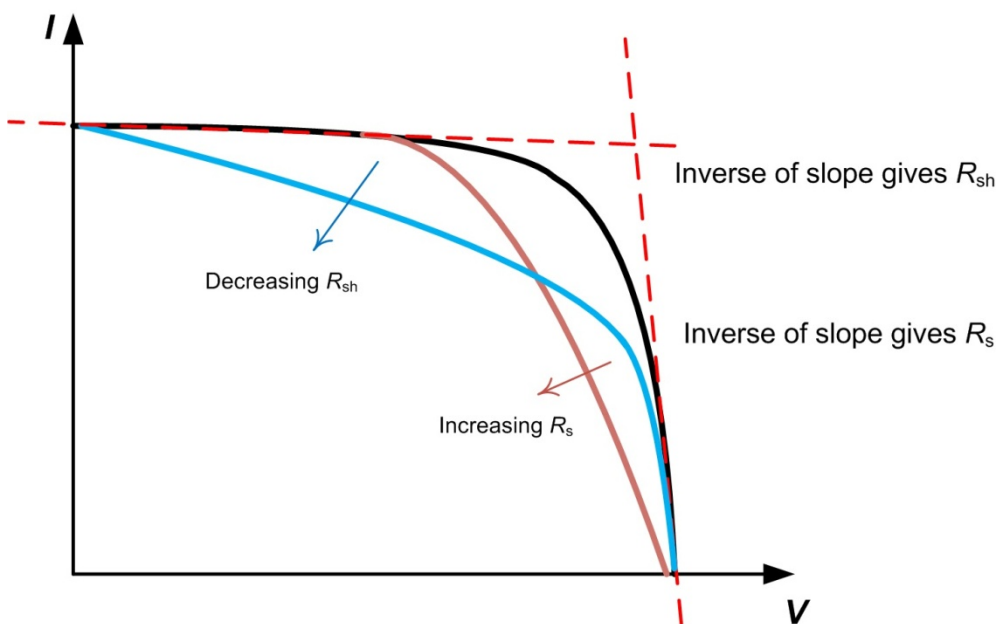


Fig. 5.2.2: Schematic $I-V$ curve of an illuminated PV module and the influence of a series resistance R_s and a shunt resistance R_{sh} to the $I-V$ curve.

5.2.3 Accuracy

For $I-V$ characteristic measurement, there are many aspects affecting measurement accuracy. To improve accuracy of measurement, each channel performance of the $I-V$ acquisition system must be calibrated in an accredited laboratory or institution to ensure proper dynamic behaviour including time response and current, voltage bias. For accurate measurement, it is important to know the module under test

characteristics, high capacitance of some high efficiency modules can influence the measurement results. Measurement problems due to high capacitive modules may be detected by comparing *I-V* characteristics measured from short-circuit current to open-circuit voltage conditions and in the reverse direction, with the other parameters unchanged. The detailed procedures are described by Mau, Virtuani, and Herman [Mau05, Virt08, Herman12].

It is strongly recommended that the spectral response of a module under test be performed before *I-V* measurement. Normally, a typical represented encapsulated cell can be a sample for spectral response measurement. To minimize the spectral mismatch effect, the reference solar device should have identical or similar spectral response to the module under test. If the *I-V* measurement is performed under outdoor condition, the pyranometer or other thermopile irradiance sensor must be calibrated against an accredited laboratory.

For all *I-V* measurements of PV cells and modules, the real time measuring result should be translated to the STC or SRC (standard report condition), so the sunlight or simulated irradiance should be measured by calibrated reference solar device which can be traced to accredited laboratory of ISO 17025 [ISO 17025]. For indoor measurement, the spectral irradiance distribution of light can not be identical to natural sunlight. It is recommended that the simulator spectrum should meet the requirement of IEC 60904-9 [IEC 60904-9] standard. On the other hand, non-uniformity of irradiance and light instability can affect the *I-V* result simultaneously. The module under test should be mounted in the area with the most homogeneous light distribution and measured in the time period of the flash with almost constant intensity level and light spectrum.

For both indoor and outdoor measurements, the environmental parameters should be monitored to keep the temperature homogeneous and constant as far as possible. As different PV modules have specific temperature coefficients, the temperature should be controlled close to the desired temperature level to reduce voltage and current correction.

At present, four laboratories maintain the World Photovoltaic Scale to give PV metrology and reference solar device to other laboratories, institutions, and manufacturers. It is commonly difficult to obtain better than 3% certified accuracy of module *I-V* characteristic for the majority of PV laboratories.

5.2.4 Effect of failures on the *I-V* curve

An *I-V* curve measured with suitable equipment as described in chapter 5.2 gives information about module failures. The interpretation of the *I-V* curve depends on the available data:

a. In case that we have only the measured *I-V* curve without information on the specific electrical values of the PV module we can evaluate the following values:

- the I_{sc} current is consistent with the cell area, cell technology and cell connections in the module - number of cells in series and strings parallel (see values in Tab. 5.2.1),

- the V_{oc} is consistent with the cell technology and cell connection in the module - number of cells in series and parallel strings, see values in Tab. 5.2.1,
- the fill factor is as expected from the module technology
- in addition the shape of the I - V curve reveals two defects:
non-active cell parts due to cell cracking or other reasons (grid defects)
short-circuit of a bypass diode.

b. If we have the specific electrical data for the PV module - from label or, even better, flash report from the manufacturer - the comparison of the measured values give a good indication of potential failures and technical problems.

c. If we have a previous I - V curve of the same PV module measured with comparable equipment and conditions such as a class AAA flasher, reference cell and module temperature, we can obviously evaluate the I - V curve for degradation effects and failures.

Tab. 5.2.1: Typical electrical values at STC conditions.

	Polycrystalline silicon cell	Monocrystalline silicon cell	Expected value for the PV module
J_{sc} Current density [mA/cm ²]	28 - 33	30 - 35	cell area * current density
V_{oc} Open curciut voltage [mV]	550 - 600	600 - 700	number of cells in series * V_{oc}
FF Fill factor	0.75 - 0.80	0.80 - 0.85	--

Deviations between measured and expected I - V curve, values obtained from the data sheets or previous measurements, could be divided into the following categories as listed in Tab. 5.2.2:

1. A lower short-circuit current I_{sc} than expected, case S1 in Tab. 5.2.2, is likely caused by the loss of transparency of the encapsulation due to browning or yellowing, glass corrosion which reduces the light trapping of the module or delamination causes optical uncoupling of the layers. These effects on the I - V curve are like a reduction of the irradiance and as shown in Tab 5.2.4 the curve shape changes differently if the effects are homogenous or heterogenous.
2. The I - V curve near I_{sc} becomes sloped. Case S4 in Tab. 5.2.2, means that the shunt resistance decreased due to shunt paths in the PV cells and/or the interconnections. Slight cell mismatch or slight non uniform yellowing, may be another cause.
3. In case S3 the slope of the I - V curve near V_{oc} is lower indicating an increase of the series resistance in the PV module. The series resistance in the module could increase by the increase of interconnections resistance, corrosion in junction box or interconnects and slacks joints.

The two previous points decrease the fill factor of the module and therefore the maximum power output of the module.

4. The I - V curve has a lower V_{oc} value than expected, case S2 in Tab. 5.2.2. Failures which lower the V_{oc} are failed cell interconnections, short circuits from cell to cell or a failure of the bypass diode. The open-circuit voltage of the module can be reduced also by the light-induced degradation (LID) of crystalline silicon modules or potential induced degradation (PID).

5. The I - V curve shows steps (see table 5.2.2 S6). The reasons of the steps in the curve could be a defect in the bypass diode, damaged cells or heavy mismatch of the PV cells in the module.

Tab. 5.2.2: Table of PV module failures detectable by the I - V curve.

* Only possible with several strings of cells protected by working bypass diodes.

			P_{max}	S1: I_{sc}	S2: V_{oc}	S3: R_{oc}	S4: R_{sc}	S5: change in slope*	S6: inflex points*
Failure	Safety	Power							
Disconnected bypass diode	B	A							
Short-circuit bypass diode	B	E	X			X			
Inverted bypass diode	B	E	X			X			
Homogeneous loss of transparency	A	C	X	X					
Heterogeneous loss of transparency	A	E	X	X				X	X
Homogeneous glass corrosion	A	D	X	X					
Heterogeneous glass corrosion	A	D	X	X				X	X
Homogeneous delamination	B	D	X	X					
Heterogeneous delamination	B	D	X	X				X	X

Homogeneous corrosion AR coating of the cells	B	<u>C</u>	X	X					
Heterogeneous corrosion AR coating of the cells	B	<u>C</u>	X	X				X	
Passivation degradation	A	<u>D</u>	X		X				
PID polarization induced degradation	A	<u>C</u>	X		X			X	
LID light-induced degradation for crystalline solar cells	A	<u>D</u>	X	(X)	X				
Short-circuited cells, e.g. by cell interconnection ribbon	A	<u>E</u>	X		X				
Solder corrosion	A	<u>C</u>	X			X			
Homogeneous soldering disconnections	B	<u>E</u>	X			X			
Broken cell interconnect ribbons	B	<u>E</u>	X			X			X
Cracked cells	A	<u>E</u>	X	X					X

P_{max} = failure is detectable as power loss

R_{oc} = open-circuit resistance (slope at V_{oc})

R_{sc} = short-circuit resistance (slope at I_{sc})

The power degradation of some of the failures mechanism mentioned in the table above is limited. The power loss caused by the corrosion of the antireflection coating is usually limited to 4% which is the initial improvement of the coating. Some others failures are limited like the delamination with values of 4%, the initial light-induced degradation with 2 - 4%, glass corrosion with maximum of 3%. Failures like cell cracks, solder corrosion, broken cell interconnects have no limits in power loss and the PV module may be unusable.

References

- [Herman12] M. Herman, M. Jankovec, M. Topic, Optimal *I-V* Curve Scan Time of Solar Cells and Modules in Light of Irradiance Level, *International Journal of Photoenergy*, Volume 2012, Article ID 151452, doi:10.1155/2012/151452
- [IEC60904-3] International Electrotechnical Commission (IEC) 60904-3 Ed. 2: Photovoltaic devices - Part 3: Measurement principles for terrestrial photovoltaic (PV) solar devices with reference spectral irradiance data, 2008
- [IEC60891] International Electrotechnical Commission (IEC) 60891 Ed.2.0 Photovoltaic devices – Procedures for temperature and irradiance corrections to measured I-V characteristics, 2009
- [IEC 60904-9] International Electrotechnical Commission (IEC) 60904-9 ed2.0: Solar simulator performance requirements, 2007-10-16
- [ISO 17025] International Organization for Standardization 17025: General requirements for the competence of testing and calibration laboratories, 2005
- [Mau05] S. Mau, Influence of Solar Cell Capacitance on the Measurement of *I-V* curves of PV Modules, Proc. 20th EUPVSEC (WIP, Barcelona, Spain, 2005), pp. 2175-2177
- [Silverman14] T. Silverman, U. Jahn, “Characterization of Performance of Thin-film Modules”, Technical Report IEA-PVPS T13-02: 2014, in preparation.
- [Virtuani08] A. Virtuani, H. Müllejans, F. Ponti, E. Dunlop, Comparison of indoor and outdoor performance measurements of recent commercially available technologies, Proc. 23rd EUPVSEC (WIP, Valencia, Spain, 2008), pp. 2713-2718

5.3 Thermography

There are basically three different types of thermography methods to detect failures in PV modules. The most common and easiest to apply technique is the thermography under steady state conditions. This method allows the analysis of PV modules in the field under working conditions. The pulse thermography and the lock-in thermography allow a more detailed view into the PV module but both techniques need to be done under lab conditions. These three techniques are described in the next three chapters.

5.3.1 Thermography under steady state conditions

Thermography or infrared (IR) imaging [Tscharner85] is a non-destructive measurement technique, which provides fast, real-time, and two-dimensional distributions of characteristic features of PV modules. It can be used as a contactless method for diagnosing some thermal and electrical failures in PV modules. The measurements can be performed during normal operation for both individual PV modules and as a scan of large scale systems. It has to be assured that the measurement is done under steady state conditions of the PV module.

The thermography measurements show temperature differences induced by an external current or by applying light to the PV module. During measurements in the dark, there is no light applied to the module but external current (typically comparable to short-circuit current I_{sc}) is supplied in the forward direction [Hoyer09]. In order to avoid thermal damage to thin-film modules it must be ensured that the I_{sc} of the modules is not exceeded by more than 30%.

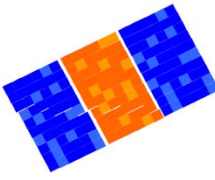
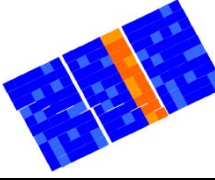
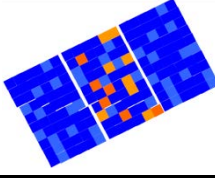
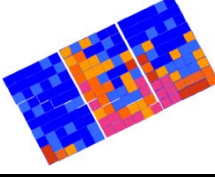
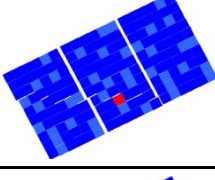
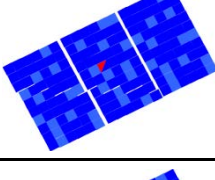
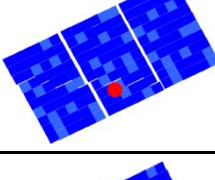
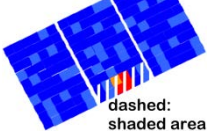
During illumination heat and current are generated by incident light (e.g. the sun) which can cause inhomogeneous temperature of the PV module. For more precise defect detection, thermography imaging is performed under illumination of the PV module and the temperature distribution of various load conditions have to be compared: short circuit, open-circuit, and at maximum power point.

By means of an appropriate IR-camera the temperature distribution can be measured. Thermography imaging is performed mostly by means of a portable, uncooled IR-camera. The wavelength of the used IR-detector is typically between 8 and 14 μm [Zamini12].

Illuminated (outdoor) thermography measurements should be performed on a sunny cloudless day, with min. 700 W/m^2 irradiation at the module array. Ideally the ambient temperature as well as the wind speed is low. The angle of view should be set as close as possible to 90° but not less than 60° to the module glass plane. The operator should be aware of reflections, e.g. buildings in the neighborhood, clouds or self radiation of operator or camera [Buerhop07]. For correct temperature measurement the camera must be set to the correct ambient temperature and the emissivity values for the surface inspected, see [Buerhop11a]. Typical emissivity values are 0.85 for the glass and 0.95 for the polymer backsheet, respectively, if the angle of view is within 90° - 60° (glass) and 90° - 45° (polymer). Measurements from the backsheet side, when possible, are more accurate than from the glass side.

When illumination is uniform and viewed under operating bias, cell temperatures may differ by only a few degrees. If the module is short-circuited or if defects are present, the temperature variations may be much larger. Multiples of 10 K temperature differences may be reached between hot spots in comparison to the normal operating parts in the vicinity. In addition it must be considered that there is a temperature gradient within the PV-plant (e.g. up to 13 K in $\sim 8 \text{ m}$ of modules on the roof) or even in a module (3-5 K), which is due to convective heat transfer [Buerhop11b]. In the Tab. 5.3.1 the possible failures which can be recognized by an IR-Camera are listed.

Tab. 5.3.1: Summary of PV module IR image patterns observed in outdoor measurements, their description, possible failure modes, and its influence on the electrical output. The table is originally from [Buerhop07] and is modified and extended.

Pattern	Description	Possible failure reason	Electrical measurements	Remarks, Chapter	Safety	Power
	One module warmer than others	Module is open circuited - not connected to the system	Module normally fully functional	Check wiring	A	System failure
	One row (sub-string) is warmer than other rows in the module	Short circuited (SC) or open sub-string - Bypass diode SC, or - Internal SC	Sub-strings power lost, reduction of V_{oc}	May have burned spot at the module 6.2.7 One diode shunted	B(f)	const. or \underline{E}
	Single cells are warmer, not any pattern (patchwork pattern) is recognized	Whole module is short circuited - All bypass diodes SC or - Wrong connection	Module power drastically reduced, (almost zero) strong reduction of V_{oc}	Check wiring 6.2.7 all diodes shunted	A when ext. SC, B(f) when Diodes SC	const. or \underline{E}
	Single cells are warmer, lower parts and close to frame hotter than upper and middle parts.	Massive shunts caused by potential induced degradation (PID) and/or polarization	Module power and FF reduced. Low light performance more affected than at STC	- Change array grounding conditions - recovery by reverse voltage 6.2.5 (PID)	A	\underline{C} (v,h,t)
	One cell clearly warmer than the others	- Shadowing effects - Defect cell - Delaminated cell	Power decrease not necessarily permanent, e.g. shadowing leaf or lichen	Visual inspection needed, cleaning (cell mismatch) or shunted cell 6.1.1 (delam.)	A B(f)	\underline{A} , \underline{B} , or $\underline{C}(m, tc, h)$
	Part of a cell is warmer	- Broken cell - Disconnected string interconnect	Drastic power reduction, FF reduction	6.2.2 (cell cracks) 6.2.4 (burn marks) 6.2.6 (interconnects)	B(f)	$\underline{C}(m, tc)$
	Pointed heating	- Artifact - Partly shadowed, e.g. bird dropping, lightning protection rod	Power reduction, dependent on form and size of the cracked part	Crack detection after detailed visual inspection of the cell possible 6.2.2 (cell cracks)	B(f)	$\underline{C}(m, tc)$
	Sub-string part remarkably hotter than others when equally shaded	Sub-string with missing or open-circuit bypass diode	Massive /sc and power reduction when part of this sub-string is shaded	May cause severe fire hazard when hot spot is in this sub-string	A, B(f)	\underline{A} , \underline{C}

dashed: shaded area

5.3.2 Pulse thermography

The pulse thermography (PT) needs an external heat source, e.g. by means of one or more simultaneous triggered powerful flashlights to generate a dynamic heat flux through a PV module. The pulse duration has to be not longer than a few milliseconds, to avoid blurry images. The flash arrangement positioned in front of the module (rear side) and its intensity should be sufficient to raise the surface temperature instantaneously about 1 K to 5 K approximately homogeneously. For a full scale PV-module several kJ lamp power is required. After excitation the surface temperature drops by $\sim 1/\sqrt{time}$. A thermographic camera with a high repetition image acquisition frequency of at least several 10 Hz, or, even better, hundreds of Hz, takes continuously images from the PV module's rear side. An inhomogeneous distribution of the material's heat capacity and thermal conductivity, i.e. differences in the thermal diffusivity, affect the evolution of the temperature distribution. The recorded changes in surface-temperature with respect to time are evaluated after a Fourier transformation of the signals in the frequency domain. The resulting pulse phase thermography images show details of the inner structure of a PV-module: bubbles in the layering, and internal electrical connections invisible through an opaque back sheet.

The penetration depth of the heat dissipation is inversely proportional to the frequency values. In Fig. 5.3.1 some examples for PT images of PV modules derived by evaluation from the back side are depicted.

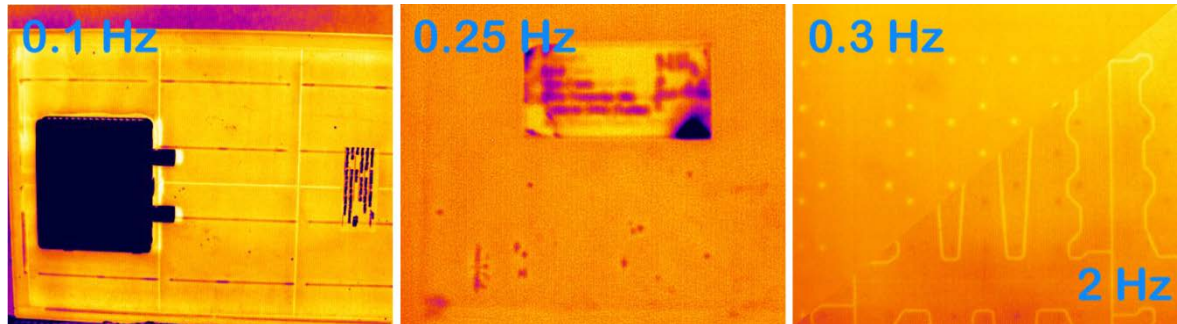


Fig. 5.3.1: Pulse phase thermography images obtained through opaque back sheets. Left hand side: backside cell interconnects between pSi-cells; Middle: bubbles within an encapsulant material; Right hand side: Interconnection structure within a back-contact module: 0.3 Hz image depicting the interconnection points, while the 2 Hz image shows the structure of the copper foil [Voronko12].

Tab. 5.3.2 shows detectable failures in PV modules with the pulse thermography method.

Tab. 5.3.2: List of failures being detectable by pulse thermography inspection. The failures are described in detail in the chapter referenced in column named “Chapter”. The code used in column “Safety” and “Power” is explained in chapter 4.3 and 4.4.

Chapter	Description	Safety	Power	Image
5.1	Allows quasi “visual inspection” of underlying layers and structures through opaque back sheet			See left side picture in Fig. 5.3.1
6.2.6	Position of string and cell interconnects. Detection of deficient soldered joints.	B (f,e,m)	<u>D/E</u>	No image available
6.2.6	Position of interconnects in back-contact modules and their connection quality.	B (f,e,m)	<u>D/E</u>	Fig. 5.3.1: upper part in right image
6.1.1 6.1.2	Inhomogeneous material properties detectable. Detects the depth, where bubbles, delamination occur	C(e)	<u>D/E</u>	Fig. 5.3.1: middle image

A disadvantage of the pulse thermography method is that a high speed and high resolution infrared camera system is required. Such infrared detector chip technology is not only expensive, but used in military infrared systems implemented in missiles and therefore export restrictions apply.

5.3.3 Lock-in thermography

Lock-in thermography (LIT) for non-destructive testing was developed by Busse [Busse92] and Breitenstein [Breitenstein03]. Using LIT the sample is excited and detected at a controlled frequency. This enhances the signal to noise ratio, so that weak heat sources can be detected. Other advantages of LIT are the low thermal impact on the sample, the influence on heat propagation and additional information from phase shifted lock-in images. The LIT method can be used to investigate crystalline [Breitenstein11] as well as thin-film modules [Tran11], [Buerhop12] or organic PV [Bachmann10].

For lock-in thermography, cooled IR-cameras in the spectral range from 2 μm to 5 μm as well as uncooled bolometers in the range from 8 μm to 14 μm are suitable. Due to the periodic excitation of the samples which is synchronized with the image recording, thermal differences in the range of 10 μK can be made visible. The lock-in algorithm provides two primary images and two derived from these: the amplitude signal and the phase signal. Since the amplitude signal is always positive, it is commonly chosen to display the resulting lock-in images in PV module testing. The phase signal, in particular, is neither affected by the emissivity nor by the power of the heat source.

The necessary excitation of the solar cells and modules can be done electrically using a voltage or current source or optically with a light source. Applying an electric current or voltage the measurement is commonly called dark lock-in thermography DLIT. Using a light source it is named illuminated lock-in thermography ILIT [Isenberg04]. This method is very charming because it is possible to work totally contactless and so it can be applied for inspection at an early manufacturing stage.

In order to detect and evaluate PV module defects, behaving as irregular heat sources, the signal intensity and expansion of the LIT measurement are important. One should use a frequency for the LIT method which allows the heat wave to flow through the packaging materials in one cycle. Therefore the lock-in frequency f is optimised for the highest image resolution if the thermal diffusion length Λ is equal to the package material thickness of the PV module

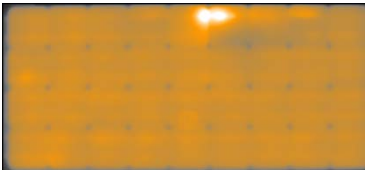
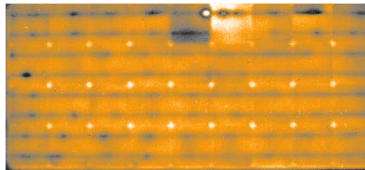
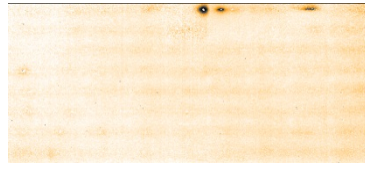
$$f = \frac{\lambda}{2\pi\Lambda^2\rho c_p}, \quad (5.3.1)$$

with the material properties: thermal conductivity k , density ρ , and specific heat capacity c_p . For typical material parameters like 0.45 mm thick EVA and 0.15 mm thick back sheet foil the thermal diffusion length λ is chosen to 0.6 mm for a DLIT measurement from the PV module rear side. Together with the material parameters $k=0.32 \text{ W/mK}$, $\rho c_p=1.19 \times 10^6 \text{ J/m}^3\text{K}$ [Wolf05] a lock-in frequency f of $\sim 0.12 \text{ Hz}$ is a good starting point for evaluations. Measurements through 3-4 mm thick glasses basically result in a lower resolution and the optimised lock-in frequency is one order of magnitude lower around 0.01 Hz.

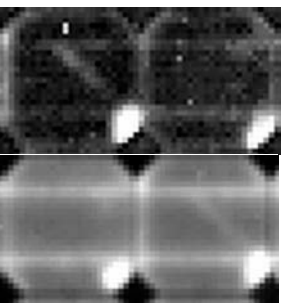
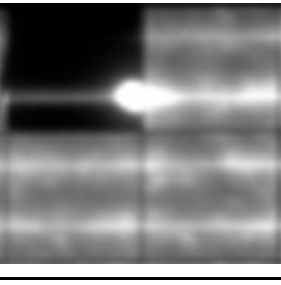
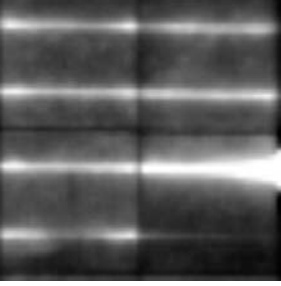
Besides the material properties the signal is influenced by various measurement parameters. With increasing period counts the defects become clearer in the image. The lock-in frequency determines the lateral heat propagation and accordingly the size of the heat affected zone and the amount of implied heat. Thus, with increasing f on the one hand the heat affected zone is reduced enabling the determination of the exact position of the heat source. On the other hand the signal intensity is lowered strongly. Varying the excitation intensity, for example low or high current or voltage, displays heat sources at different working regimes of the module, which can be dominated by parallel or series resistance. Table 5.3.3 shows IR-images of the same module using standard and lock-in thermography.

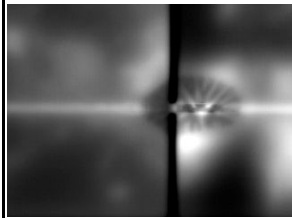
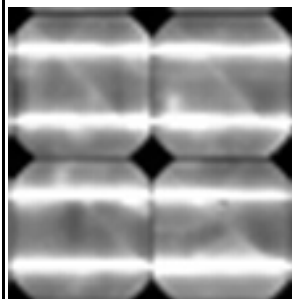
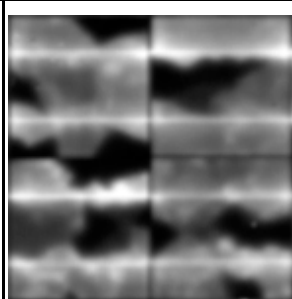
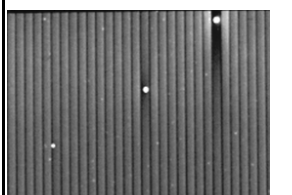
Using LIT irregular heat sources and temperature distributions can be visualized. Even small ones, which are buried by stronger neighbor sources using standard thermography, show up due to the enhanced local resolution. Thus, various types of cell and module defects, e. g. shunts with linear and non-linear behavior, can be distinguished. The exact number and position of defects can be determined. The knowledge about the defect characteristics enables investigating the defect origin and its impact on the module performance. Tab. 5.3.4 lists possible failures which have been detected in crystalline and thin-film modules using lock-in thermography.

Tab. 5.3.3: Three IR-images of the same crystalline PV-module with defects, left: PV module continuously excited, middle and right: DLIT-images, PV module periodically excited, amplitude (middle) and phase (right), measured from the front side, $f = 0.1$ Hz, $I = 5$ A, spatial resolution about 2 mm/pixel, nominal STC-power 115 W, STC-power (8 years running time) 50 W.

Thermography under steady state conditions	Lock-in thermography, periodically excited	
Temperature image	Amplitude image	Phase image
		

Tab. 5.3.4: Overview of defects and failures in solar cells and PV modules visualized using lock-in thermography. Images taken with I_{sc} as current amplitude.

Chapter	Description	Safety	Power	Amplitude image
6.2.4	Edge isolation shunt. To identify a linear shunt the intensity of the shunt area should stay mostly constant for images taken at 10% of I_{sc} (upper image) and 100% of I_{sc} (lower image). Edge isolation shunt occurs only at the edge of the cells.	B(f)	A	
	Cell shunted by cell interconnect ribbon: No current flowing through the cell.	B(f)	A	
6.2.6	Broken cell interconnect ribbon	B(f)	A	

	Medium sized bubbles in encapsulant material	A	<u>A</u>	
6.2.2	Cell cracks type A/B.	B	<u>C</u>	
6.2.2	Cell cracks type C	B(f)	<u>C</u>	
6.3.2	Local ohmic shunt or non-linear impedance	B(m)	<u>E</u>	

References

- [Bachmann10] J. Bachmann, C. Buerhop-Lutz, C. Deibel, I. Riedel, H. Hoppe, C. J. Brabec, V. Dyakonov, Organic Solar Cells Characterized by Dark Lock-in Thermography, *Solar Energy Materials and Solar Cells* **94** (2010), pp. 642-47
- [Buerhop07] C. Buerhop, U. Jahn, U. Hoyer, B. Lerche, S. Wittmann: "Überprüfung der Qualität von Photovoltaik-Modulen mittels Infrarot-Aufnahmen", www.sev-bayern.de/content/downloads/IR-Handbuch.pdf (2007)
- [Buerhop11a] C. Buerhop, D. Schlegel, C. Vodermayer, M. Nieß: Quality control of PV-modules in the field using infrared-thermography, 26th EUPVSEC (WIP, Hamburg, Germany, 2011), pp. 3894 – 3897
- [Buerhop11b] C. Buerhop, H. Scheuerpflug, R. Weißmann: The Role of Infrared Emissivity Of Glass on IR-Imaging of PV-Plants, Proc. 26th EUPVSEC (WIP, Hamburg, Germany, 2011), pp. 3413 – 3416
- [Buerhop12] Cl. Buerhop, J. Adams, F. Fecher, C. J. Brabec, Lock-in Thermographie an Dünnschichtmodulen, *ep Photovoltaik aktuell*, no. **7/8** (2012) pp. 37-41

- [Breitenstein03] Breitenstein, O., M. Langenkamp, Lock-in Thermography, Advanced Microelectronics 10. Berlin: Springer, 2003
- [Breitenstein11] O. Breitenstein, H. Straube, Lock-in Thermography Investigation of Solar Modules, Proc. 26th EUPVSEC (WIP, Hamburg, Germany, 2011), pp. 1451-1453
- [Busse92] G. Busse, D. Wu, and W. Karpen, Thermal Wave Imaging with Phase Sensitive Modulated Thermography, *Journal of Applied Physics* **71** (1992) pp. 3962
- [Hoyer09] U. Hoyer, A. Burkert, R. Auer, C. Buerhop-Lutz, Analysis of PV Modules by Electroluminescence and IR Thermography, Proc. 24th EUPVSEC (WIP, Hamburg, Germany, 2009), pp. 3262-3266
- [Isenberg04] Jörg Isenberg, Neue Infrarotmeßtechniken für die Photovoltaik, Dissertation, KOPS, 2004
- [Tran11] T. M. Tran, B. E. Pieters, M. Siegloch, A. Gerber, C. Ulbrich, T. Kirchartz, R. Schäffler, U. Rau, Characterization of Shunts in Cu(in, Ga)Se₂ Solar Modules Via Combined Electroluminescence and Dark Lock-in Thermography Analysis, Proc. 26th EUPVSEC (WIP, Hamburg, Germany, 2011), pp. 2981-2985
- [Tscharner85] R. Tscharner, K.H.S. Rao, A.V. Shah, Evaluation Of Photovoltaic Panels With Ir. Thermography, Proc. SPIE 0520, Thermosense VII: Thermal Infrared Sensing for Diagnostics and Control, 130(March 20, 1985); DOI: 10.1117/12.946143
- [Voronko12] Y. Voronko, G. Eder, M. Weiss, M. Knausz, G. Oreski, T. Koch, K. A. Berger, Long term Performance of PV Modules: System optimization through the application of innovative non-destructive characterization methods, Proc. of 27th EU-PVSEC, Frankfurt 2012, p. 3530-3535
- [Wolf05] A. Wolf, P. Pohl, R. Brendel, Determination of thermophysical properties of thin-films for photovoltaic applications, Proc. 31st IEEE PVSC (IEEE, Florida, USA, 2005), pp. 1749-1752
- [Zamini12] S. Zamini, R. Ebner, G. Újvári, B. Kubicek, Non-destructive techniques for quality control of photovoltaic modules: Electroluminescence imaging and infrared thermography, *Photovoltaics International* **15** (2012), pp. 126-135

5.4 Electroluminescence

The PV test module is supplied by a dc current to stimulate radiative recombination in the solar cells [Fuyuki05]. This electroluminescence (EL) emission is detected by a commercially available silicon charged coupled device (CCD) camera.

EL imaging is done in a dark environment because the amount of infrared radiation near 1150 nm emitted by the solar module is low compared to the radiation emitted by the background lighting. The dark environment is useful but not necessary to decrease the background “noise” during the EL imaging. Additionally a high pass edge filter at 850 nm may be used to reduce interfering light from other sources. The resolution of the camera should be at least high enough that the fingers of the solar cells in the module can be clearly identified. The noise of the camera output has to be as low as possible. To reduce the influence of stray light an image without dc current through the PV module may be taken and subtracted (dark field subtraction).

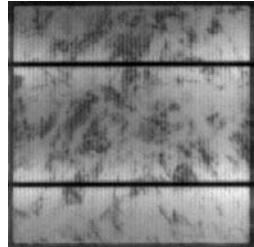
The resulting image is free of stray light then. Outdoor characterisation is also possible in the dark, or by using dark field subtraction or lock-in technique together with a sensitive camera.

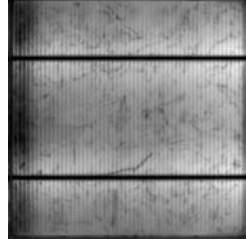
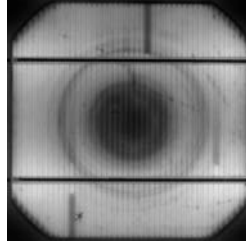
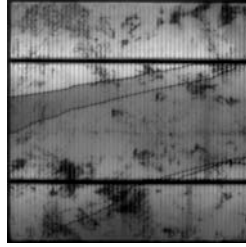
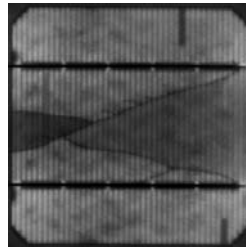
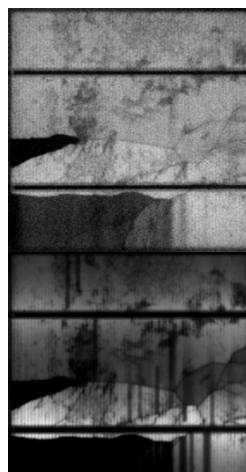
Table 5.4.1 summarizes all effects being detectable with electroluminescence for wafer-based PV modules. The table 5.4.1 also shows the influence of the effects to the electrical parameters of a PV module.

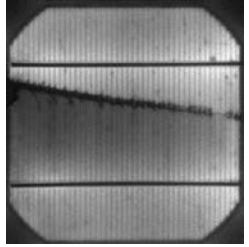
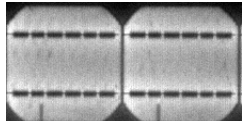
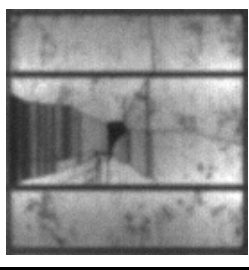
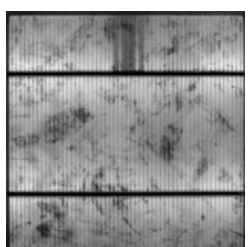
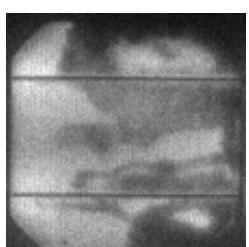
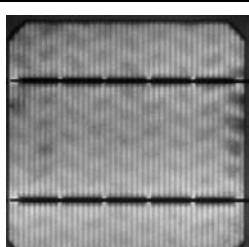
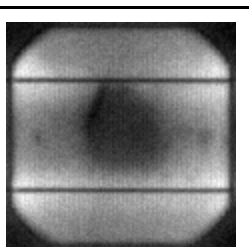
Using EL imaging, it is especially possible to detect cell cracks in photovoltaic modules. Cell cracks appear as dark lines on the solar cell in the EL image. Especially in multi crystalline solar cells, crystallographic defects typically also appear as dark lines. Therefore the detection of cell cracks by EL imaging has not been automated successfully yet. Hence, cell cracks are detected by a person with training in how to recognize cell cracks in photovoltaic cells and modules. A well trained person can detect cracks by looking at an EL image of a solar module. For recognition of cracks in PV modules made of multi crystalline wafers we define criteria to identify cell cracks:

1. A cell crack appears as a dark grey line in an EL image. The width and the greyscale should be mostly constant over the whole length of the crack.
2. A crack orientated in an angle of $+45^\circ$ to about $+5^\circ$ to the fingerprint of the solar cell should partly run parallel to the fingers of the solar cell so that the crack appears as a wavy step function.
3. Wafers that have been neighbours in the ingot may be found in a PV module. These wafers can be used to check whether a detected dark grey line is a defect structure of the silicon or a cell crack.
4. If the EL intensity changes abruptly at a dark grey line it is a cell crack. In this case the crack already reduces the conductivity of the metallisation across the crack.
5. It is quite unlikely to find a cell crack not starting or ending at the busbar or the edge of the cell except for cross cracks. Cross cracks are quite likely to be found in the middle of the cell.

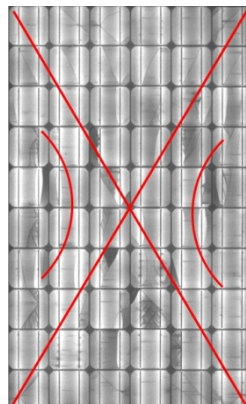
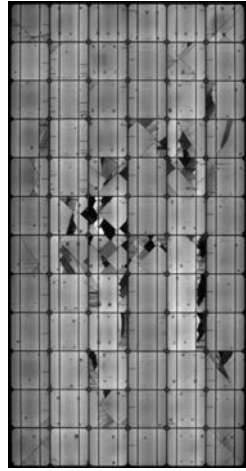
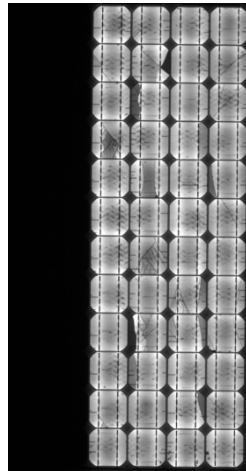
Tab. 5.4.1: List of failures being detectable by electroluminescent inspection. The failures are described in detail in the chapter referenced in column named “Chapter”. The code used in column “Safety” and “Power” is defined in Tab. 4.4.1 and 4.4.2.

Chapter	Description	Safety	Power	Image
	No module failure			
	Crystal dislocations in a multi crystalline wafer	A	A	

	Edge wafer	A	<u>A</u>	
	Striation rings	A	<u>A</u>	
	Cell failures			
6.2.2	Cracks in solar cell modus A. The cell has a crack but the crack does not influence the current flow over the crack (no crack resistance)	B	<u>C</u>	
6.2.2	Cracks in solar cell modus B+(A). The cell has a crack and the crack influences the current flow to the cell interconnect ribbon of the cell. However the cell is still connected.	B(f)	<u>C</u>	
6.2.2	Cracks in solar cell modus C+(B+A). The cell has a crack and the crack completely isolates cell part(s) from the cell interconnect ribbon. An EL image taken at about 1/10 of the rated current (upper image) of the PV module is more capable to reveal isolated cell parts as one taken at the rated current (lower image), compare lower left parts of the two images.	B(f)	<u>C</u>	

6.2.2	Cross crack line/cross crack	B(f)	A	
	Finger failure A, often identical finger interruptions on some cells in a PV module	A	A	
6.2.2	Finger failure B, finger interuptions along cell cracks.	B(f)	C	
	Finger failure C, also called gridfinger interruptions caused by soldering (GICS) [WENDT09]	B(f)	C	
7.6.1	Humidity corrosion	A	E	
	Contact forming failure A, temperature inhomogeneities of the transport belt during the firing process of the cell process lead to a tire like imprint	A	A	
	Contact forming failure B, temperature inhomogeneities during the firing process of the cell process lead to center edge gradient of contact resistance of the cell finger metalisation	A	A	

6.2.4	Shunt fault on solar cell	B(f)	A	
	Shunt fault due to cell interconnect	B(f)	A	
6.2.6	Disconnected cell interconnect	B(f)	A	
	Cell pattern in a PV module			
6.2.5	Potential induced degradation (PID). PID PV modules can be identified with EL images taken at 1/10 of the rated current in an early stage, before a power loss can be noticed. [Berger13]	A		
6.2.2	Repetitive induced cell cracks in the production	B(f)	C	

6.2.2	Heavy homogeneous mechanical load. The overall crack pattern in the module looks like a X-crack pattern. The X-crack pattern is visualized in the image by the red lines.	B(f)	C	
6.2.2	Tilt over PV module. Many dendritic like cracks are located mainly in the cells in the middle of the module.	B(f)	C	
6.2.7	Shunted by pass diode or break in current flow somewhere in the string.	B(f)	E	

References

[Berger13] K.A. Berger, B. Kubicek, G. Újvári, G. Eder, Y. Voronko, M. Weiss, G. Oreski, M. Knausz, T. Koch, J. Wassermann, *Innovative, non destructive methods for investigations of PV-modules* (in German: „Innovative, nichtzerstörende Methoden zur Untersuchung von Photovoltaikmodulen“), Proc. 28th Symposium Photovoltaische Solarenergie (OTI, Bad Staffelstein, Germany, 2013), Regensburg 2013, ISBN 978-3-943891-09-6

[Fuyuki05] T. Fuyuki, H. Kondo, T. Yamazaki, Y. Takahaschi, Y. Uraoka, Photographic surveying of minority carrier diffusion length in polycrystalline silicon solar cells by electroluminescence, *Applied Physics Letters* **86** (2005), p. 262108

5.5 UV fluorescence

The UV fluorescence (FL) of Ethylene Vinyl Acetate (EVA) was used for the first time to analyze the discolouration of photovoltaic (PV) modules by Pern et al. in 1997 [Pern97]. Due to exposure of EVA to sunlight, especially the UV spectrum, molecules in the encapsulation decompose to form lumophores. In the publication of Pern, a source of 315 nm UV light was used to excite the lumophores in the EVA which emit fluorescent light in the range of 325 nm to approx. 800 nm. A correlation between features in UV fluorescence images and cell cracks was recently presented [Schlothauer10]. Schlothauer et al. used EL images to identify the cell cracks in a cell of a PV module and correlate them with the UV fluorescence image. The fluorescent degradation product was found to change to a non fluorescent product along the edges of and the cracks in the solar cells, when they are oxidized by oxygen diffused through the back sheet to the EVA front layer of the module [Pern96]. This effect is called photobleaching and can be used to determine the number, position and orientation of cell cracks in PV modules, even in a dark outdoor environment.

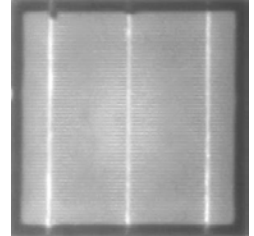
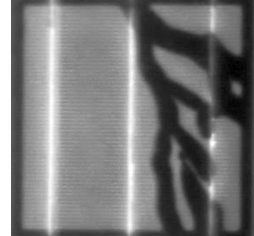
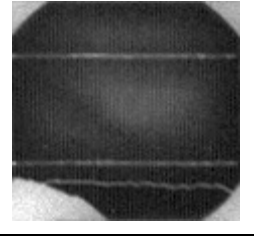
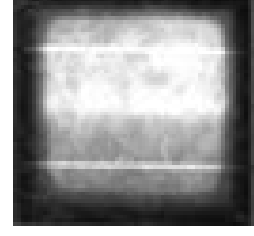
The species involved in the fluorescence which may indicate or facilitate material degradation may be examined using fluorescence spectroscopy [Silverstein91]. First an emission spectrum is obtained by monitoring the response to a particular excitation wavelength, such as 315 nm. Then an excitation spectrum is obtained by monitoring at a particular fluorescent wavelength and scanning the wavelength of the excitation signal. Examination may be iteratively repeated until each fluorescence peak is correlated with a corresponding excitation spectrum. The technique may be applied to hydrocarbon and silicone encapsulation [Pern93, Miller12]. However this technique needs direct access to the encapsulant because typically used front glasses or back sheets are intransparent for UV light below 350 nm. Therefore the PV module has to be destroyed for a full fluorescence spectroscopy analysis. In fluorescence spectroscopy and FL imaging, the intensity is proportional to the lumophore concentration and the wavelength is characteristic to the lumophore species.

For FL imaging, an array of black light sources may be used for excitation. The black light should emit light of wavelength ranging from 310 nm to 400 nm. Most of the photons with higher energy than 350 nm will be absorbed in the front glass of most modules and will not reach the lamination material. Photons with lower energy than 400 nm would make it more difficult to differentiate between excitation light and fluorescent emission. The source lamp used to illuminate a PV module typically has a light intensity at module surface of approx. 10-100 W/m². The encapsulation material fluoresces in the wavelength interval from 400 nm to approx. 800 nm [Pern97, King00, Schlothauer10]. A long pass filter in front of the camera objective lens can be used to block the excitation light of the black light from entering the camera. A typical exposure time for the FL image is in the order of 10 s.

The PV module has to be exposed to sunlight for some time to develop lumophore species capable of emitting a sufficient signal from the UV fluorescence. Typically, the longer the exposure to UV light is the more intensive the fluorescent emission will be. To get a sufficient fluorescence signal, the module should have been exposed to an UV dose of approx. 80 kWh/m², e.g. this correlates to about 1.5 year outdoor exposure in Germany. Table 5.5.1 summarizes all effects being detectable with the FL method.

Using FL imaging, it is especially possible to detect cell cracks in cells of photovoltaic modules [Koentges12]. Cell cracks appear as a dark bar on the solar cell in the FL image. A cell crack is much easier to be identified than in an EL image. Due to the bleaching at the frame of regular cells, cracks at the cell edge are not detectable. Furthermore FL images show sometimes along the interconnector grey zones. In this case cell cracks near the interconnector are difficult to identify.

Tab. 5.5.1: List of failures being detectable by FL inspection. The failures are described in detail in the chapter referenced in column named “Chapter”. The code used in column “Safety” and “Power” is explained in chapter 4.3 and 4.4.

Chapter	Description	Safety	Power	Image
	No failure	A	A	
6.2.2	Cell cracks	B(f)	C	
6.2.2	Isolated cell part, reverse biasing of the not isolated cell part increases fluorescence	B(f)	C	
6.2.6	Disconnected cell interconnect. The current flows only through one cell interconnect ribbon and heats one cell side more intensely than the other and therefore creates more lumophores.	B(f)	A	

References

- [King00] D. L. King, M.A. Quintana, J.A. Kratochvil, D.E. Ellibee and B.R. Hansen, Photovoltaic module performance and durability following long-term field exposure, *Progress in Photovoltaics: Research and Applications* **8** (2000), pp. 241-256 doi: 10.1002
- [Koentges12] M. Köntges, S. Kajari-Schröder, I. Kunze, Cell cracks measured by UV fluorescence in the field, Proc. 27th EUPVSEC (WIP, Frankfurth, Germany, 2012), pp. 3033-3040
- [Miller12] D. C. Miller, M. T. Muller, M. D. Kempe, K. Araki, C.I E. Kennedy, S. R. Kurtz, Durability of Polymeric Encapsulation Materials for Concentrating Photovoltaic Systems, *Progress in Photovoltaics: Research and Applications* **21**(4) (2012) doi: 10.1002/pip.1241
- [Pern93] F. J. Pern, Luminescence and absorption characterization of ethylene-vinyl acetate encapsulant for PV modules before and after weathering degradation, *Polym. Deg. Stab.* **41** (1993), pp. 125-139
- [Pern96] F.J. Pern, Factors that affect the EVA encapsulant discoloration rate upon accelerated exposure, *Solar Energy Materials and Solar Cells* **41-42** (1996), pp. 587-615
- [Pern97] F.J. Pern, S.H. Glick, Improved Photostability of NREL Developed EVA Pottant Formulations for PV Module Encapsulation, Proc. 26th IEEE PVSC, (IEEE, Anaheim, USA, 1997)
- [Schlothauer10] J. Schlothauer, S. Jungwirth, B. Röder, M. Köhl, „Flourescence imaging- a powerful tool for the investigation of polymer degradation in PV modules”, *Photovoltaics International* **10** (2010), pp. 149-154
- [Silverstein91] R .M. Silverstein, G. C. Bassler, T. C. Morrill, Spectrometric Identification of Organic Compounds: Fifth Edition. John Wiley and Sons Inc.: New York, 1991, Chapter 7: ultraviolet spectrometry

5.6 Signal transmission method

Originally the Signal Transmission Device (STD) [Kato10] is not designed for detecting PV module failure but for maintenance in the field of electric work such as detection of earth-leakage points and wired routes in walls.

Applying this STD to a PV system, especially to the dc circuit of a PV array, makes it possible to detect local disconnection of interconnect ribbons in PV modules and open-circuit failure of bypass diodes (BPD) in junction boxes.

Fig. 5.6.1 shows the appearance of a STD, which is small, lightweight, and inexpensive. It consists of two parts: a transmitter and a receiver. The transmitter sends small alternating test signal current into a connected circuit and the receiver can detect magnetic flux generated by this test signal current.



Fig. 5.6.1: An example of the Signal Transmission Device (STD).

Fig. 5.6.2 depicts a schematic procedure for detecting local disconnection of interconnect ribbons in PV modules. At first one must stop the PV system operation. Next the transmitter is connected to a target module string at the PV combiner box and the test signal current automatically starts to be transmitted to the module string. The dotted light blue lines in Fig. 5.6.2 visualise the test signal path. Subsequently the receiver is moved along the interconnect ribbons on the rear or front side of each PV module. When the cell interconnect ribbons are both connected to the solar cells the receiver detects the test signal. But it cannot detect the signal current on a disconnected point of the cell interconnect ribbon indicated as "A" in Fig. 5.6.2. If all (typically two or three) cell interconnect ribbons of one cell are disconnected, indicated as "B" in Fig. 5.6.2, no signal can be detected anywhere on the disconnected sub-module because the signal passes through the bypass diode integrated in the disconnected sub-module.

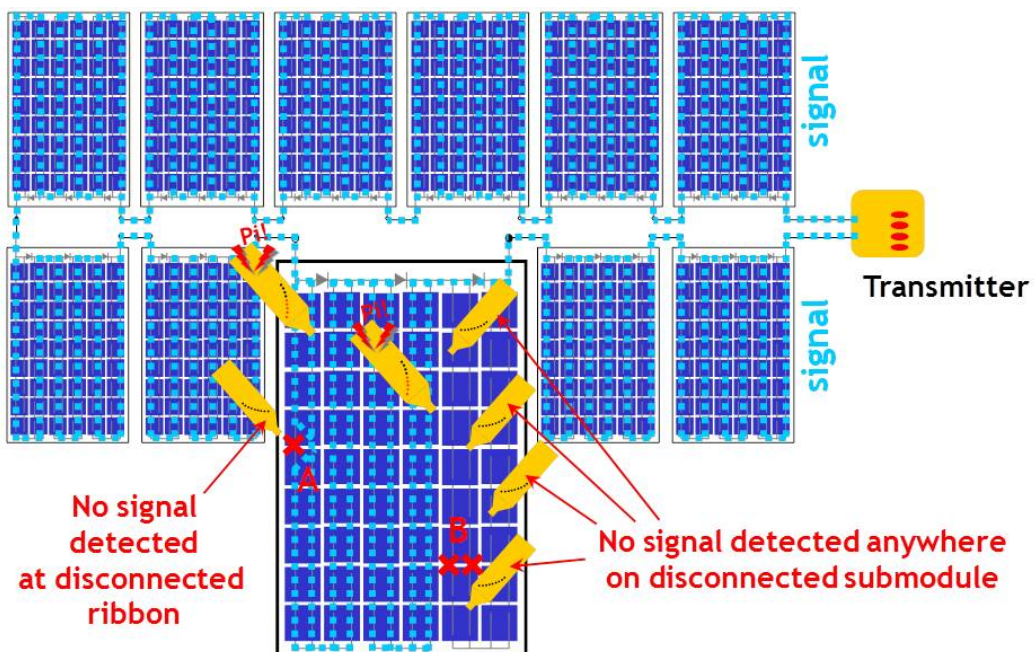


Fig. 5.6.2: A schematic procedure for detecting local disconnection of interconnect ribbons in PV modules.

Figure 5.6.3 depicts a schematic procedure for detecting bypass diode failures in PV modules. In order to check the bypass diode failure, especially open-circuit failure, e.g. a rubber sheet is used to block the sunlight on sub-module in addition to the STD.

As outlined above, the PV system must stop operation first. After connecting the transmitter to the module string, the rubber sheet is layed on one sub-module to activate the bypass diode. Subsequent the receiver is moved along the interconnect ribbons on the rear side of the PV module.

If the bypass diode is activated, indicated as "C" in Fig. 5.6.3, due to partial shading by the rubber sheet, no signal current is detected on the sub-module because it goes through the bypass diode. In case of an open-circuit bypass diode, one can detect the test signal on the sub-module, indicated as "D" in Fig. 5.6.3, even if the sub-module is shaded.

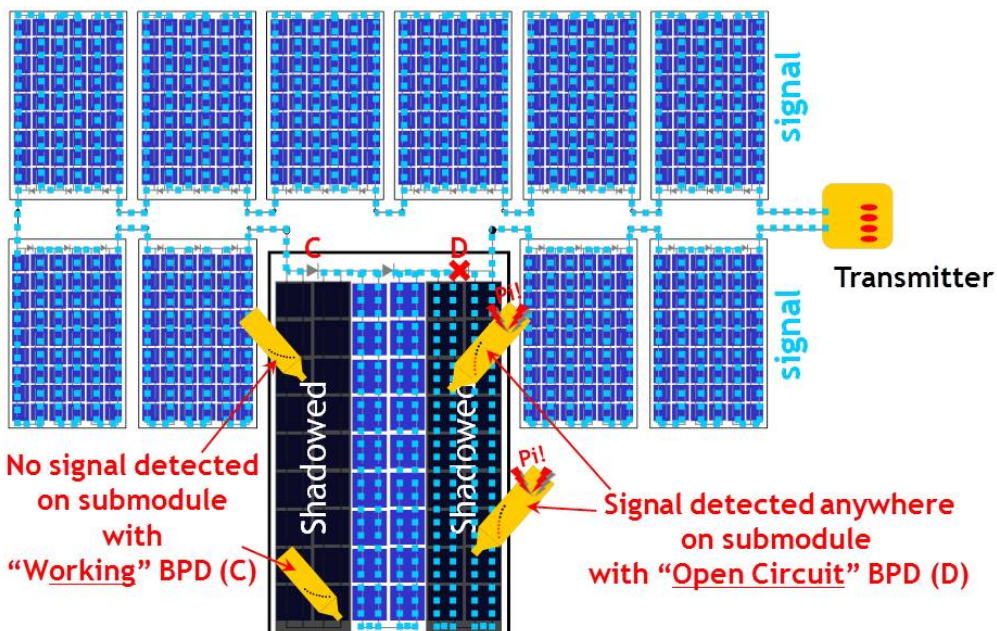


Fig. 5.6.3: A schematic procedure for detecting open-circuit bypass diode failures in PV modules.

Fig. 5.6.4 is an example of the STD detection of disconnected cell interconnect ribbons in a working PV module. An EL image indicates that two solar cells have disconnected cell interconnect ribbons on the left half of them. The STD detection easily indicates these disconnections of the left-side interconnect ribbons. Table 5.6.1 shows a summary of all failures which are detectable by the STD method.

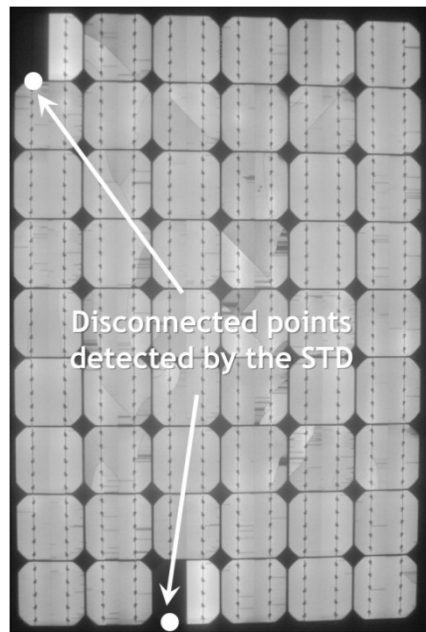
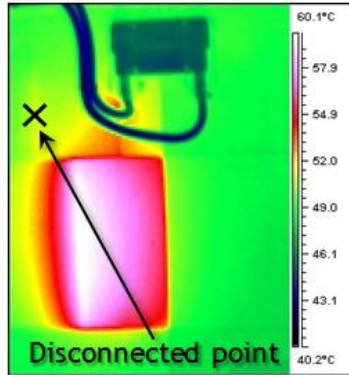
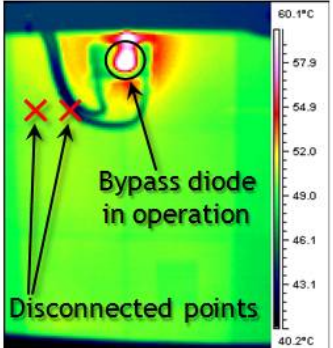


Fig. 5.6.4: The detection results of the STD detected at a working PV module are inserted into the EL image of the PV module. The EL image indicates that two solar cells, on which finger grids are separated for the two cell halves, have disconnected cell interconnect ribbons on the left half of them. Both results completely match.

Most EL observations must be indoors and are expensive, but the STD has the advantages that it is a cheap and easily applicable method in the field without removing PV modules.

Tab. 5.6.1: List of failures being detectable by STD inspection. The failures are described in detail in the chapter referenced in column named “chapter”. The code used in column “Safety” and “Power” is explained in chapter 4.3 and 4.4.

Chapter	Description	Safety	Power	Image
5.3.8	One disconnected cell interconnect ribbon: No signal detected at the disconnected ribbon.	B(f)	C	
5.3.8	All cell interconnect ribbons of one cell are disconnected or disconnected string interconnect: No signal detected anywhere on the disconnected submodule.	B(f)	E	
5.3.9	Open-circuit bypass diode: Signal detected anywhere on the shaded submodule.	C(f)	A	no image available

References

[Kato10] K. Kato, Taiyoko Hatsuden Sisutem no Fuguai Jirei Fairu, p.38-40 published from Nikkan Kogyo Shimbun, 2010 (in Japanese)

6 Failures of PV modules

PV modules fail for a wide variety of reasons. Failures related to how the module is connected to the PV system and common packaging failures are common to all modules. These are indicated in the Tab. 6.0.1 in the general category. Some defects are observed only in some module types; these are indicated in the table for each technology. Some of the defects are not even caused by the module but by external sources or intrinsic effects which are already taken into account by the manufacturer by printing the module label. These lists are not prioritized, nor are all

possible failure mechanisms included. More details are provided in the following sections.

Tab 6.0.1: Known and anticipated failure modes and degradation mechanisms for each PV technology.

Known and anticipated failure modes & degradation mechanisms	Chapter references
General	
Quick connector reliability	4.3.3
Delamination	6.1.1
Glass breakage	4.3.1, 6.1.4, 6.4.1, 7.2
Junction box failure	6.1.3
Wafer-based silicon modules	
Cell cracks	6.2.2, 6.2.3, 7.1, 7.2
Delamination	6.1.1
EVA discolouration	6.2.1, 6.2.3, 7.3
Burn marks	6.2.4
Potential induced degradation	6.2.5, 7.5
Fatigue of ribbon due to thermal cycling	6.2.6
Bypass diode failure	6.2.7
Junction box failure	6.1.3
Light-induced cell degradation	4.2
Thin-film Si	
Initial light degradation (a-Si)	4.2
Annealing instabilities (a-Si)	4.2
Shunt hot spots	6.3.2
Thin-film CdTe	
Cell layer integrity – backcontact stability	6.4.2
Busbar failure - mechanical (adhesion) and electrical	6.3.1
Shunt hot spots	6.3.2
Thin-film CIGS	
Shunt hot spots	6.3.2

6.1 Review of failures found in all PV modules

In the following chapters PV module failures are described which can be found in nearly all PV module types. The most similar part of all different kinds of modules is the laminate. Therefore laminate failures are discussed here in a general way.

6.1.1 Delamination

The adhesion between the glass, encapsulant, active layers, and back layers can be compromised for many reasons. Thin-film and other types of PV technology may also contain a transparent conductive oxide (TCO) or similar layer that may delaminate from an adjacent glass layer [Jansen03]. Typically, if the adhesion is compromised because of contamination (e.g. improper cleaning of the glass) or environmental factors, delamination will occur, followed by moisture ingress and corrosion. Delamination at interfaces within the optical path will result in optical reflection (e.g., up to 4%, power loss D and safety class A, at a single air/polymer interface) and subsequent loss of current (power) from the modules.

Delamination may be relatively easy to see, as shown in Tab. 5.1.3. In theory, the detachment of interfaces might be quantified using a reflectometer. Pulse and lock-in thermography, as described in chapter 5.3.2 and 5.3.3, may be used to detect delaminations that cannot be identified visually. X-Ray tomography and an ultrasonic scanner may also be used to examine less overt delaminations in higher resolution, but both require a greater examination time [Veldmann11].

In EVA encapsulation, the adhesion promoter (intended for glass interfaces) is generally the least stable additive, limiting the shelf-life of the EVA even more so than the peroxide used for cross-linking. Factors affecting the durability of the interfaces within a PV module may include UV, temperature, and/or moisture. For example, the delamination of Polyethylene Terephthalate (PET) containing backsheet is known to be affected by the hydrolysis of PET [McMahon59], which limits its ability to be examined in accelerated testing using the “damp-heat” test condition. Delamination may be more likely at the interface between EVA and the solar cell, because the interfacial strength may initially be more limited there than at the EVA/glass interface. On the other hand, UV degradation and subsequent embrittlement, may limit the long-term adhesion of interfaces exposed to the sun.

The new pathways and subsequent corrosion following after delamination reduce module performance, but do not automatically pose a safety issue. The delamination of the back sheet, however, may enable the possibility of exposure to active electrical components. The delamination of the backsheet may also result in an isolation fault (safety class C(e)). Failure of the rail bond may free a module from its mounting system, posing a hazard to personnel or property within the installation site. The detachment of the junction-box may also allow for exposure to active electrical components in addition to the possibility of electrical arcing. A few instances of arc-initiated fires have been reported from PV installation sites.

The adhesive strength of encapsulation/glass and encapsulation/cell interfaces are most commonly examined using double cantilever beam (DCB) [ISO25217] measurements, compressive shear tests [Chapuis12], or overlap shear tests [Kempe09]. The advantage of a fracture mechanics-based approach like DCB is that adhesion (and its degradation) can be related to its underlying fundamental principles. The adhesive strength of a flexible front sheet or back sheet may be measured with a 180° peel test [ISO8510].

6.1.2 Back sheet adhesion loss

The back-sheet of a module serves to both protect electronic components from direct exposure to the environment and to provide safe operation in the presence of high DC voltages. Back-sheets may be composed of glass, or polymers, and may incorporate a metal foil. Most commonly, a back-sheet is made up of a laminate structure with a highly stable and UV resistant polymer, often a fluoropolymer on the outside, directly exposed to the environment, an inner layer of PET, followed by the encapsulant layer. Recently new designs have been implemented which (amongst other materials) may use a single layer of PET, formulated for UV and thermal stability. The choice of material depends on cost, what sort of mechanical strength is needed, the need for electrical isolation, and whether or not water vapor must be excluded from the package.

When a rear glass is used instead of a back-sheet, it may fail by breaking. This can happen because of improper mounting, impact from hail, impact from windblown objects, or any other type of mechanical stress. If the module is constructed as a thin-film device on the backsheet (e.g. substrate CIGS), then this presents a significant safety hazard in addition to significant or, more likely, complete power loss for that module. Along the cracks there may be a small gap and some voltage which is capable of producing and sustaining an electric arc. If this happens in conjunction with failure of a bypass diode, the entire system voltage could be present across the gap creating a large and sustained arc which is likely to melt glass possibly starting a fire. However, if a glass backsheet were to break in a typical crystalline Si module, there would still be a layer of encapsulant to provide a small measure of electrical isolation.

When a module is constructed with glass front- and back-sheets, there may be additional stresses enhancing delamination and/or glass breakage. Without proper control of lamination, excess encapsulant may be pushed out from the sides of the module causing the glass to bend slightly. This results in the presence of significant tensile stress in the encapsulant at the edge of the module which will then have a higher propensity to delaminate. Similarly, tempered glass is not perfectly flat and the presence of structure with the cell materials will lead to further residual mechanical stresses. All these stresses act to increase the probability of delamination and glass breakage both of which may lead to serious performance and safety concerns.

Backsheet materials may also be constructed with a metal foil in a polymeric laminate structure to provide a moisture impermeable structure that is lightweight, and potentially flexible. This construction produces a number of additional safety

concerns. Here there is the need to provide a more robust electrical insulation layer between the cells and the metal foil. Any small breach in electrical isolation over the entire surface of the foil will result in the entire foil being charged at system voltage. Thus there is a larger area over which one must be concerned with electrical insulation. Furthermore, a metal foil will act as a high voltage capacitor with the cells serving as one of the electrodes. Because of these specific safety concerns, the IEC standards community is currently drafting language into IEC 61730 [IEC61730] to address this concern.

Lastly, but most commonly, modules are laminated with a polymeric laminate backsheet construction, as in typical crystalline Si modules. With multiple layers, there are a number of interfaces which may delaminate in response to heat, thermal cycling, mechanical stress, humidity, UV light, or other physical or chemical stresses. If delamination occurs forming bubbles (as seen in Tab. 5.1.3) in a central, open area of the back, it will not present an immediate safety issue. That area would likely operate slightly hotter as heat does not conduct out the back as well, but as long as the bubble is not further disturbed and broken or expanded, the performance and safety concerns are minimal.

However, if delamination of the backsheet occurs near a junction box, or near the edge of a module there would be more serious safety concerns. Delamination at the edge may provide a direct pathway for liquid water to enter a module during a rainstorm, or in response to the presence of dew. That can provide a direct electrical pathway to ground creating a very serious safety concern. Similarly, delamination near a junction box can cause it to become loose, putting mechanical stress on live components and breaking them. A break here is more likely to cause failure of the connection to a bypass diode and possibly result in an unmitigated arc at full system voltage.

If the module is not correctly formulated for adhesion, the cell surfaces are not properly prepared (e.g. residual flux), the foil parts of the backsheet are not well adhered or are sensitive to UV, or if gas forms inside of the module because of too much flux from soldering or vaporization of water in the EVA, the back encapsulant sheet may not be well adhered and bubbles may form on cell surfaces. During periods of high humidity, especially when dew forms on the module because of radiative cooling at night, water droplets may form within the bubbles. Liquid water, especially when combined with high voltage, may cause significant and irreversible damage to cell components. This type of degradation can quickly make a module unsafe and/or inoperable.

There are many different forms and compositions of backsheet materials. Each of these has a unique set of potential failure modes which must be considered when designing a PV module package.

6.1.3 Junction box failure

The junction box (JB) is the container fixed on the backside of the module which protects the connection of cell strings of the modules to the external terminals. Generally the junction box contains the bypass diodes to protect the cells in a string in case of hot spot or shadowing. Observed failures in the field are:

- a) Poor fixing of the junction box to the backsheet. Some adhesive systems are good for short-term pull but poor for long term adhesion [WOL10].
- b) Opened or badly closed j-boxes due to poor manufacturing process.
- c) Moisture ingress which cause corrosion of the connections and the string interconnects in the junction box
- d) Bad wiring causing internal arcing in the j-box. This failure is particularly dangerous because the arcing can initiate fire.

Not reliable soldering contacts of the string interconnects could cause high a resistance and consequent heating in the junction box. In extreme cases the fire danger increases. These bad soldering contacts are caused by low soldering temperature or chemical residuals of the previous production process on the solder joints.



Fig. 6.1.3: Junction box failures: Left photo shows an open junction box in the field, the middle one a poorly bonded JB on the backsheet, and the right one a JB with poor wiring.

6.1.4 Frame breakage

Many PV modules have been designed and applied for heavy snow load regions. To test and certify the PV modules for the heavy snow load reagions the snow load test of the IEC 61215 [IEC61215] was used. Regarding real snow load characteristics, the mechanical load test cannot apply extraordinary stress to the framing section at the lower part of a module at an inclined exposure. Snow loads creep downhill and intrude into the potential space between the frame edge and top surface. The ice formed by compression of the lower snow areas pushes against the exposed tip of the frame.

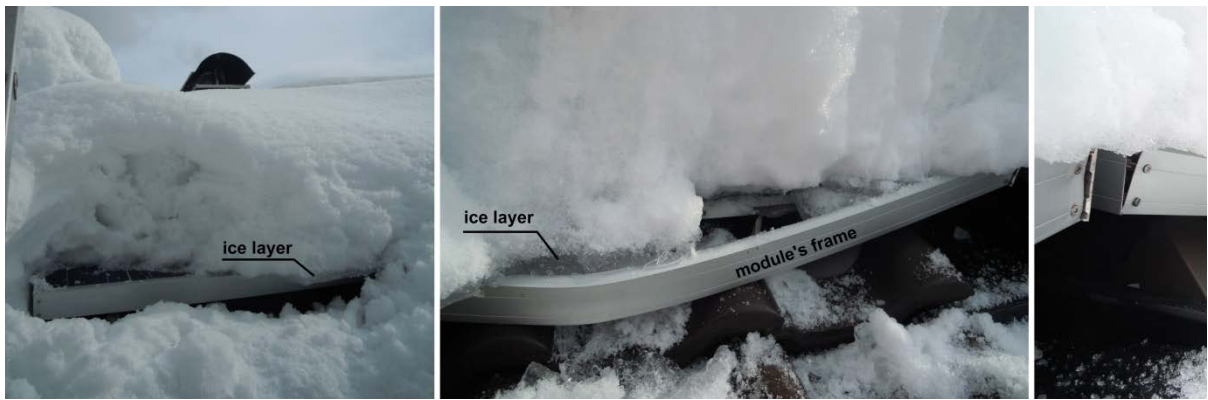


Figure 6.1.4: Damaged module frames after heavy snow load of 1.2 m, melted down to 35 cm, in winter 2012. Alpine location at 620 m a.s.l., tilt angle 25°. 60 cell modules with dimensions 1660 mm x 990 mm, 50 mm Al-frame.

Left hand side: Ice layer slides over module's edge;

Middle: Ice bends frame; Right: Failure of the corner screw joints [Leitner12].

The inclined surface or top of the module simply allows the snow to shift the load to the lower parts of the module, which also induces a torque at the clamped spots. This behaviour is amplified by a higher gravitational force compared with the centre or top of the module. Figure 6.1.5 illustrates this relationship, while simplifying the difference between horizontally and vertically long-term snow impacts.

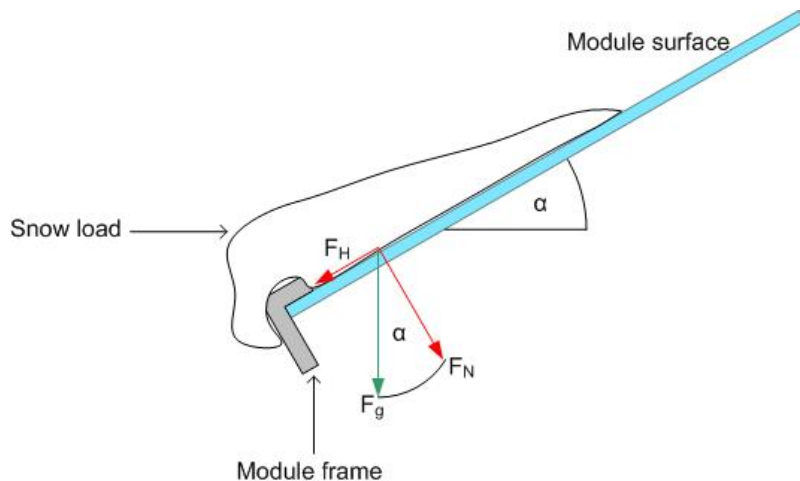


Figure 6.1.5: Introduction of snow loads, difference between load vectors.

As a function of the inclination angle, the downhill force increases the stress to the bottom of the module, potentially resulting in a lack of resistance for maintaining the structural integrity of the glass. This kind of deformation has been observed in the field, with subsequent damage to the superstrate. If the frame is detached from the glass the PV module is destroyed and must be exchanged.

In general, snow loads on PV modules can be summarized in terms of mainly four characteristics, which are used to develop a new test method described in chapter 7.2:

- Vertical loads acting on an inclined surface break down into two component-related forces: the normal force F_N and the downhill force F_H . The force F_R is the friction between the snow and glass and counteracts F_H .
- Snow sliding down the surface is inhomogeneously distributed on the surface of the module.
- Inhomogeneous loads cause moments and torques in the lower part of the module along the axial direction of the test specimen. The lower module clamps are subject to large moments.
- Low temperatures ($<0^\circ\text{C}$) may cause embrittlement of the adhesives and further reduce stability. Creeping may occur at higher temperatures.

References

- [IEC61730-1] International Electrotechnical Commission (IEC) 61730-1: Photovoltaic (PV) module safety qualification - Part 1: Requirements for construction, 2004-10-14
- [ISO25217] ISO 25217:2009 Adhesives -- Determination of the mode 1 adhesive fracture energy of structural adhesive joints using double cantilever beam and tapered double cantilever beam specimens, International Electrotechnical Commission: Geneva, 1–24 (2009)
- [ISO8510] ISO 8510-2:2006 Adhesives -- Peel test for a flexible-bonded-to-rigid test specimen assembly -- Part 2: 180 degree peel, International Electrotechnical Commission: Geneva, 1–6 (2006)
- [Chapuis12] V. Chapuis, S. Pélisset, M. Raeis-Barnéoud, H.-Y. Li, C. Ballif, L.-E. Perret-Aebi, Compressive-Shear Adhesion Characterization of PVB and EVA at Different Curing Times Before and After Exposure to Damp-Heat Conditions, *Prog. Photovolt: Res. Appl.* (2012), doi: 10.1002/pip.2270
- [Jansen03] K. W. Jansen, A. E. Delahoy, A Laboratory Technique for the Evaluation of Electrochemical Transparent Conductive Oxide Delamination from Glass Substrates, *Thin Solid Films* **423** (2003), pp. 153–160
- [Kempe09] M.D. Kempe, M. Kilkenny, T.J. Moriconi, Accelerated stress testing of hydrocarbon based encapsulants for medium-concentration CPV applications, Proc. IEEE PVSC (IEEE, Philadelphia, PA, USA, 2009), pp. 001826–001831
- [Leitinger12] Pictures submitted by M. Leitinger
- [McMahon59] W. McMahon, H.A. Birdsall, G.R. Johnson, C.T. Camilli, Degradation Studies of Polyethylene Terephthalate, *J. Chem. Eng. Data* **4** (1), (1959), pp. 57-79
- [Veldmann11] D. Veldman, I. J. Bennett, B. Brockholz, and P. C. de Jong, Non-Destructive Testing of Crystalline Silicon Photovoltaic Back-Contact Modules, Proc. 37th IEEE PVSC (IEEE, Seattle, USA, 2011), pp. 3237 - 3240
- [WOL10] J. Wohlgemuth, D.W. Cunningham, A. Nguyen, G. Kelly, D. Amin, Failure Modes of Crystalline Si Modules, PV Module Reliability Workshop 2010 (NREL, Golden, USA, 2010)

6.2 Review of failures found in silicon wafer-based PV modules

The most common PV modules are made of wafer-based silicon solar cells. Therefore a large knowledge base has been accumulated for the most PV module failures of this type. However even for this type of PV modules some effects like potential induced degradation and snail tracks have been studied in detail in the last 3 years for the first time. Therefore their description shows the current state and is not a final presentation. Even the other module failure descriptions arise from older PV modules which may differentiate them from current module and material designs.

6.2.1 EVA discolouration

One of the most overt degradation mechanisms for PV modules is the discolouration of the ethylene vinyl acetate (EVA) or other encapsulation materials. This type of degradation is predominantly considered to be an aesthetic issue. Discolouration may become apparent to an observer before module current (therefore power production) can be confirmed to decrease, but EVA discolouration is expected to contribute < 0.5%/a of the ~0.8%/a degradation that is commonly seen for Si modules [Jordan11]. Examples of the discolouration of EVA are shown in Tab. 5.1.3.

EVA is usually formulated with additives, including UV and thermal stabilizers. But if the choice of additives and/or their concentrations are inadequate, the EVA may discolor as shown in Tab. 5.1.3. To explain, interaction between incompatible additives in the field may produce discolouring chromophore species [Holley98] or the depletion of additives (such as the UV absorber) over time [Shioda11] may render the EVA vulnerable to damage. The patterns of discolouration observed in the field can be very complex because of the diffusion of oxygen or the products of reaction, such as acetic acid [Pern97], generated when heat and UV light interact with EVA. The presence of oxygen photobleach chromophores, creating a ring of transparent EVA where no discolouring chromophore species are present, around the perimeter of a wafer-based cell. It is quite common to see symmetric patterns and sometimes multiple rings based on the effects of limited chemical diffusion, both into and out of EVA and the existence of multiple chemical pathways that produce similar chromophore species. A photo in Tab. 5.1.3 shows an example where a single cell is far darker than any of the adjacent cells. This typically implies that the most discolored cell was at higher temperature than the surrounding cells, perhaps because of a lower photocurrent of the cell compared to the other cells in the module or the cell being located above the junction box.

Unless discolouration is very severe and localized at a single cell, where it could cause a substring bypass-diode to turn on, the discolouration of EVA does not present any safety issues (safety class A). While it is uncommon for EVA discolouration to induce other failures within the cell, discolouration may correlate to: significant thermal history (high temperature in the field), the generation of acetic acid [Pern98] and concomitant corrosion [Weber12], and the embrittlement of the EVA [Dhere98].

There is some evidence that discolouration of EVA may be a contributor to the slow degradation that is seen in the majority of silicon modules. The median degradation rate of ~0.5%/a was reported for a summary of ~1800 studies of silicon module degradation [Jordan11]. This degradation was found to be dominated by loss of short-circuit current. Of these, ~60% reported observation of discolouration. A total loss of ~10% in the module performance appears as a severe discolouration, implying that EVA discolouration is unlikely to account for the full decrease in performance observed for the majority of silicon modules. To conclude, the EVA discolouration is classified into the power loss category $D(t,uv)$ with a slow saturating time dependence depending on UV radiation and temperature.

References

- [Dhere98] N. G. Dhere, K. S. Gadre, Tensile Testing of EVA in PV Modules. Proc. Int. Solar Energy Conf. Solar Engineering 1998, ASME 1998, Albuquerque, NM, (1998), pp. 491-497
- [Jordan11] D.C. Jordan, S.R. Kurtz, Photovoltaic Degradation Rates—an Analytical Review, *Prog. Photovolt: Res. Appl.* (2011) doi: 10.1002/pip.1182
- [Jordan12] D.C. Jordan, J.H. Wohlgemuth, S.R. Kurtz, Technology and Climate Trends in PV Module Degradation, 27th EUPVSEC (WIP, Frankfuth, Germany, 2012), pp. 3118-3124 (<http://www.nrel.gov/docs/fy13osti/56690.pdf>)
- [Holley98] W. W. Holley, Agro SC, Advanced EVA-based encapsulants: final report, NREL/SR-520-25296 (1998)
- [Pern97] F.J. Pern, Ethylene-vinyl acetate (EVA) encapsulants for photovoltaic modules: degradation and discoloration mechanisms and formulation modification for improved photostability, *Angew. Makromol. Chem.* **252** (1997), pp. 195-216.
- [Shioda11] T. Shioda, UV-accelerated test based on analysis of field-exposed PV modules, *Proc. SPIE* 8112, Reliability of Photovoltaic Cells, Modules, Components, and Systems IV, 81120I (San Diego, California, USA, 2011); doi:10.1117/12.894597
- [Weber12] U. Weber, R. Eiden, C. Strubel, T. Soegding, M. Heiss, P. Zachmann, K. Nattermann, H. Engelmann, A. Dethlefsen, No. Lenck, Acetic Acid Production, Migration and Corrosion Effects In Ethylene-Vinylacetate-(EVA-) Based PV Modules", Proc. of 27th EUPVSEC, (WIP, Frankfurth, Germany, 2012) pp. 2992-2995

6.2.2 Cell cracks

Photovoltaic cells are made of silicon. This makes photovoltaic cells very brittle. Cell cracks are cracks in the silicon substrate of the photovoltaic cells that often cannot be seen by the naked eye. Cell cracks can form in different lengths and orientation in a solar cell. In the manufacturing process for solar modules a number of photovoltaic cells are embedded into a solar module. In today's PV modules most often 60 photovoltaic cells are built in per module. In the following the number of cell cracks considered to be normal and what this means in terms of expected cell crack rate for the product are discussed. The wafer slicing, cell production [Pingel09], stringing and the embedding process during the production of the solar cell and module

causes cell cracks in the photovoltaic cells. Intrinsic manufacturing process variation causes cell cracks during solar module manufacturing. Especially the stringing process of the solar cells has a high risk for introducing cell cracks to the cells [Gabor06]. After finishing the production, a great source for cell cracks is the packaging/transport and reloading of PV modules [Reil10]. At last the installation of PV modules is a great source for cell cracking if the module e.g. drops or someone steps on the module [Olschok12]. A mean cracking distribution over all modules from various manufactures analysed at the ISFH and TÜV Rheinland is shown in Fig. 6.2.1 [Koentges11]. However all these cell cracking is not necessarily a module failure, because the reason for the failure is an external source, see Chapter 4.3.2.

But there are also cell cracks introduced during production. These are discussed in the following. For each production line under constant conditions it is possible to specify the probability p to have a cell crack in a solar cell. If one takes $n=60$ cells of the produced cells to make a PV module, the probability p_k to have a certain number k of cells with cell cracks in the PV module is given by the binomial distribution:

$$p_k = \binom{p}{k} \cdot (1 - p)^{(n-k)} \quad (6.2.1)$$

In other words Eq. (6.2.1) gives the probability (p_k) for a PV module (with n cells) to have k cracked cells if one knows the probability (p) of cell cracks during production. Therefore the best way to assess a quality criterion for PV modules is to use the binomial distribution to describe the number of cracks per module directly after production. An example for a distribution of cell cracks in production is given in Fig. 6.2.1. The binomial distribution describes this production-caused cell crack distribution well.

There are three different sources of cell cracks during production; each has its own occurrence probability p :

1. Cracks starting from the cell interconnect ribbon are caused by the residual stress induced by the soldering process. These cracks are frequently located at the end or starting-point of the connector, because there is the highest residual stress [Sander11]. This crack type is the most frequent.
2. The so called cross crack, which is caused by needles pressing on the wafer during production.
3. Cracks starting from the edge of the cell are caused by bouncing the cell against a hard object.

Once cell cracks are present in a solar module, there is an increased risk that during operation of the solar module short cell cracks can develop into longer and wider cracks. This is because of mechanical stress [Kajari11] caused by wind or snow load and thermo mechanical stress [Sander11] on the solar modules due to temperature variations caused by passing clouds and variations in weather.

Furthermore there are some typical crack patterns in a PV module detectable by electroluminescence imaging which can be assigned to a certain cause. Examples of these crack patterns are shown in Tab. 5.4.1. A repetitive crack pattern which appearance is turned by 180° from one string to the neighbour string is caused by a production failure (typically caused by the stringer) before the lamination of the PV module. This repetitive crack pattern can not be created after the lamination.

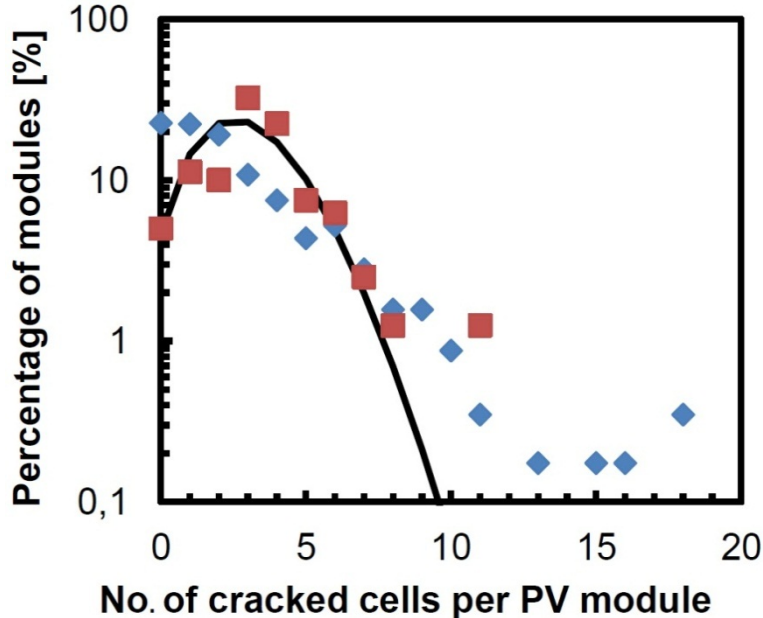


Fig. 6.2.1: Logarithmic histogram of 60 cell PV modules showing a specific number of cracks per PV module. The red squares show the crack distribution of PV modules (#80) directly after production from one manufacturer. The blue diamonds show the crack distribution (#574) of PV modules found in the field [Koentges2012]. The straight line depicts the binomial distribution of equation (6.2.1) for $p=5\%$.

Cracks beyond the cell interconnect ribbons appear as a finger failure type C, compare Tab. 5.4.1. This failure type typically indicates a high strain at the solder joint. PV modules with this kind of failure typically show more of this failure after thermomechanical stress and lead e.g. to a higher power loss in the TC200 test than PV modules without this failure type [Wendt09].

PV modules showing dendritic like solar cell crack patterns have been exposed to a heavy mechanical load [Koentges11] or a high acceleration. Typical reasons for the heavy mechanical loads are wrong packaging during transport, dropping of a PV module parallel to the ground, tilting over of a PV module or very heavy snow load. This crack pattern indicates that the crack has occurred after the lamination process. A cell with a dendritic crack pattern is not possible to be machined in a production line. In our experience PV modules with a dendritic crack pattern in the cells show higher power loss in humidity freeze tests than modules with other crack patterns.

Depending on the crack pattern of the larger cracks, the thermal, mechanical stress, and humidity may lead to “dead” or “inactive” cell parts that cause a loss of power output from the affected photovoltaic cell. A dead or inactive cell part means that this particular part of the photovoltaic cell no longer contributes to the total power output of the solar module. When this dead or inactive part of the photovoltaic cell is greater than 8% of the total cell area, it will lead to a power loss roughly linearly increasing with the inactive cell area [Koentges10]. This rule holds for PV modules with 230 Wp with 60 cells, 156 mm edge length, and 3 bypass diodes. Finally an inactive area of 50% or more will lead to a power loss of one third of the solar module power as the bypass diode is activated and shortcuts this part of the solar module. This happens because of the failure of one cell in one of the three sub strings in the solar module.

For PV module strings, the power loss is much more dramatically depending on the inactive area. The dependency between inactive cell area and power loss is compared in Fig. 6.2.2 for a single PV module and a string of 20 PV modules simulated for PV modules [Koentges08]. The Fig. 6.2.2 shows, that for a high but typical string length of solar modules the power loss due to inactive cell areas raises much steeper at 8% inactive cell area than it does for a single PV module. Therefore an inactive cell area of more than 8% is not acceptable. Besides the risk of power loss there is a chance of hot spots due to inactive cell parts greater than 8%. This happens if the cracked cell has a localised reverse current path in the still active cell part. Due to the missing cell area the cell is driven into reverse bias and the full current can flow along the localised path. This may cause hot spots and therewith burn marks (chapter 6.2.4).

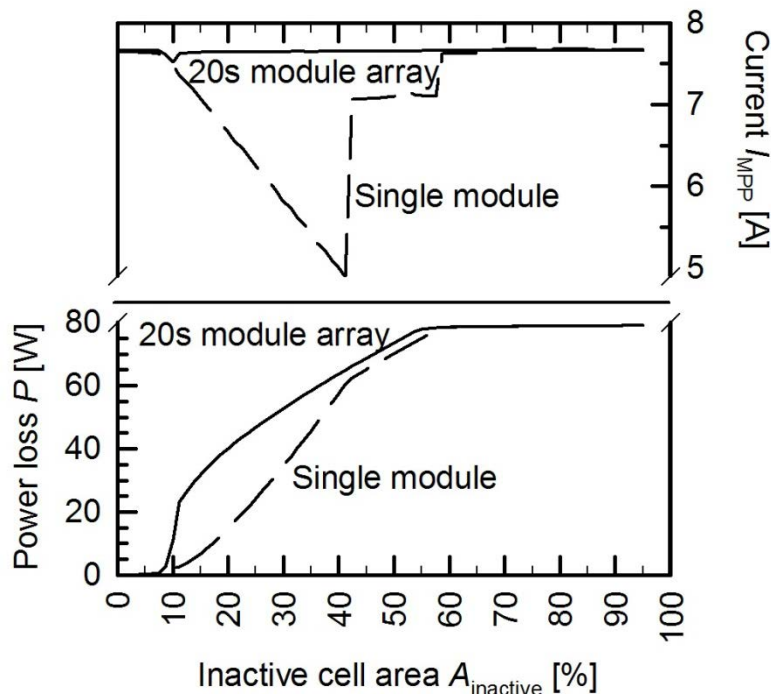


Fig. 6.2.2: Simulation of the power loss of a single 230 Wp PV module with a single solar cell having a varying inactive cell area. The simulated power loss of a 20 PV modules array containing this defective module is also shown. More than 8 % of inactive cell area in the 20s module array leads to a much higher power loss compared to the stand-alone PV module. These simulations depend on the reverse bias characteristics assumed for the silicon modules.

The higher the number of cell cracks in a solar module, the higher the chance that a PV module will develop longer and wider cracks in the course of its service life. A humidity freeze accelerated aging test being a combination of test procedure 10.11 and 10.13 defined in the standard IEC 61215 shows a correlation between the number of cracks and power loss (Fig. 6.2.3). A higher number of cracked cells per module show a higher power loss after the accelerated aging test [Koentges10]. Due to the dependence of the power loss on the orientation of the cell crack in a solar cell, the correlation between the number of cell cracks and power loss is very noisy. However for greater statistics the mean power loss risk should be linear with the number of cells with cell cracks as can be assumed from Fig.6.2.3.

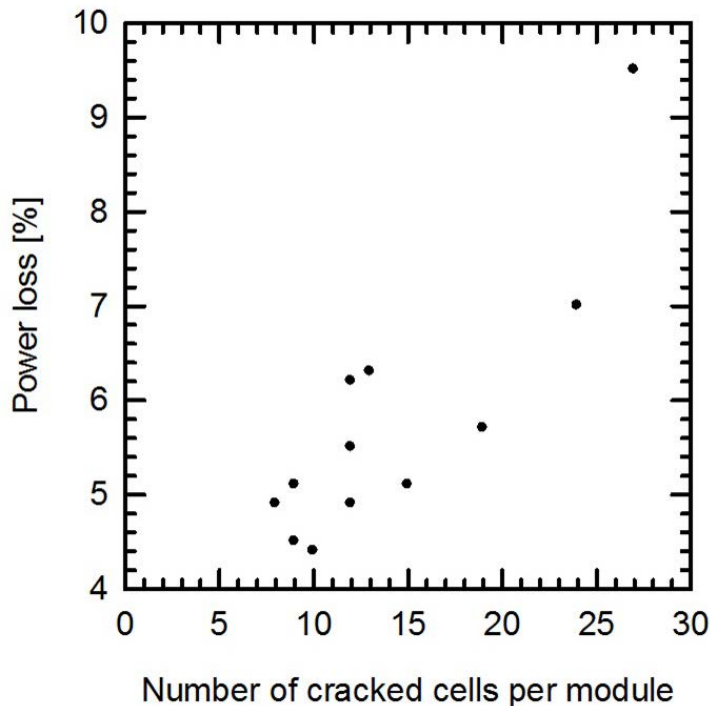


Fig. 6.2.3: The power loss after a test sequence of mechanical load and 200 humidity freeze cycles correlates with the number of cells cracked in the mechanical load test. Each point represents a single PV module. A bias power loss of about 3% is caused by glass corrosion.

The crack development and speed of isolation of cracked cell parts in PV modules being in service live is not known, yet. There have been seen PV modules with plenty of cracked cells, but there was even after two years in the field no significant power loss detectable. However there are examples in the literature showing that cell cracks can have a dramatic impact on the output of PV modules. In a solarpark with 159 PV modules with 165 Wp nearly 50% of the PV modules show a power loss of ~10% or more after 6 years of operation [Buerhop11]. Even 3.8% of the modules show cell cracks that force the bypass diode to bypass the cracked sub-module.

References

- [Buerhop11] C. Buerhop, D. Schlegel, C. Vodermayer, M. Nieß: Quality control of PV-modules in the field using infrared-thermography, 26th EUPVSEC (WIP, Hamburg, Germany, 2011), pp. 3894-3897
- [Gabor06] A. M. Gabor, M. M. Ralli, L. Alegria, C. Brodonaro, J. Woods, L. Felton, Soldering induced damage to thin Si solar cells and detection of cracked cells in modules, Proc. 21st EUPVSEC (WIP, Dresden, Germany, 2006), p. 2042-2047
- [Kajari11] S. Kajari-Schröder, I. Kunze, U. Eitner, M. Köntges, Spatial and orientational distribution of cracks in crystalline photovoltaic modules generated by mechanical load tests, *Sol. Energy Mater. Sol. Cells* **95**(11):6 (2011), doi: 10.1016/j.solmat.2011.06.032
- [Koentges08] Köntges M., Bothe K., Elektrolumineszenzmessung an PV-Modulen, ep Photovoltaik aktuell, 7/8, 36-40, 2008

[Koentges10] Köntges M., Kunze I., Kajari-Schröder S., Breitenmoser X., Bjørneklett B., Quantifying the Risk of Power Loss in PV Modules Due to Micro Cracks, 25th EuUPVSEC (WIP, Valencia, Spain, 2010) and Köntges M., Kunze I., Kajari-Schröder S., Breitenmoser X. and Bjørneklett B., The risk of power loss in crystalline silicon based photovoltaic modules due to micro cracks, *Sol. Energy Mater. Sol. Cells* **95**(4) (2011) p. 1131-1137

[Koentges11] M. Köntges, S. Kajari-Schröder, I. Kunze, U. Jahn, Crack statistic of crystalline silicon photovoltaic modules, Proc. 20th EUPVSEC (WIP, Hamburg, Germany, 2011), p. 3290-3294

[Koentges12] M. Köntges, S. Kajari-Schröder, I. Kunze, Crack Statistic for Wafer-Based Silicon Solar Cell Modules in the Field Measured by UV Fluorescence, *IEEE Journal of Photovoltaics* **3**(1) (2012) pp. 95-101, doi: 10.1109/JPHOTOV.2012.2208941

[Olschok12] C. Olschok, M. Pfeifer, M. Zech, M. Schmid, M. Zehner, G. Becker, Untersuchung von Handhabungsfehlern bei der Montage und Installation von PV Modulen, 27. Symposium Photovoltaische Solarenergie (OTTI, Bad Staffelstein, GER, 2012), p. 202

[Pingel09] S. Pingel, Y. Zemen, O. Frank, T. Geipel and J. Berghold, Mechanical stability of solar cells within solar panels, Proc. 24th EUPVSEC (WIP, Dresden, Germany, 2009), p. 3459-3464

[Reil10] F. Reil, J. Althaus, W. Vaaßen, W. Herrmann, K. Strohkendl, The Effect of Transportation Impacts and Dynamic Load Tests on the Mechanical and Electrical Behaviour of Crystalline PV Modules. Proc. 25th EUPVSEC (WIP, Valencia, Spain, 2010), p. 3989 – 3992

[Sander11] M. Sander, S. Dietrich, M. Pander, and M. Ebert, S. Schweizer, J. Bagdahn, Investigations on crack development and crack growth in embedded solar cells, Proc. Reliability of Photovoltaic Cells, Modules, Components, and Systems IV, 811201 (SPIE, San Diego, California, USA, 2011); doi:10.1117/12.893662

[Wendt09] J.Wendt, M. Träger, M. Mette, A. Pfennig, B. Jäckel, The Link Between Mechanical Stress Induced by Soldering and Mircos Damages in Silicon Solar Cells, Proc. of 24th EU-PVSEC (WIP, Hamburg, Germany, 2009), p. 3420-3424

6.2.3 Snail tracks

Figure 6.2.4 shows typical images of “snail tracks” found in the field. A snail track is visible by the human eye. A snail track is a grey/black discolouration of the silver paste of the front metallisation of screen printed solar cells. In the PV module the effect looks like a snail track on the front glass of the module. The discolouration occurs at the edge of the solar cell and along usually invisible cell cracks. The discolouring typically occurs 3 month to 1 year after installation of the PV modules. The initial discolouring speed depends on the season and the environmental conditions. During the summer and in hot climates snail tracks seem to occur faster.

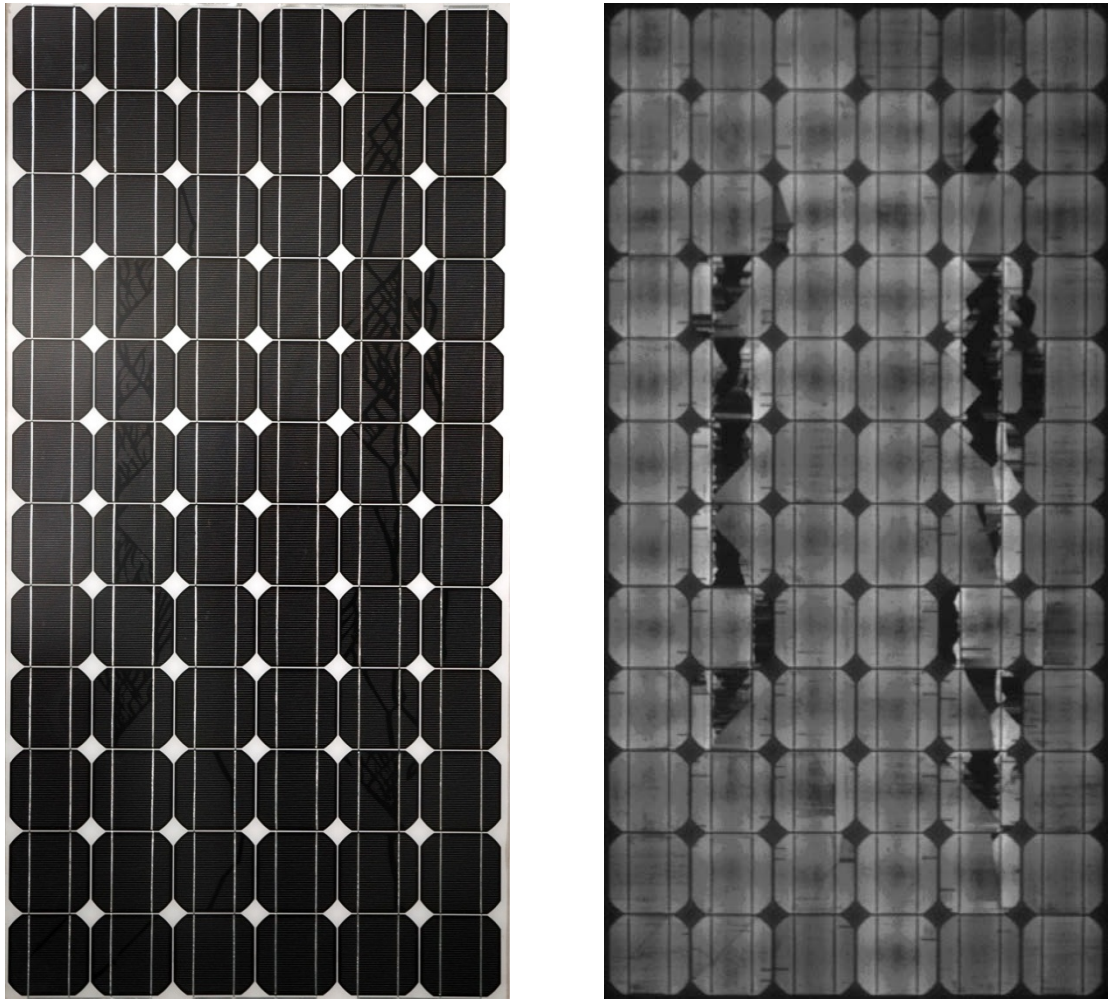


Fig. 6.2.4: Left: photograph of a snail track PV module. Right: EL image of the same snail track PV module. A snail track occurs along the edges of a solar cell and along cell cracks [Koentges08].

The origin of the discolouration of the silver paste is not clear. However in the region of the snail track discolouration along the silver finger of the front side cell metallisation shows nanometer sized silver particles in the EVA above the silver finger. These silver particles cause the discolouration. The silver particles are compounds of sulfur, phosphorus or carbon, depending on the module looked at [Richter12, YI-Hung12, Richter13]. So there may be different causes for snail tracks. Furthermore the discolored silver finger is more porous than normal silver fingers [Richter13]. This may reduce the conductivity of the silver finger especially along the crack line of the cells.

Common IEC 61215 testing will not show up snail tracks reliably [Philipp13]. To create snail tracks cell cracks should be present in the module of interest. Therefore a mechanical test should be included in a snail track test. Furthermore the combination of UV radiation and temperature seem to play an important role [Berghold12]. Berghold suggested a combined mechanical load, UV, and humidity freeze test to test for snail tracks [Berghold12] as shown in Fig. 6.2.5a.

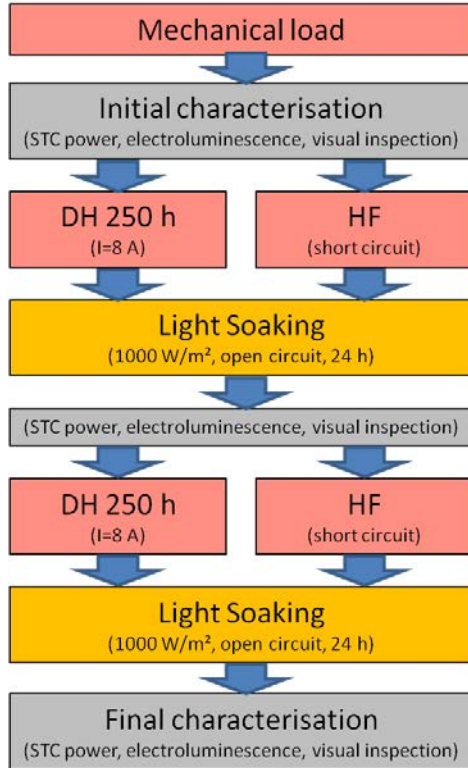


Fig. 6.2.5a: Suggested test procedure to provoke snail tracks in PV modules [redrawn from Berghold12].

On the material side the choice of the EVA and the back sheet material seems to be important for the snail track occurrence. The snail track does not depend on the kind of silver paste used for the cell production. Snail tracks have been found in a great variety of solar modules and manufacturers. PV modules being affected by snail tracks show a tendency to high leakage currents as can be seen in Fig.6.2.5b.

The growth speed of the snail track discolouration must be very slow or it saturates directly after the first occurrence. We know no case where the discolouration itself leads to a measurable power loss of the PV module. However the snail tracks make cell cracks in the solar cell visible which can reduce the PV module power, see chapter 6.2.2. Due to the observed porous silver finger in snail track affected modules the isolation of cracked cell parts may be accelerated more than it would be without snail tracks.

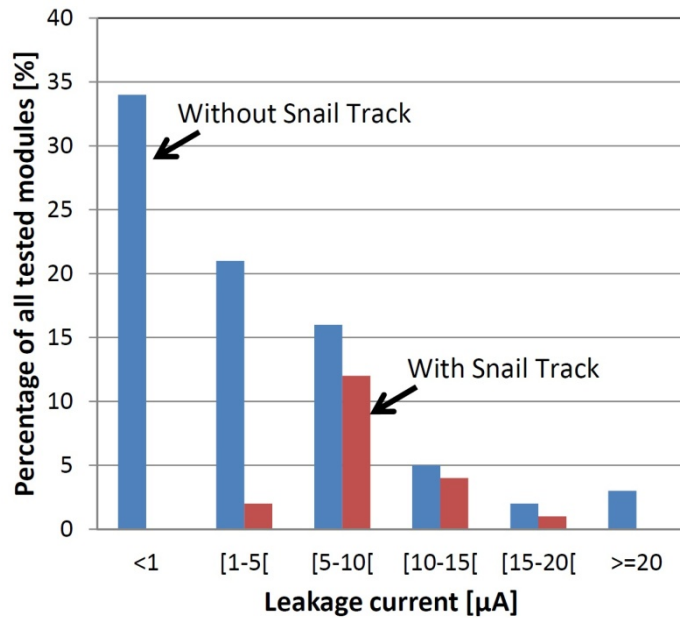


Fig. 6.2.5b: Histogram of leakage current measured in wet leakage testing for snail track affected panels. Given percentage values are relative to the number of all tested PV modules [Berghold12].

References

- [Berghold12] J. Berghold, M. Roericht, Anja Böttcher, S. Wendlandt, M. Hanusch, S. Koch, P. Grunow, B. Stegemann, Electrochemical corrosion within solar panels, 27th EUPVSEC (WIP, Frankfurt, Germany, 2012), p. 3511
- [Koentges08] Köntges M., Bothe K., Elektrolumineszenzmessung an PV-Modulen, *ep Photovoltaik aktuell 7/8*, 2008, pp. 36-40
- [Philipp13] D. Philipp, C. Peike, T. Kaltenbach, S. Hoffmann, I. Dürr, "Schneckenfspuren" - Schadenanalyse und Möglichkeiten der Früherkennung, 28th Symposium Photovoltaische Solarenergie (OTTI, Staffelstein, Germany, 2013), p. 071
- [Richter12] S. Richter, M. Werner, S. Swatek, C. Hagendorf, Understanding the Snail Trail Effect in Silicon Solar Modules on Structural Scale, 27th EUPVSEC (WIP, Frankfurt, Germany, 2012), pp. 3439 - 3441
- [Richter13] S. Richter, M. Gläser, M. Werner, M. Sander, S. Meyer, S. Dietrich, M. Ebert, C. Hagendorf, Schneckenfspuren: Ursachenanalyse und Testverfahren, Proc. of 28th Symposium Photovoltaische Solarenergie (OTTI, Staffelstein, Germany, 2013), p. 082
- [Yi-Hung12] Yi-Hung (Ivan) Chou, Wen-Yao Chou, Shr-Ming Shiu, Yu-Chen Chien, Shih-Yu Huang, Sunny Chi, Ethan Wang, Robert Struwe, Chemical Analysis and Proposed Generating Mechanism For Snail Tracks Contamination of EVA Encapsulated Modules, 27th EUPVSEC (WIP, Frankfurt, Germany, 2012), pp. 3132 - 3136

6.2.4 Burn marks

One of the most common failures sometimes observed in silicon modules is associated with parts of the module that become very hot because of solder bond failure, ribbon breakage (chapter 6.2.6), localized heating from application of reverse current flow (chapter 6.2.2) or other hot spots [Degraaff11].

Solder bond and ribbon failures can be caused by thermal fatigue. The failures may be hastened because of the increased resistance and associated heating as the joint begins to fail and current still flows through it. As the temperature increases, the resistance may also increase until the temperature is hot enough to discolor both the front and/or back encapsulation. Examples are shown in Table 5.1.3. Such failures may occur at any metal-semiconductor or metal-metal interconnection including within a ribbon or other metallic conductor.

A second type of burn mark occurs because a cell or part of a cell is forced into reverse bias. Sometimes this occurs because part of the module is shaded; it can also occur because of nonuniformities within the module including cracked cells (chapter 6.2.2) or defects that cause shunting. In some cases, the reverse current flow causes heating that further localizes the current flow, leading to a thermal runaway effect and the associated burn mark.

Burn marks are often associated with power loss, but if redundant electrical interconnections are provided, a failed solder bond may have negligible effect on the power output. If all solder bonds for one cell break, then the current flow in that string is completely blocked and an electric arc can result if the current cannot be bypassed by the bypass diode and the system operates at high voltage. Such an arc can cause a fire.

An electric arc is a so-called thermal plasma discharge with the particles temperature high enough to dissociate and ionize the medium to an extent that it is electrically conductive (plasma state). In the case of DC fault arcs in PV systems the arc is burning in an air plasma, modified by evaporated material from conductors and insulating material components. The minimum arc temperature is above 6000 K to keep the matter of a free burning arc in the plasma state and a minimum voltage (depending on electrode material and current) exists allowing for a stable burning dc arc, see Fig. 6.2.6. For a brief introduction into the matter of electrical contacts, related material, and arc plasma issues see [Rieder00, Rieder01].

With the PV generator characteristics depicted in Fig. 6.2.6 it would be possible to operate a serial arc with 200 mm maximum length resulting in 6 kW of dissipated power. By means of the power of a single 60 cell 240 W_p standard module a maximum arc length approx. 2-5 mm may be reached. The *I-V* characteristic of PV systems (stabilized current source) fits perfectly to generate stable arcing conditions. If the arc and PV characteristics intersect in 2 points, the point with the higher current is the stable operating point. Because of its high temperature an arc evaporates adjacent material resulting in fluid dynamic forces. Additionally the electromagnetic Lorentz-force acts onto the arc plasma. Therefore the arc length

and its voltage are not completely constant, causing a high frequency noise pattern that may be used for detection of arc faults [Bieniek11].

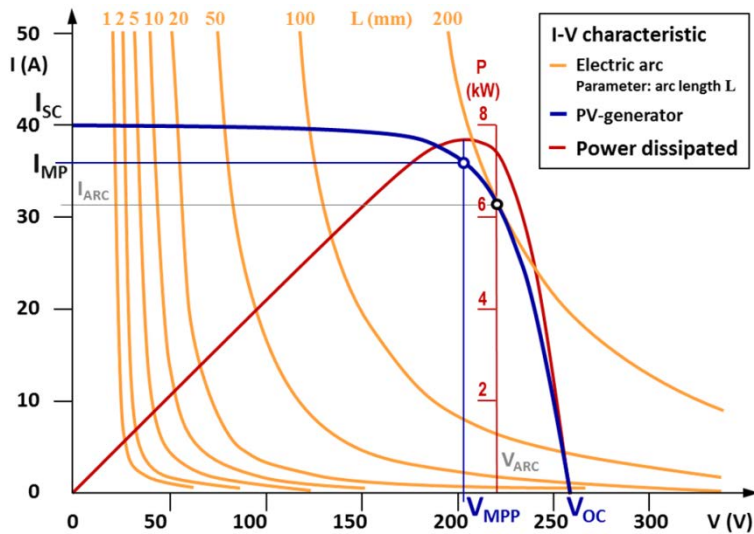


Fig. 6.2.6: I-V characteristics of free burning DC arcs in air on copper electrodes depending on arc length (in orange, from [Rieder55]) in comparison with typical PV system characteristics (blue curve).

Burn marks can usually be identified as such visually. If there is a question about whether the existence of the burn mark requires replacement of the module, an infrared image under illuminated and/or partially shaded conditions will quickly identify whether the area is continuing to be hot and/or whether current flow has stopped in that part of the circuit.

References

- [Bieniek11] S. Bieniek, H. Behrends, G. Bettenwort, T. Bülo, A. Häring, M. Hopf, M. Kratochvil, C. Merz, T. Wegener: Fire prevention in PV plants using inverter integrated AFCI. 4DO.4.6. 26th EU-PVSEC (WIP, Hamburg, Germany, 2011), p. 3199-3203
- [Degraaff11] D. DeGraaff, R. Lacerda, Z. Campeau, Degradation Mechanisms in Si Module Technologies Observed in the Field; Their Analysis and Statistics, Presentation at PV Module Reliability Workshop 2011 (NREL, Denver, Golden, USA, 2011), http://www1.eere.energy.gov/solar/pdfs/pvmrw2011_01_plen_degraaff.pdf
- [Rieder55] W. Rieder: Stability of shunted dc arcs. (German: Die Stabilität geshunteter Gleichstromlichtbögen) Elin-Z 7(1955) ISSN: 0302-2560, Vienna, p.145-149
- [Rieder00] W. Rieder, Elektrische Kontakte: Eine Einführung in ihre Physik und Technik. ISBN-13: 9783800725427. Vde Verlag GmbH, 2000 - 56 pages.
- [Rieder01] W. Rieder, Electrical Contacts. An Introduction to their Physics and Applications. ISBN-13: 9780780396395. IEEE 2001 - 90 pages

6.2.5 Potential induced degradation

During the last years underperforming of silicon wafer-based PV systems were found with a “new” failure mode of PV modules. High efficiency n-type cells evolved potential induced power degradation at positive polarity from cells to ground [Swanson05]. This effect is called polarization. More recently, several different module types with (standard) p-type cells degraded in negative polarity strings, [Pingel10]. Typically only a fraction of the modules have power losses and only in strings with a distinct voltage polarity with respect to ground. The power losses are more pronounced the higher the voltage is, and this PV module failure mode was therefore called “potential induced degradation” (PID). In crystalline Silicon wafer-based PV modules PID is to some extent a reversible polarization effect, for p- and n-type cells, at negative and positive potential, respectively. The PID effect causes cell shunts and therefore a reduction of I - V curve fill factor, see Fig.6.2.7.

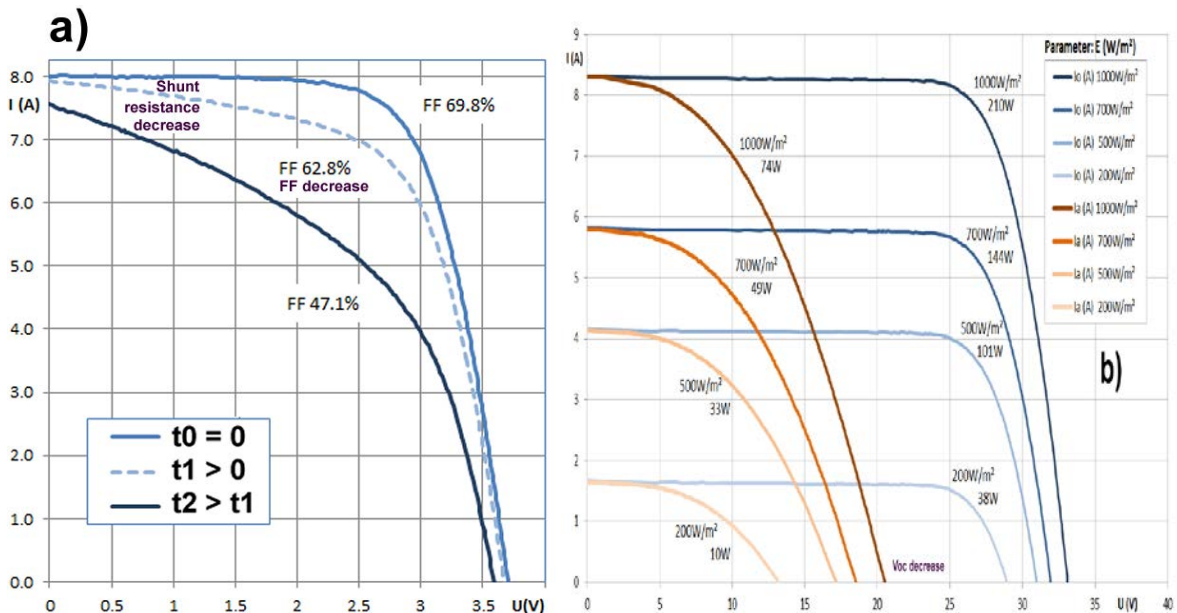


Fig. 6.2.7: I - V curves of PV modules with polycrystalline cells. On the left a): I - V curves measured at STC from a 2x3-cell-module kept in a climate chamber at 60°C/85% rel. humidity; $t_0 \dots t_1$: 96 h at -1000 V, $t_1 \dots t_2$: 96 h and -1500 V between cells and frame. The power is decreasing with increasing PID effect over time. On the right b): I - V curves of a fielded (la) and initial (lo) 6x9-cell-module at ± 400 V system voltage measured under various Irradiation levels [Berger13].

If some cells in a module remain at the original short-circuit current value, the module’s short-circuit current is almost unchanged. In early stages, the PID caused power degradation effect at high irradiation conditions is small, while more pronounced at low light conditions [Mathiak12], therefore not easy to detect within a power plant’s monitoring data. Additionally even massive PID has often no visual effects, so a huge number of unreported cases may exist [Bagdahn12, Berghold10]. The Fig. 6.2.8 depicts schematically the electric circuit and a cross section view of a framed (cSi) module.

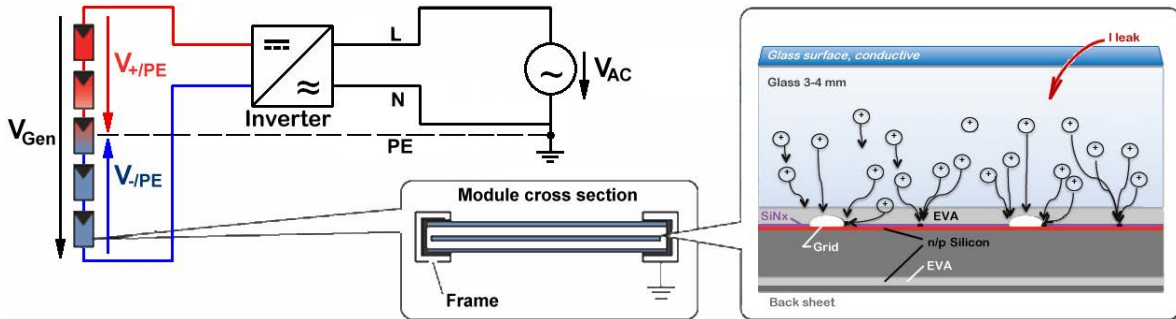


Fig. 6.2.8: On the left: Schematics of a PV array connected to the grid by means of a transformerless inverter. Middle: Module cross section. On the right: Detail drawing of the cross section next to the (grounded) frame. Left and middle part from [PID-TI-UEN113410], right figure from [Hacke12a].

Electrochemical degradation in PV modules was addressed as early as 1978 [Hoffman78]. The effect was described as the migration of ions from the front glass through the encapsulant to the anti-reflective coating (SiN_x) at the cell surface [Mon89] driven by the leakage current in the cell to ground circuit. This leakage current is typically in the order of μ A and its value is strongly depending on material properties, the surface conditions and humidity as well as module temperature and the applied voltage, see Fig. 6.2.9 a) [Hacke11].

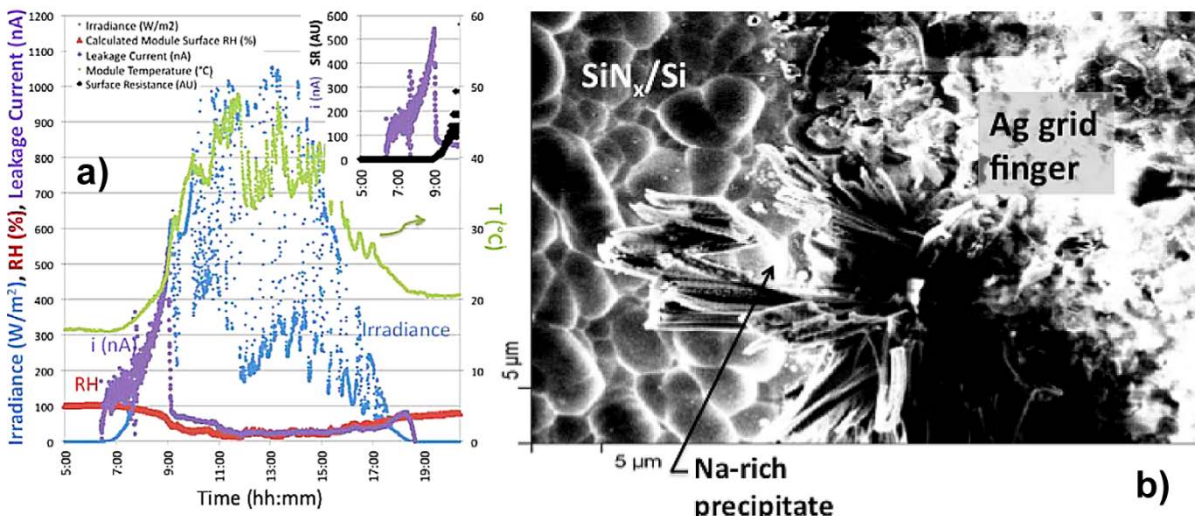


Fig. 6.2.9: a): Irradiance, humidity, leakage current, and temperature during daytime [Hacke11]. b): AES imaging of the SiN_x/Si boundary [Hacke11].

Several experiments were performed to elaborate a microscopic model which explains the effect.

In-depth investigations of the cell-encapsulant boundary by means of Auger Electron Spectroscopy (AES) [Hacke11], see Fig. 6.2.10 b), detects sodium rich regions at the antireflection coating-Si interface.

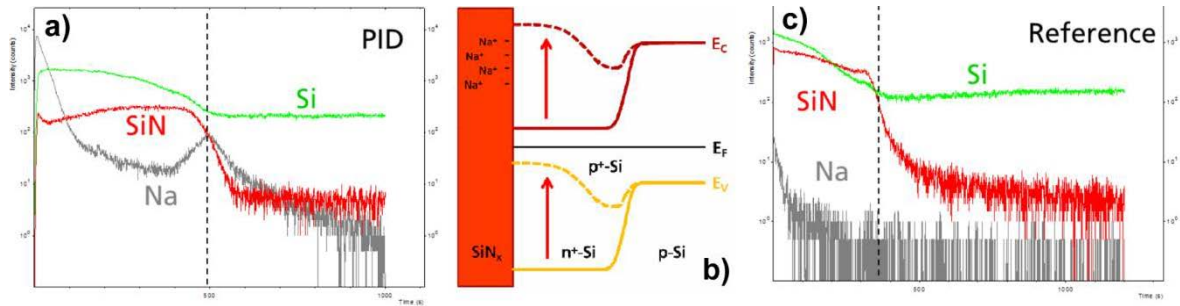


Fig. 6.2.10: a) and c): Depth profiles recorded by means of time of flight SIMS (a) with, and c) without PID, respectively. c): AES imaging of the SiN_x/Si boundary. b): Original band gap structure, and by PID changed energy levels (dashed lines) [Naumann12].

Also secondary ion mass spectroscopy (SIMS) [Naumann12], Fig. 6.2.10, with (a), and without (c) PID, respectively give evidence of Sodium ions trapped in the so called K-centers of the silicon nitride anti reflective coating. This positive space charge forms a double-layer with electrons changing the semiconductor's band gap structure, see middle drawing of the energy band model in Figure 6.2.10 b), causing the shunted paths in the p-n junction of the cell.

Additional impurity models were presented, whereby positive ions are attracted to the cell and the impurities themselves cause recombination in the junction and where charge accelerates by an electrical potential over silicon nitride causing lattice damage [Hacke12].

As depicted in Fig. 6.2.7 the *I-V* curve measurement (see chapter 5.2) e.g. at STC and at low light conditions gives clear evidence of PID. Infrared Thermography, see Tab. 5.3.1 in chapter 5.3, is a suitable method in the field, when the array is illuminated and operating at (maximum) power (point), Fig.6.2.11.

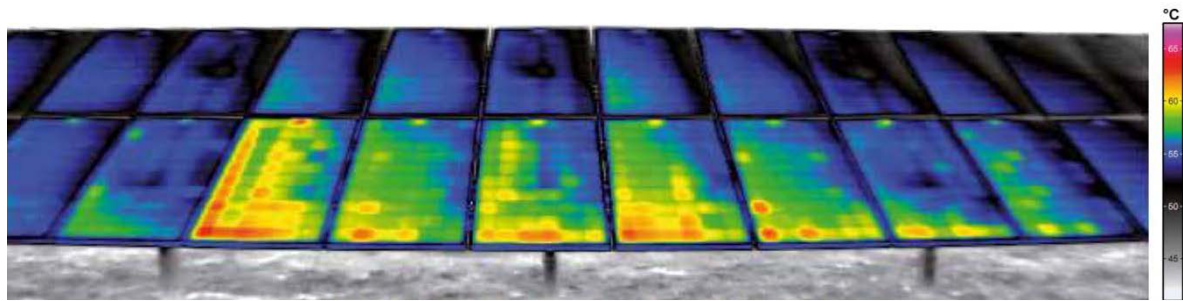


Fig. 6.2.11: Operating module array investigated by thermography under illumination. The negative module voltage decreases from the right to the left side, and the power losses heating the modules in the shunted areas are also increasing from the right to the left [Weinreich13].

Figure 6.2.12 shows electroluminescence images made at 10% and 100% I_{sc} and a thermographic image made at 100% I_{sc} . The images are made from the same PV module studied in Fig. 6.2.7 b). In contrast to the array with the outdoor

thermography depicted in Fig. 6.2.11, this module was rack mounted in landscape position. While cells with a black EL-image in the middle and upper parts are heated through the shunts, the cells in the lowest row are shunted with very low resistance, resulting in a dark part in the thermographic image.

Up to now safety problems directly related to the PID are not reported, but “medium” degraded cells have higher temperatures (hot spots), while low resistive shunting of severe degraded cells have less temperature, cf. Fig. 6.2.12. Hot spots and corrosion may cause delamination between cells and encapsulant, possibly exposing the inner circuitry of the module to the ambient, see chapter 6.1.1.

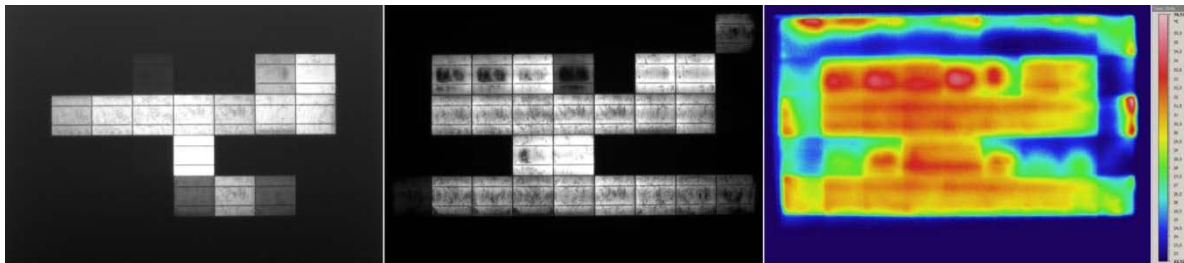


Fig. 6.2.12: Fielded 6×9-cell-module with the I - V curves depicted in Fig. 6.2.7 (b), investigated with electroluminescence images made at 10% I_{sc} (left), 100% I_{sc} (middle) and dark IR thermography at 100% I_{sc} (right) [Berger13].

How severe the power losses due to PID are depends on the ambient conditions and system configuration, as well as module design parameters. For a given PV module design the value of the leakage current (and its time integral) can be an indicator for the PID effect in some circumstances. Figure 6.2.13 depicts measured values for the leakage current between the cells and the module frame over the applied voltage (with parameters temperature and rel. humidity), the relative air humidity at constant voltage, and reciprocal abs. temperature (with three different variants for contacting the module’s outer surface) [Hoffmann12].

These variable accelerating factors result in the complex variation of the outdoor leakage current as depicted in Fig. 6.2.9 a). Additionally the glass surface conductivity is lowered during rainfall and through pollutants, e.g. salt mist near by the sea. The power degradation in the field may evolve within several months and can reach almost 100%. Figure 6.2.14 gives an example, cf. schematic diagram in Fig. 6.2.7. The fill factor degradation can be modeled with increased second-diode pre-exponential and ideality factor and a decreasing shunt resistance in a two-diode model [Hacke11a].

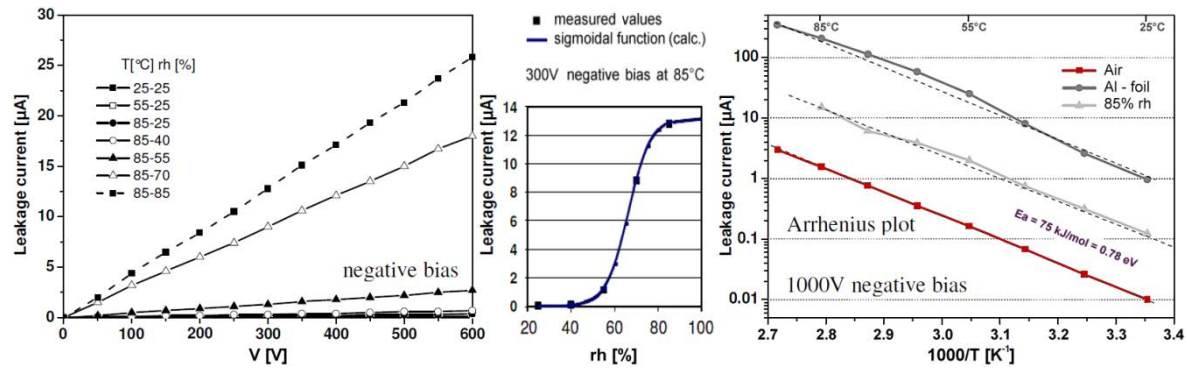


Fig. 6.2.13: Measured values for the leakage current (LC) between cells and module frame. Left side: voltage dependency of LC, with parameters temperature and humidity. Middle: LC as function of the humidity measured (squares) and approximation by a sigmoid function (blue curve). The effect of humidity in the climatic chamber is time dependent. This is due to condensation at the module [Mathiak12]. Right side: Arrhenius plot of LC with three different variants for contacting the module's outer surface: frame only, in (dry) air; front glass and frame additional covered with aluminum foil; frame only contacted, but 85% rel. humidity applied. Modified, from [Hoffmann12].

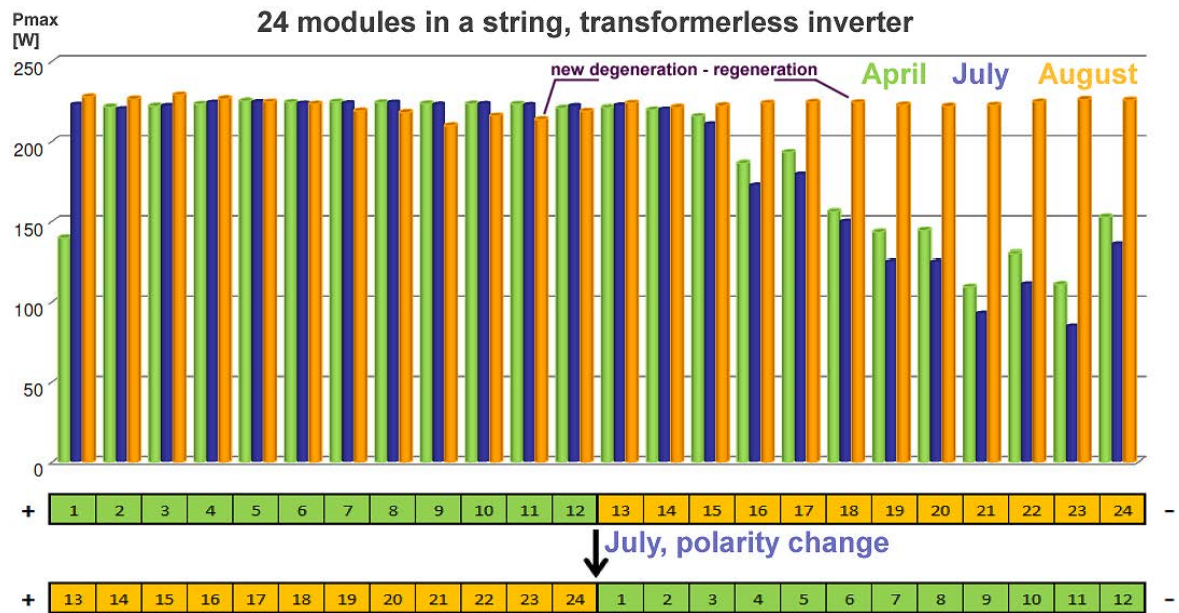


Figure 6.2.14: Measured power for individual PV modules at STC dependent on the module's position in the string. The power losses at negative potential are still increasing until the polarity is changed and recovery to the original P_{max} values takes place [Herrmann12].

Quick recovery is often possible within hours by applying a reverse voltage, low resistive contact to glass and frame, and at elevated temperature. PID occurring at higher temperatures (85°C) is much less reversible [Pingel12]. Some recovery can also be achieved by voltage and temperature alone, but with much longer time constants. Recovery can be achieved by applying reverse voltage during nighttime.

But this may need several months or even years without adequate accelerating factors [Mathiak13], cf. Fig. 6.2.13. A climate model for the outdoor module power degradation prediction based on measurements as depicted in Fig. 6.2.13 and local site specific climate profiles was presented in [Raykov12], including the regeneration processes. Further literature concerning the regeneration process can be found in [Pingel12], [Koch12], [Nagel12], [Taubitz12], and [PID-TI-UEN113410].

The module design has a fundamental influence if and how a prone module is affected by PID. The Tab. 6.2.1 lists the effects of conditions and measures on different levels from the environmental and system influences down to cell design aspects and gives references for further information on these topics.

Table 6.2.1: Factors influencing PID.

Design level	Influence on / accelerating factor	References
<i>Environmental conditions (Micro-, macroclimate)</i>	<ul style="list-style-type: none"> • Temperature • Humidity, rain, and condensation • Insolation(-distribution) • Aerosols <ul style="list-style-type: none"> • Surface conductivity, leakage current, ion mobility, chemical reactivity • Surface and encapsulant bulk conductivity, leakage current • Fraction of energy yield at low light conditions • Surface conductivity, leakage current 	[Raykov12] [Hoffmann12] [Berghold12] [Hoffmann12] [Hacke11] [Berger13] [Mathiak12]
<i>System related factors</i>	<ul style="list-style-type: none"> • Operating and open circuit system voltage • Inverter topology and array potentials • Reverse array polarity during nighttime • Grounding concept <ul style="list-style-type: none"> • Leakage current • Array polarity levels (DC + AC content), leakage current, and polarity • Recovery • Conductivity of ele. path, leakage current 	[AE13] [Berghold12] [Herrmann12] [PID-TI-UEN113410]
<i>Module level</i>	<ul style="list-style-type: none"> • Mounting orientation (angle, portrait or landscape orientation) • Frame and mounting on structure <ul style="list-style-type: none"> • Wetness, number of cells next to the lower edge with higher surface conductivity, soiling, temperature, and leakage current • Conductivity of electrical path, leakage current 	[Herrmann12] [Berghold12] [Richardson11] [Raykov12] [Herrmann12]

<ul style="list-style-type: none"> • Encapsulant material and thickness • Back-sheet material • Front cover material • Front cover surface treatment and coating 	<ul style="list-style-type: none"> • Bulk resistivity, ion mobility, leakage current • Water vapour transmission rate (WVTR), encapsulant's water content, bulk resistivity, chemical reactivity, leakage current • Electrical conductivity, sodium ion concentration, ion mobility, leakage current • Surface conductivity, soiling, leakage current 	
<p><i>Cell (manuf.) level</i></p> <ul style="list-style-type: none"> • Anti-reflective coating (ARC) thickness and homogeneity, Si/N ratio • Surface structure • Emitter depth • Doping, p- or n-type semiconductor 	<ul style="list-style-type: none"> • No ARC - no PID, conductive coating on ARC arrests PID, higher refracting index of SiNx lowers PID (but increases reflective losses) • Reduction of “attractive” K-centers • Emitter sheet resistivity influences PID • Wafer base resistivity influences PID 	<p>[Hacke12] [Nagel12] [Pingel10] [Raykov12] [Naumann12] [Koch12] [Koch12a] [Schutze11] [Richardson11]</p>

References

[AE213] AE Solar Energy: *Understanding Potential Induced Degradation*, White Paper of Advanced Energy, Doc. ENG-PID-270-01, 8 p. Bend, Oregon 2013

[Bagdahn12] J. Bagdahn, S. Dietrich, M. Ebert, J. Fröbel, C. Hagendorf, S. Großer, D. Lausch, V. Naumann, Potential induced degradation of crystalline Silicon photovoltaic modules, Presentation, technical seminar 6 (materials and reliability) at the PV Japan, Oct. 2012

[Berger13] K.A. Berger, B. Kubicek, G. Újvári, G. Eder, Y. Voronko, M. Weiss, G. Oreski, M. Knausz, T. Koch, J. Wassermann, Innovative, non destructive methods for investigations of PV-modules (in German: „Innovative, nichtzerstörende Methoden zur Untersuchung von Photovoltaikmodulen“), Proc. 28th Symposium Photovoltaische Solarenergie (OTI, Bad Staffelstein, Germany, 2013), Regensburg 2013, ISBN 978-3-943891-09-6

[Berghold10] J. Berghold, O. Frank, H. Hoehne, S. Pingel, B. Richardson, M. Winkler, Potential Induced Degradation of solar cells and panels, Proc. 25th EUPVSEC (WIP, Valencia, Spain, 2010), pp. 3753-3759

[Berghold12] J. Berghold, S. Koch, S. Lehmann, S. Wendlandt, M. Leers, A. Preiß, S. Pingel, P. Grunow, PID and correlation with field experiences (in German: “PID

und Korrelation mit Felderfahrungen.“) 27th Symposium Photovoltaische Solarenergie (OTTI, Bad Staffelstein, Germany, 2012), Regensburg 2012

[Hacke11] P. Hacke, K. Terwilliger, R. Smith, S. Glick, J. Pankow, M. Kempe, S.K.I. Bennett, M. Kloos, System voltage potential-induced degradation mechanisms in PV modules and methods for test, Proc. 37th PVSC (Seattle, Washington, USA 2011), pp. 814-820, 19-24

[Hacke11a] P. Hacke, R. Smith, K. Terwilliger, S. Glick, D. Jordan, S. Johnston, M. Kempe, S. Kurtz, Testing and Analysis for Lifetime Prediction of Crystalline Silicon PV Modules Undergoing Degradation by System Voltage Stress, Proc. 38th PVSC (IEEE, Austin, Texas, USA, 2011), pp. 814–820

[Hacke12] P. Hacke, S. Glick, S. Johnston, R. Reedy, J. Pankow, K. Terwilliger, S. Kurtz, Influence of impurities in module packaging on potential-induced degradation, Presentation at the 22nd Workshop on Crystalline Silicon Solar Cells & Modules: Materials and Processes. Vail, Colorado, July 22–25, 2012. Technical report NREL/TP-5200-56301, 10 p., Sept. 2012, 32p.

[Hacke12a] P. Hacke, Potential induced Degradation in Crystalline Silicon PV Modules: Evaluation of Durability, Presentation at PV Japan 2012, Dec. 5-7 2012

[Herrmann12] W. Herrmann, G. Mathiak, Potential induced degradation (PID) in crystalline Silicon PV-modules (in German: “Potential-Induzierte Degradation (PID) bei kristallinen Silizium PV-Modulen, Presentation at 9th Workshop Photovoltaik-Modultechnik, Nov. 2012, TUV Rheinland, Cologne

[Hoffman78] A.R. Hoffman and R.G. Ross, Environmental Qualification Testing of Terrestrial Solar Cell Modules, 13th IEEE PVSC, Washington DC 1978, pp. 835–842

[Hoffmann12] S. Hoffmann, M. Koehl, Effect of humidity and temperature on the potential-induced degradation, *Prog. Photovolt. Res. Appl.* 2012, doi: 10.1002/pip.2238

[Koch12] S. Koch, D. Nieschalk, J. Berghold, S. Wendlandt, S. Krauter, P. Grunow, Potential induced degradation effects on crystalline silicon cells with various antireflective coatings, Proc. 27th EUPVSEC, (WIP, Frankfurt, Germany, 2012), pp. 1985-1990

[Koch12a] S. Koch, J. Berghold, O. Okoroafor, S. Krauter, P. Grunow, Encapsulation influence on the potential induced degradation of crystalline silicon cells with selective emitter structures, Proc. 27th EUPVSEC (WIP, Frankfurt, Germany, 2012), pp. 1991-1995

[Mathiak12] G. Mathiak, M. Schweiger, W. Herrmann, E. Eikelboom, M. Sedlacek, M. Heijo Al Rifai, Potential-induced degradation - comparison of different test methods and low irradiance performance measurements, Proc. 27th EUPVSEC (WIP, Frankfurt, Germany, 2012), pp. 3157-3162

[Mathiak13] G. Mathiak, Potential induced Degradation (PID) for crystalline PV Modules - Analysis and Counter measures (in German: „Potentialinduzierte Degradation (PID) bei kristallinen PV-Modulen - Analyse und Gegenmaßnahmen“), Proc. 28th Symposium Photovoltaische Solarenergie (OTTI, Bad Staffelstein, Germany, 2013), Regensburg 2013, ISBN 978-3-943891-09-6, pp. 272-273

[Mon89] G.R. Mon, L.C. Wen, R.S. Sugimura, R.G. Ross, Jr., Reliability studies of photovoltaic module insulation systems, 1989 IEEE - CH2788-8/89/0000-0324 pp. 324-329

[Nagel11] H. Nagel, Possible cause for PID of crystalline silicon cells, Sophia Workshop PV Module Reliability, Lugano, Switzerland, 2012

[Nagel12] H. Nagel, R. Pfeiffer, A. Raykov, W. Wangemann, Lifetime warranty of crystalline silicon modules for potential-induced degradation, Proc. 27th EUPVSEC (WIP, Frankfurt, Germany, 2012), pp. 3163-3166

[Naumann12] V. Naumann, C. Hagendorf, S. Grosser, M. Werner, J. Bagdahn, Micro Structural Root Cause Analysis of Potential Induced Degradation in c-Si Solar Cells, SiliconPV: April 2012, Leuven, Belgium, *Energy Procedia* **27** (2012), pp. 1-6

[PID-TI-UEN113410] SMA: Technical Information on PID, Doc. PID-TI-UEN113410, Version 1.0. SMA Solar Technology AG, Niestetal, Germany. Undated, 4 pages. <http://files.sma.de/dl/7418/PID-TI-UEN113410.pdf> (15.5.2013)

[Pingel10] S. Pingel, O. Frank, M. Winkler, S. Daryan, Potential Induced Degradation of solar cells and panels, Proc. 35th PVSC (IEEE, Hawai, US, 2010), pp. 002817 - 002822

[Pingel12] S. Pingel, S. Janke, O. Frank, Recovery methods for Modules Affected by Potential Induced Degradation (PID), Proc. 27th EUPVSEC (WIP, Frankfurt, Germany, 2012), pp. 3379-3383

[Raykov12] A. Raykov, H. Nagel, D. Amankwah, W. Bergholz, Climate model for potential induced degradation of crystalline silicon photovoltaic modules, Proc. 27th EUPVSEC (WIP, Frankfurt, Germany, 2012), pp. 3399-3404

[Richardson11] W. Richardson, *Potential Induced Degadation*. NREL PV-Reliability Workshop Febuary 1st, 2011, 37p.

http://www1.eere.energy.gov/solar/pdfs/pvmrw2011_26_csi_richardson.pdf

[Schutze11] M. Schütze, M. Junghänel, M.B. Koentopp, S. Cwikla, S. Friedrich, J.W. Müller, and P. Wawer, Laboratory study of potential induced degradation of silicon photovoltaic modules, Proc. 37th PVSC (IEEE, Seatle, Washington, USA, 2011), pp. 821-826

[Swanson05] R. Swanson, M. Cudzinovic, D. DeCeuster, V. Desai , J. Jürgens, N. Kaminar, W. Mulligan, L. Rodrigues-Barbarosa, D. Rose, D. Smith, A. Terao, and K. Wilson, The Surface Polarization Effect in High-Efficiency Silicon Solar Cells, 15th PVSEC (Shanghai, China, 2005), 4p. 2805d1306844541

[Taubitz12] Christian Taubitz, Matthias Schütze, Max B. Koentopp, Towards a kinetic model of potetial-induced shunting, 27th EUPVSEC (WIP, Frankfurt, Germany, 2012), pp. 3172-3176

[Weinreich13] B. Weinreich, Field study module and generator quality based on thermography measurements of 100 MW (in German: „*Feldstudie zur Modul- und Generatorqualität auf Basis thermografischer Messungen über 100 MW*“), Proc. 28th Symposium Photovoltaische Solarenergie (OTTI, Bad Staffelstein, Germany, 2013), Regensburg 2013, ISBN 978-3-943891-09-6

6.2.6 Disconnected cell and string interconnect ribbons

Conventional wafer-based crystalline silicon PV modules have numbers of solar cells, which are interconnected in series with cell interconnect ribbons to obtain higher voltage. These cell interconnect ribbons are connected from the front side to the rear side of the solar cells. A series of interconnected cells is called a string. These cell strings itself are typically interconnected in series or sometimes in parallel by string interconnect ribbons.

In such conventional interconnected PV modules, we sometimes find weakened cell or string interconnect ribbons and following disconnections. Especially the so-called ribbon kink between the cells and the joint between the cell interconnect ribbon and the string interconnect [Munzo8] are prone for fatigue breakage. There may be several possible causes of this PV module failure. Poor soldering in the PV module production process of the connection between cell interconnect ribbon and string interconnect is the most important reason for disconnections. A too intense deformation during the fabrication of the ribbon kink between the cells mechanically weakens the cell interconnect ribbon. A narrow distance between the cells promotes cell interconnect ribbon breakage. Physical stress during PV module transportation, thermal cycle, and/or hot spots by partial cell shading during long-term PV system operation forces mechanical weak ribbon kinks to break [Kato2].

A ribbon breakage may be detected by EL, IR imaging, UV imaging or the signal transmission method, compare chapter 5.3, 5.4, 5.5, and 5.6. In Fig. 6.2.14 an IR and EL image of a module with three disconnected cell interconnects are depicted on the left and right hand side, respectively.

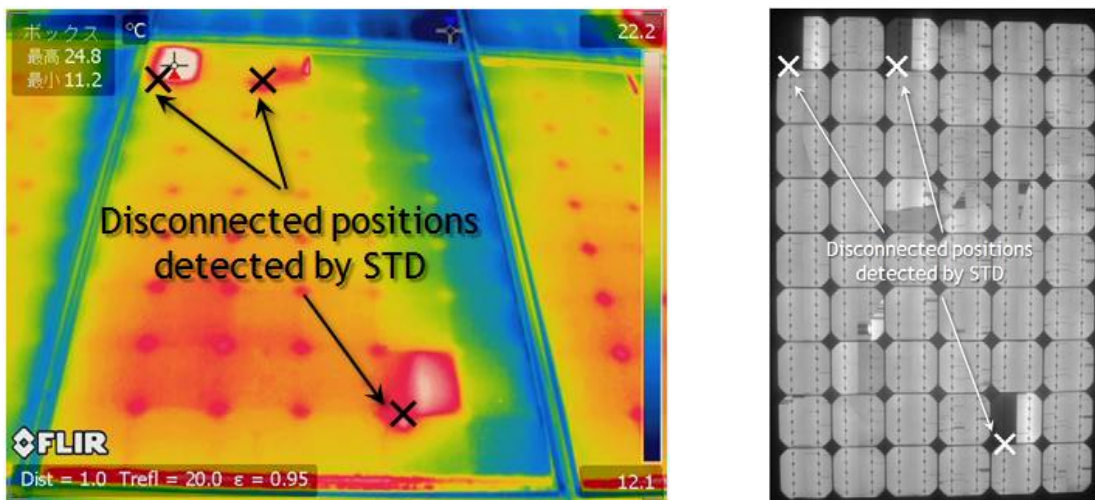


Fig. 6.2.14: Left: An example of disconnected cell interconnections found in the field (IR image). Right: The corresponding EL image of the same PV module.

Figure 6.2.15 left and right represent an IR image and the I-V characteristic curve (measured at standard test condition) of one PV module, locally in which one interconnect ribbon is electrically disconnected. In this image the disconnected position detected by the STD is also given. As shown in the I-V characteristic curve, only this one disconnection among many interconnection results in 35% power loss.

But on this stage (“failure stage 1”) safety risk may be not so high because the temperature of this hot spot cell does not increase to more than around 100°C. This module failure is categorised into safety class B(f,m,e).

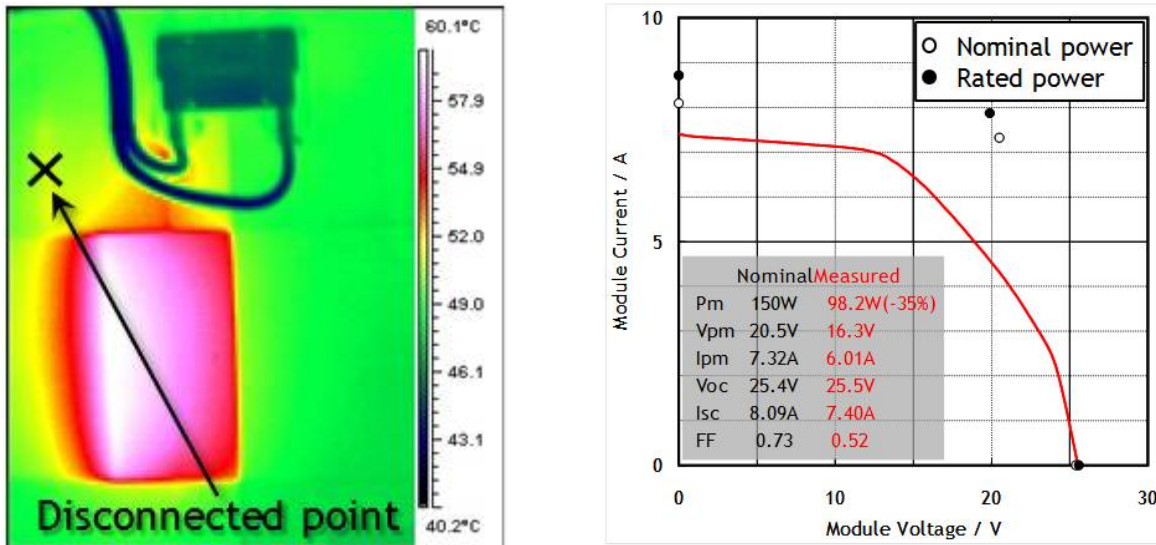


Fig. 6.2.15: Left: an IR image of a PV module where one interconnect ribbon is locally disconnected (“failure stage 1”). Right: I - V curve (indoor STD) of a PV module in which one interconnect ribbon is locally disconnected (“Failure Stage 1”). The Nominal and initial rated I - V curve parameters are plotted into the graph.

Fig. 6.2.16 left and right hand sides show an IR image and the I - V characteristic curve (also measured at standard test condition) of another PV module. On this stage (“failure stage 2”) a sub-module has given up power generation since both interconnect ribbons are electrically disconnected and current flow constantly goes through a bypass diode during daytime. The I - V characteristic curve of this PV module indicates 46% power loss. On this failure stage 2, safety risk heavily depends on the durability of this bypass diode. This module failure is still categorised into safety class B(f,m,e), because a further failure (diode becomes defective) must occur until this failure leads to a safety issue.

A photograph of one PV module on the “final stage” is shown in Fig. 6.2.17 on the left and right side, respectively. The cover glass has been completely broken and many burn marks can be seen on the back sheet. As one can imagine, this situation is that the bypass diode, which had worked during daytime, has been worn out to be open-circuit state. As a result, the generated current went back to the failed cell string and generates heat at the disconnected position. The cover glass breakage was caused by rapid increase in temperature.

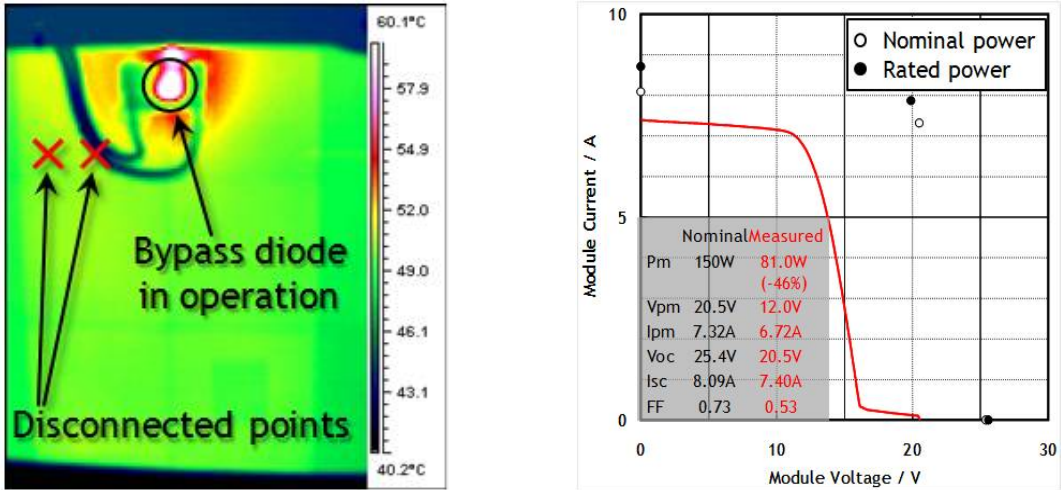


Fig. 6.2.16: Failure stage 2. Left: an IR image of a PV module with two parallel cell interconnect ribbons locally disconnected. Right: $I\text{-}V$ curve measurement (indoor STD) of PV module with two parallel cell interconnect ribbons locally disconnected.



Fig. 6.2.17: Final stage. Left: glass breakage of a PV module caused by broken cell interconnect ribbons. Right: burn marks on the PV module rear side caused by broken cell interconnect ribbons.

Figure 6.2.18 shows an IR image of this final stage PV module. The highest temperature observed at the disconnected position reaches over 500°C . This module failure is categorised into safety class C(f,m,e), because it may cause a fire, open electrical conducting parts to the user and destroy the mechanical integrity of the module. The power loss occurs stepwise therefore this failure mode is power loss class E.

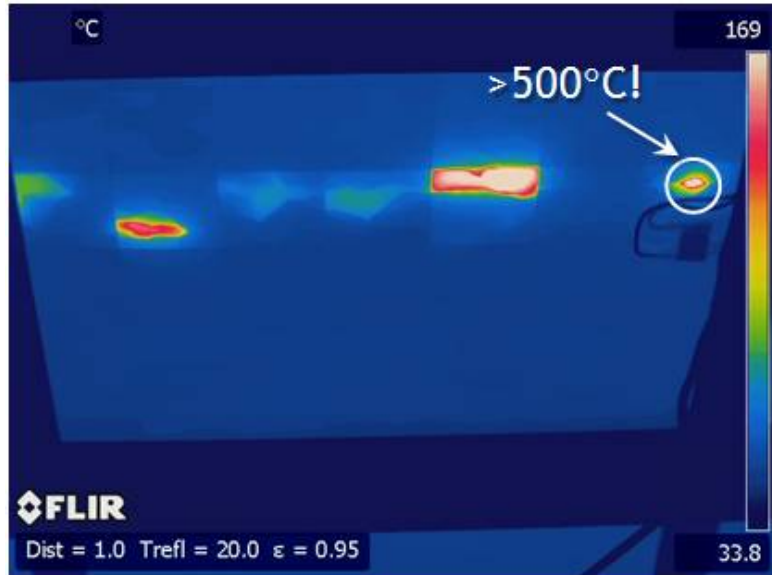


Fig. 6.2.18: An IR image of the “final stage” PV module (observed from rear side).

Figure 6.2.19 represents the trend in number of these PV module failures happening in a PV system. Bypass diodes play a very important role in conventional crystalline silicon PV modules as “safety valves” in case some electrical fatigue occurs in the cell strings.

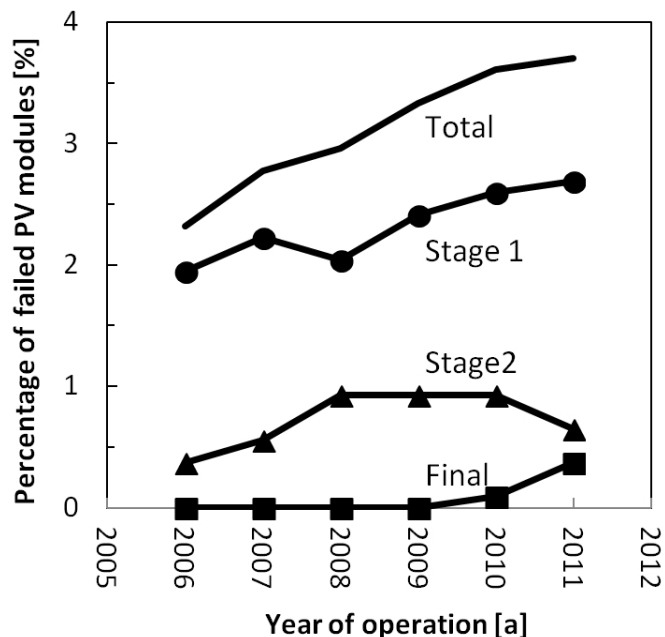


Fig. 6.2.19: Annual trend in number of modules with cell interconnect ribbon failures happening in a PV system. The system consists of 1080 PV modules in total and was built in 2004.

6.2.7 Defective bypass diode

In parallel to a certain number of solar cells bypass diodes are integrated into the PV module. These bypass diodes reduce the power loss caused by partial shading on the PV module. Besides the power loss the diode avoids the reverse biasing of

single solar cells higher than the allowed cell reverse bias voltage of the solar cells. If a cell is reversed with a higher voltage than it is designed for the cell may evolve hotspots [Hermann09] that may cause browning, burn marks or, in the worst case, fire. Typically, Schottky diodes are used as bypass diodes in PV modules. Schottky diodes are very susceptible to static high voltage discharges and mechanical stress. So they must be handled with care and human contact without grounding must be avoided.

Consequently, many bypass diode failures may occur. But it is difficult to find them because they only attract attention when the PV modules have severe mismatch in the individual *I-V* characteristic of single cells, e.g. caused by shading or disconnected parts of a cell due to cell cracks.

To our knowledge there is only one published non representative study on defective bypass diodes of crystalline PV modules [KATO02]. The study has been conducted on a PV system over car parks at the National Institute of Advanced Industrial Science and Technology (Japan) which operated 53 units of 4 kWp. The total number of single crystalline PV modules with 180 W_p nominal power amounts to 1272.

Fig. 6.2.20 left shows a rear side of one PV module with burn marks. Both left and center sub-modules have some burn marks. *I-V* curves measured outdoors are given in Fig. 6.2.20 right. The black, red, green, and blue curves indicate measurements without partial shade, with partial shade on the left sub-module, with partial shade on the center sub-module and with partial shade on the right sub-module, respectively. The blue curve has 1/3 reduction in voltage compared with the black curve. This means that the bypass diode integrated into the right sub-module works well. On the other hand, both red and green curve have different shapes from the blue one, that is, a small amount of current can be measured without reasonable voltage drop. These results point out that the bypass diodes combined into the left and center sub-modules operate in open circuit. Its cause is not yet confirmed but possible options are defective bypass diodes or soldering disconnection between the bypass diode and the metal contact inside the junction box.

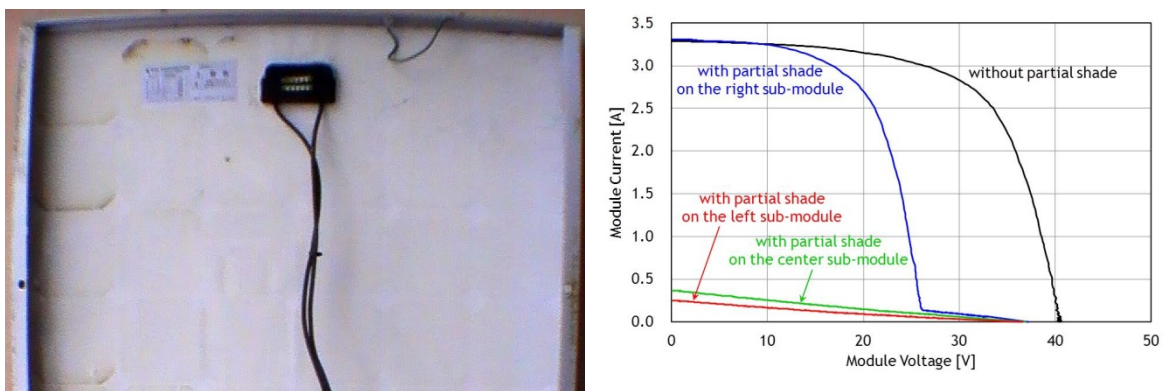


Fig. 6.2.20: A rear side view (left) and a measured *I-V* characteristic curve (right) of a PV module with burn marks.

The system shows 47% of modules with defective bypass diodes, see Fig. 6.2.21. 3% of the defective PV modules also show burn marks on sub-modules. The sub-modules with burn marks always have defective bypass diodes.

The burn marks are found along cell edges on the back sheet such as pictures shown in Fig. 6.2.22. All of these PV modules are partially shaded by neighbor trees, streetlights, and PV installation. Edge isolation faults on the solar cell level are under normal condition no problem, but when the bypass diode is in open-circuit the current is driven in reverse through the shunts of the solar cells and burns the encapsulation.

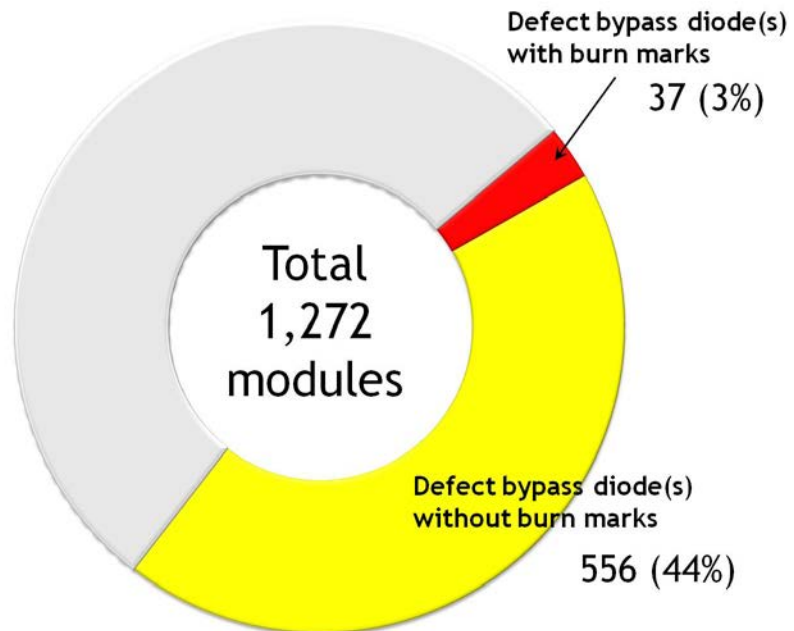


Fig. 6.2.21: A result of bypass diode check for 1272 180 Wp PV modules of one type. The diagram shows the number and percentage of PV modules with one or more defective bypass diodes. The PV modules have been in the field for about four years.



Fig. 6.2.22: Burn marks caused by open-circuit bypass diodes.

References

- [Hermann09] W. Herrmann, W. Wiesner, W. Vaaßen, Hot Spot Investigations on PV Modules - new Concepts for a Test Standard and Consequences for Module Design with Respect to Bypass Diodes, Proc. 26th PVSC (IEEE, Anaheim, CA, USA, 1997), pp. 1129-1132

[Kato02] K. Kato, "PVResQ!": A Research Activity on Reliability of PV System from an user's viewpoint in Japan, Proc. Optics + Photonics 8112 (SPIE, San Diego, California, USA, 2011), 811219

6.3 Review of failures found in thin-film modules

For thin-film PV modules there are far fewer experiences accumulated in the past years than for crystalline Si PV modules. Also the variety of different thin module types is much broader than for crystalline Si PV modules. Therefore many module failures are very specific for a certain manufacturer. In the following chapters the focus is on failures which can be found in a broader range of PV module types.

6.3.1 Micro arcs at glued connectors

For thin-film PV modules various techniques are used to connect the string interconnect to the cells and to each other. The most common techniques are ultrasonic soldering, soldering and conductive gluing. For conductive gluing the pressure on the connection area is an important factor for the electrical conductivity. In some cases when the pressure is not sufficient the connection loses its conductivity and the PV module loses up to 100 % of power. The here-described failure affects mainly the FF of the I - V curve, see chapter 5.2.4. Due to the contact loss micro arcs appear at the connecting areas, compare Fig. 6.3.1. To confirm that this failure occurs one may press/clamp the PV module at the suspected connection points between string interconnect and cell or string interconnect to string interconnect. The FF of the module should increase by increasing the pressure to the connection point. In the evaluated cases the failure occurs in the first year after installation. There are no known safety issues or follow-up failures. So this failure has the safety class A.

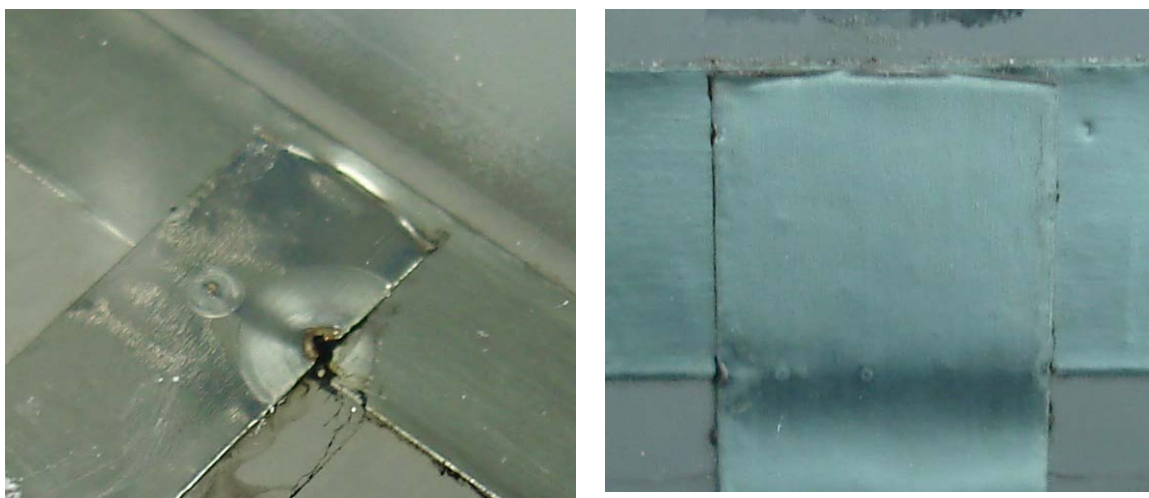


Fig. 6.3.1: Micro arcs which occur if the conductive glue on the string interconnect has an insufficient contact.

6.3.2 Shunt hot spots

The electrical performance of thin-film modules strongly depends on the quality of the deposition process. As an example Fig. 6.3.2 shows the electroluminescence image of an a-Si module, in which shunts are clearly visible as dark and bright areas. Two types of shunts must be differentiated:

- a) Type A shunts that originate from the manufacturing process.
- b) Type B shunts that originate from reverse bias operating of cells. These shunt paths are follow-up failures and are caused by shading of modules/cells in a PV system.

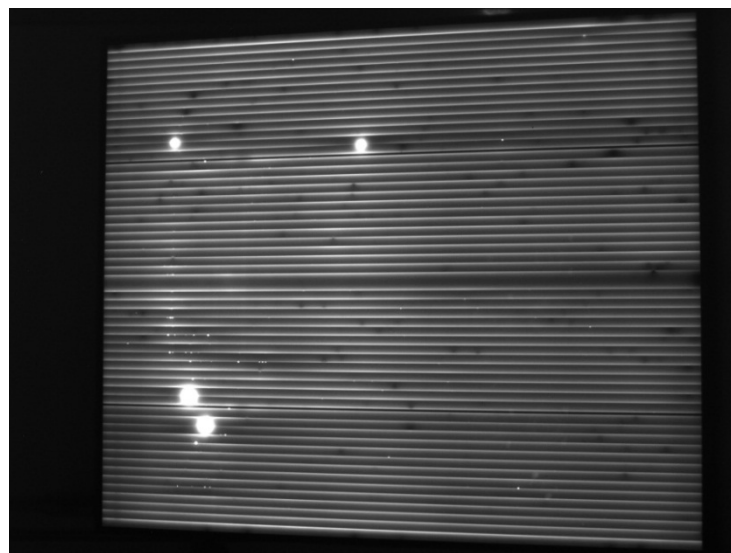


Fig. 6.3.2: Electroluminescence image of an a-Si thin-film module. Dark areas are shunts originating from the production process (type A shunt). Bright spots are severe shunt paths formed by hot-spot operation (type B shunt).

Type A shunts in thin-film solar cells can be found at typical positions in the module:

- a) At cell interconnection lines: Imperfect laser scribing process (scribe lines P1, P2, P3). The laser beam may cause crystallisation to some extent, see Fig. 6.3.3 a).
- b) Cell area: any particles or impurities generated during processing, particles on the glass surface or TCO surface roughness (pinholes).
- c) Edge of active cell area: imperfect edge insulation process (i.e. sand blasting).

Shunts in thin-film solar cells can be easily made visible by EL imaging. Alternatively lock-in thermography (see chapter 5.3.3) can also be applied as a visualisation technique for shunts. This technique enables the distinction of weak and strong electrical shunts caused by type A fabrication defects [Buerhop10].

Major subsequent failures are damage caused by reverse bias operation of thin-film cells. This condition occurs in a module when a cell is producing less current compared to the operating current of the module. Typically for thin-film modules this is caused by shading. When such a condition occurs, the affected cell or group of

cells is forced into reverse bias. Thin-film cells are extremely sensitive to reverse bias operation. Accordingly a junction breakdown will easily occur and a shunt path is formed (type B shunt) or an already existing shunt of type A carries the current. Module current will concentrate in the shunt path and power dissipation will lead to point-focal heating (hot-spot heating), that can cause severe module damage; compare Fig. 6.3.3 c).

The hot-spot operational behaviour of thin-film and crystalline silicon PV technologies under shading is very different. This is due to the fact that for thin-film modules preventive measures using bypass diodes may not be possible to limit the reverse voltage at affected cells. Table 6.3.1 gives an overview of the hot-spot behaviour of the two technologies.

Tab. 6.3.1: Comparison of hot-spot behaviour of thin-film and crystalline silicon PV modules

	Thin film PV modules	Crystalline silicon PV modules
Formation of hot-spot shunts	Cells are very sensitive to junction breakdown if operated under reverse bias voltage. Visual appearance of damages can be very different (pins, small area spots, worm-like trails). Figure 6.3.3 gives some examples of hot-spot damage observed during laboratory hot-spot testing (IEC 61646).	Cells are tolerant against reverse bias operation if protective measures with bypass diode are well designed.
Measures for prevention of hot-spot heating	Formation of hot-spot shunts cannot be avoided. The damage is clearly visible and is normally spread across the affected group of cells. Various technologies apply an additional laser scribe to divide cells into electrically isolated parts. This measure shall reduce potential hot-spot damage.	Bypass diodes are implemented in the interconnection circuit of cells. Reverse voltage at a shaded cell is limited to an uncritical value to prevent pn junction breakdown. For example, 20 serially connected cells per bypass diode can lead to reverse voltage up to approx. -12 V.
Hot-spot heating	This is a minor failure mechanism as shunts are typically spread across the cell and the module is operated at low current. Because no heat strengthened glass is used, hot-spot heating can be critical at the module edges (risk of glass breakage).	Operating temperature of a shaded cell depends on the leakage current distribution in the cell area and the current density. Even if no junction breakdown occurs overheating can occur, such as melting of encapsulant or back insulation, break-up of soldering joints or breakage of glass.

Power loss	<p>Power loss due to the formation of hot-spots is dependent on the technology and the number of affected cells. Typically a significant power loss will occur as a group of cells is affected. If no protective measures with a bypass diode between the module terminals are taken, the power loss of the system can by far exceed the power of the affected module. Power loss category E(s).</p>	<p>Power loss due to the formation of hot-spot is normally insignificant as typically a single cell is affected. Power loss category A(s).</p>
Safety issues	<p>As overheating normally does not occur, module safety is only affected for glass breakage. This may cause mechanical instability of the module and electrical shocks are possible. Safety class B(e,m).</p>	<p>Module safety is affected if overheating causes delamination or melting of polymeric materials. Safety class B(e).</p>
Other	<p>Cleaning of thin-film modules with tools producing shadow is critical as reverse bias operation of cells will occur.</p> <p>Any short-circuit operation of a thin-film module shall be avoided. Due to the production tolerance in cell performances, reverse biased operation of cells with low I_{sc} will occur and lead to module damages. In particular, this issue shall be considered by calibration labs if a continuous light source or natural sunlight is used for measurements.</p>	<p>Cleaning measures are uncritical regarding formation of hot-spots</p>

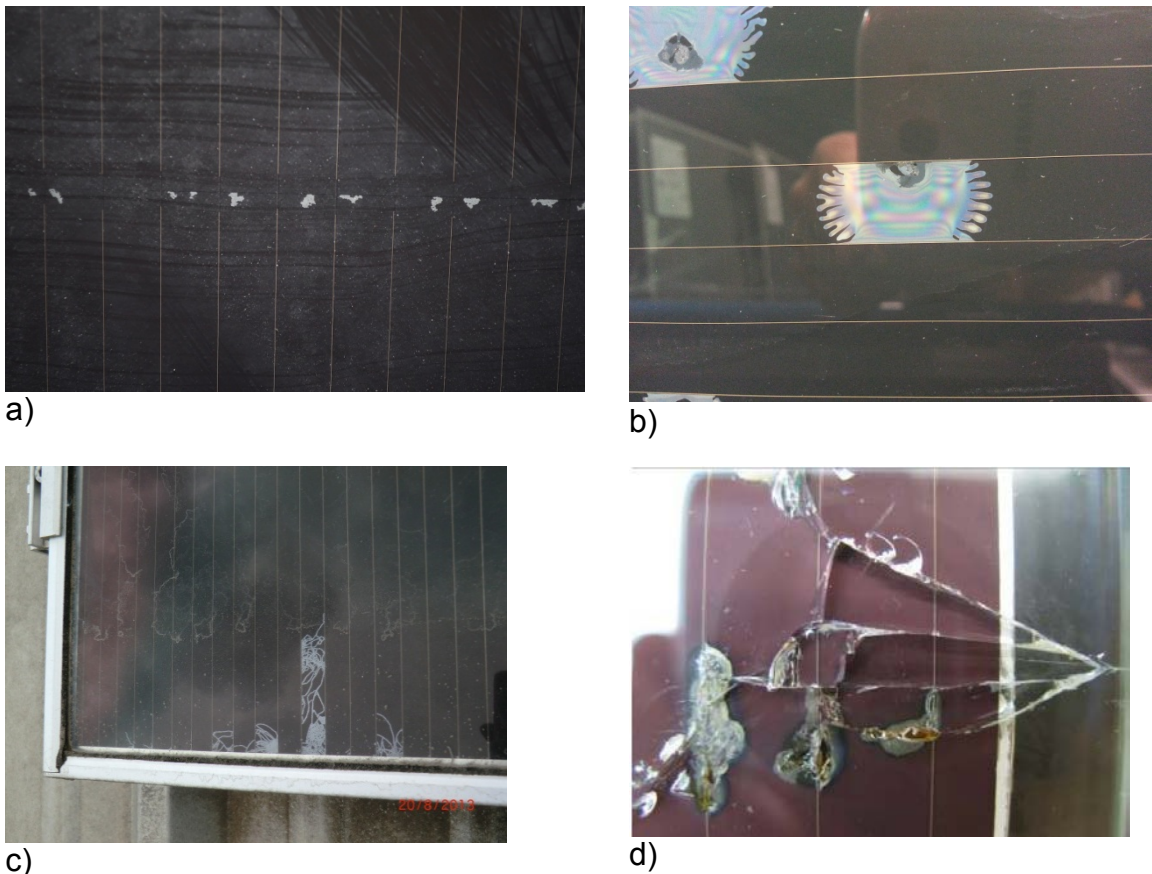


Fig. 6.3.3: Module damages and failures observed for hot-spot testing of thin-film modules in accordance with IEC 61646: a) Formation of hot-spot shunts along a laser scribing line, b) Formation of hot-spot shunts at the cell interconnection associated with large-area cell damage, c) Formation of hot-spot shunts associated with worm-like cell damage, d) Glass breakage through high temperature gradient and not tempered glass [Wendlandt11].

References

[Buerhop10] Cl. Buerhop, J. Bachmann, Infrared analysis of thin-film photovoltaic modules, *Journal of Physics* **214** (2010), p.012089

[Wendlandt11] St. Wendlandt, Hot Spot Risk Assessment of PV Modules, Investors day, PI Berlin, 28th September 2011, Berlin, Germany

6.4 Review of specific failures found in CdTe thin-film PV modules

Most current CdTe devices use glass as front and back-sheets. The front-sheet glass is used as a “superstrate” for building the stack of functional thin-films, starting with the front contact, which is a transparent conductive oxide (TCO), next CdS is deposited as the buffer layer (n-type) and then CdTe (p type). Finally the back contact is deposited. Several barrier layers are needed to prevent diffusion between

layers, see Fig. 6.4.1. After cell scribing and contact ribbon arrangement, an encapsulant like EVA is put in place. Then the edge sealing is positioned on the module border and the connector exits, before completion of the module with adding the backsheet made of tempered glass and gluing the junction-box.

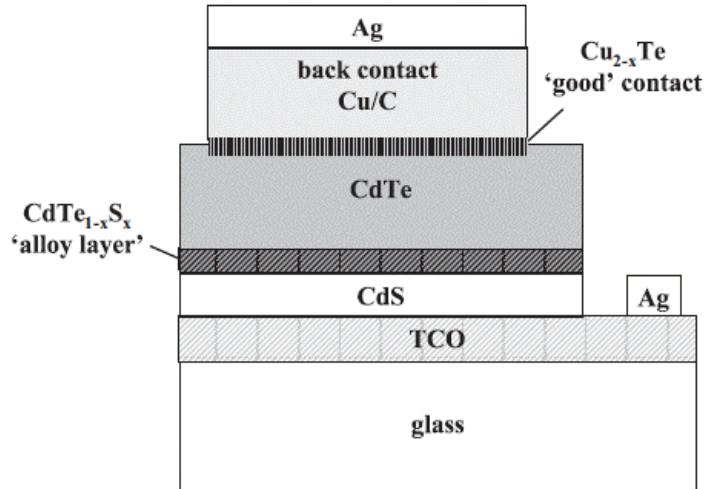


Fig. 6.4.1: Typical CdTe cell design, taken from [Visoly-Fisher03].

6.4.1 Front glass breakage

One of the inconveniences of the superstrate concept is that the front glass goes through the different processing steps, and therefore hardening or tempering is basically excluded. Indeed, thermal tempering needs an initial high temperature which would be harmful for the deposited thin-films, followed by very quick air cooling, also not compatible with the thin-film process.

Thermal tempering of 3.2 mm thick glass allows having more than 100 MPa of compressive stress [Daudeville98, Gardon80] in the front surface subjected to potential impact, while the same surface of annealed or slightly hardened glass for the CdTe module front-sheet will not exceed 1 to 5 MPa of compressive stress. Therefore, front glass breakage can occur at lower impact stress. Once the glass is broken, it is very easy to know what type of tempering or hardening was initially in the glass. Tempered glass fragments in small pieces, all over the sheet. The number of fragments per unit of surface (5x5cm²) is a good indication of the level of tempering or hardening stress.

A second reason for glass breakage comes from impact stresses on the glass edge. This type of breakage is common for CdTe modules. Frameless modules are more subject to edge breakage than framed modules. It is worth mentioning that differentiating both breakage origins need little glass breakage expertise, since the impact location can be readily found on non-tempered glass, since fragmentation is not occurring.

References

[Daudeville98] L. Daudeville, H. Carré, Thermal tempering simulation of glass plates: Inner and edge residual stresses, *Journal of Thermal Stresses* **21** (1998), pp. 667-689

[Gardon80] G. Robert, Thermal tempering of glass, *Glass science and technology* **5** (1980), pp. 145-216

6.4.2 Back contact degradation

Back contacts in commercial CdTe devices are pretty hard to conceive. The main reason for that is the energy needed to extract the charges from the CdTe. Cu, Mo, C or Ag are typically used for this purpose, but other components are needed for fine tuning, like Cd or Te based alloys.

Many studies have dealt with the stability of the back-contact [Jenkins03, Albin09]. Recently, First Solar published an introduction to the subject [Strevet12] and interesting degradation kinetics. Depending on climate, one may expect a first initial degradation of 4 to 7%, over the first one to three years, depending on climate and system interconnection factors. High temperature climates tend to accelerate this initial stabilisation.

Starting in the second year of operation and every year after, a yearly degradation rate of 0.5 to 0.7% can be expected, depending on temperature climate conditions, see Fig. 6.4.2.

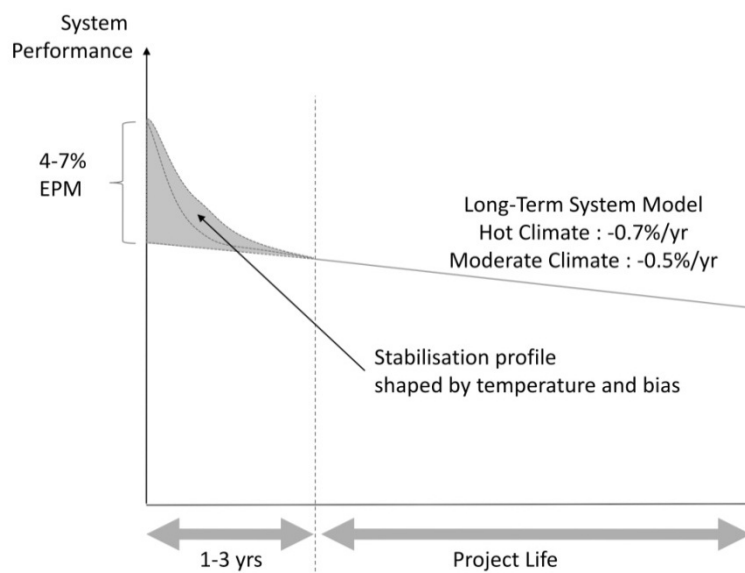


Fig. 6.4.2: Time dependence of degradation caused by Cu diffusion from the back contact into the CdTe absorber [Strevet12, modified]. EPM is the abbreviation for Engineered Performance Margin.

Both phases are attributed to grain boundary diffusion of copper from the back contact as discussed by Cahen et al. [Cahen01], see Fig. 6.4.3. Cu from the Cu-rich back-contact area migrates through the CdTe/CdS interface. The process of

diffusion can be accelerated in the laboratory by performing accelerated life tests under increased temperature and cell bias. When installed modules experience prolonged open-circuit conditions, cell bias is increased compared to the typical voltage conditions at the maximum power point and the degradation also increases.

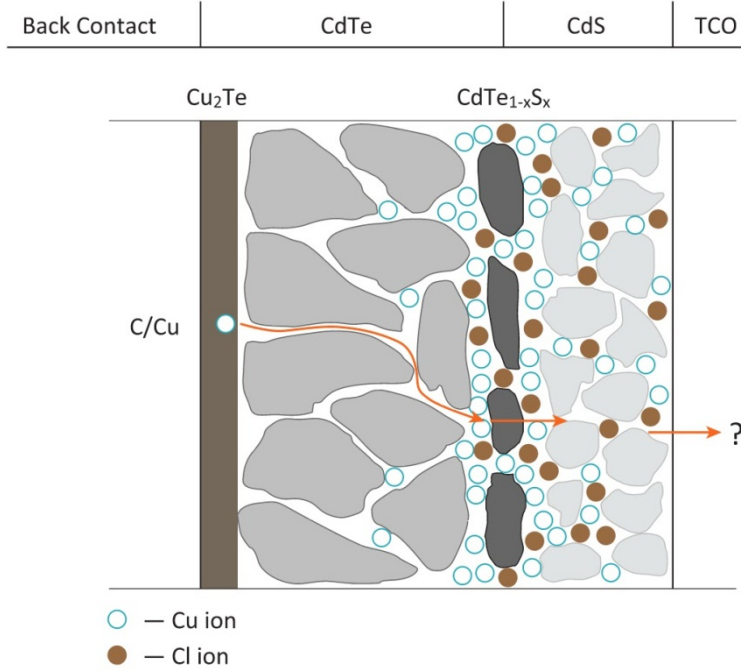


Fig. 6.4.3: Copper migration through a CdTe device [Strevet12].

By Visoly-Fisher [Visoly-Fisher03] and [Carlsson06] a second degradation mechanism is identified. Oxidation of the CdTe back surface in an O₂/H₂O containing environment creates a back-contact barrier. This barrier results in a roll-over as seen in the *I-V* curve, see Fig. 6.4.4. However, no detailed module degradation kinetics is available.

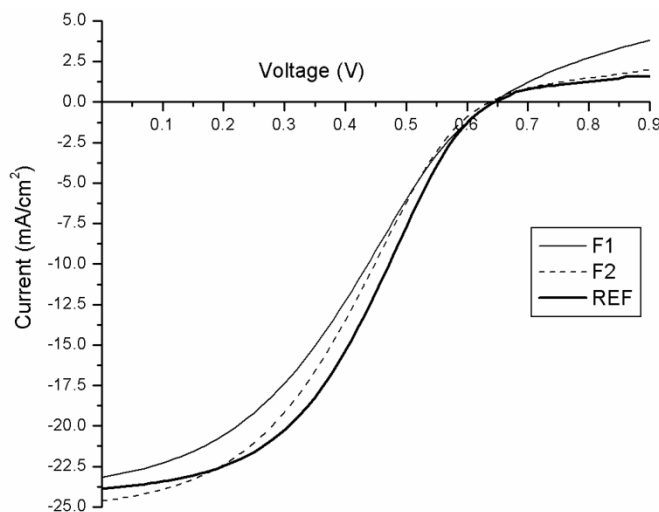


Fig. 6.4.4: Roll-over seen in *I-V* curve of CdTe devices [Carlsson06]. Both field-deployed modules F1 and F2 show a decrease in P_m and FF relative to the reference. The decrease in rollover is more pronounced for module F1.

References

- [Albin09] D.S. Albin, R.G. Dhere, S.C. Glynn, W.K. Metzger, The direct correlation of CdTe solar cell stability with mobile ion charge generation during accelerated lifetime testing, Proc. 34th PVSC (IEEE, Philadelphia, PA, USA , 2009), pp. 001903-001908
- [Cahen01] D. Cahen, G. Hodes, K. Gartsman, Overcoming degradation Mechanisms in CdTe Solar Cells, second annual report 2001, NREL/SR-520-29416, <http://www.nrel.gov/docs/fy01osti/29416.pdf>
- [Carlsson06] Th. Carlsson, A. Brinkman, Identification of degradation mechanisms in field tested CdTe modules, *Progress in photovoltaics: research and applications* **14** (3) (2006), pp. 213-224
- [Jenkins03] Jenkins, C., A. Pudov, M. Gloeckler, S. Demtsu, T. Nagle, A. Fahrenbruch, J. Sites, CdTe Back Contact: Response to Copper Addition and Out-Diffusion, NREL/CD-520-33586, 2003, pp. 900-903
- [Korevaar11] B.A. Korevaar, R. Shuba, A. Yakimov, H. Cao, J.C. Rojo, T.R. Tolliver, Initial and degraded performance of thin-film CdTe solar cell devices as a function of copper at the back contact, *Thin Solid Films* **519** (2011), pp. 7160-7163
- [Strevel12] N. Strevel, L. Trippel, M. Gloeckler, First Solar, Performance characterization and superior energy yield of First Solar PV power plants in high-temperature conditions, *Photovoltaics International*, August 2012, pp. 148-154
- [Visoly-Fisher03] I. Visoly-Fisher, K. Dobson, J. Nair, E. Bezalel, G. Hodes, D. Cahen, Factors affecting the stability of CdTe / CdS Solar cells deduced from stress tests at elevated temperature, *Adv. Funct. Mater.* **13** (2003), pp. 289-299

7 Adapting testing methods to failure mechanism for PV modules

In the following chapters not-yet-standardized testing methods are discussed and described. These methods may lead to standards in the future. A majority of TASK13 experts agree that these tests are important missing not standardized test methods to assess the reliability of PV modules in the field.

7.1 Mechanical loads caused by transport

In the IEC standards for type approval testing of photovoltaic modules (IEC 61215/61646) it is noticeable that mechanical load testing (test code 10.16) is only considering static loads. To estimate and characterize also the performance and lifetime behaviour of PV modules in regards to dynamic loads, additional tests need to be carried out under different load parameters. Various mechanical stresses in reality can be expected by transportation, wind, and thermo-mechanical loads [Reil10]. To analyse the influence under adapted simulations, a test procedure is worked out to evaluate the mechanical and electrical behaviour of different crystalline PV modules.

To estimate the influences from vibration-wise impacts on PV modules, truck transportation simulations are carried out on complete shipping stacks and single resonance frequencies of single modules are determined. Electroluminescence images and IV measurements are used as characterization tools for the identification of the induced state of mechanical and electrical degradation.

7.1.1 Determination of resonance frequencies of single PV modules

Mainly three kinds of measuring are applied to estimate the resonance frequency of a module, (1) by the decay curve determination, (2) the resonance frequency spectrum as a result of sinusoidal excitation, and (3) by a broadband noise excitation (not shown here). Because a PV module consists of several individual interlayers and attached components, such as a j-box, the vibrating behavior correlates to the character of multi-mass oscillators, which indicates the complexity of determining exact resonance frequencies by the decay curve. The modules are placed flat on the ground (sunny side up) and excited at the center, where on the opposing back, an acceleration sensor was attached. Resonances for 18 individual PV modules were found between 5.5 Hz and 18 Hz.

By using a sinusoidal excitation, the module's deflection is measured under a constant acceleration of $1g$ (g is the gravity constant) for a maximum excitation length of 5 mm between 3.5 Hz and 15 Hz. Resonances are found around 11 Hz. For this method, the modules were fixed at the short frame elements each on the opposing sides and excited by two synchronized servo-hydraulic rods. Figure 7.1.1 shows EL images indicate clearly the destruction of single cells distributed over the whole module. In this case a total power loss of 8% is induced.

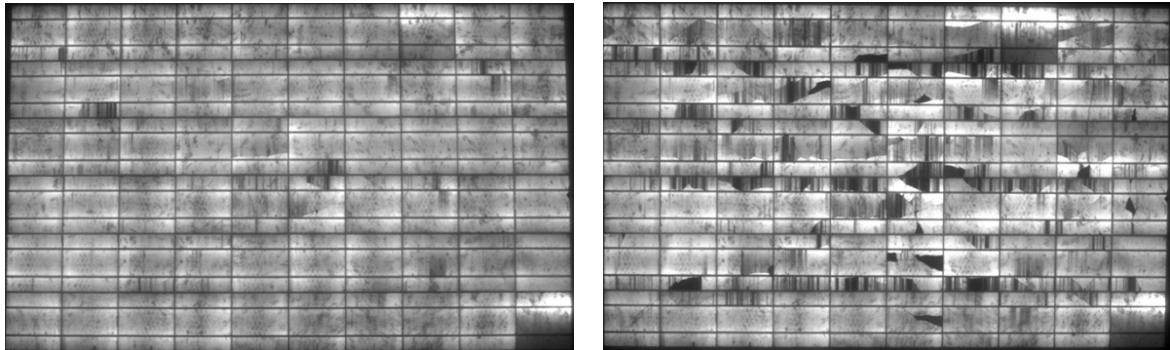


Fig. 7.1.1: Electroluminescence image before (left) and after (right) resonance search.

7.1.2 Transport and environmental testing of silicon wafer-based PV modules in a shipping stack

The simulation method used for transport testing of PV modules was adapted from standards ASTM D 4169/4728. In Appendix X1.1. of ASTM D 4728-2006 conditions for truck transportation are specified by the power spectral density (PSD)-spectrum and Assurance level II with $g_{RMS} = 0.52g$ under 180 minutes of testing

[ASTM1,ASTM2]. This standard formed the basis for the transport testing of PV modules, including the above resonance frequencies within the frequency range for vibration simulation [ASTM2]. Complete shipping stacks of products undergo in reality, depending on the road conditions, different impacts, and vibrations that have to be regarded. In terms of PV modules, the transport inside a truck is a common way to carry PV modules from the manufacturer to the distributor and end customer. Complete module stacks, with standing and flat modules, are exposed to this testing method [IEC62759-1]. As yet, several other tests were conducted with complete shipping stacks without having an indication that either standing or flat module orientation is more or less severe. The shipping stack in total has to be regarded which means that also the pallet, foil, strap bands, attachments or elements for suspension have to be evaluated. Not only the orientations of the modules is the qualifying argument.

Subsequently, ten new modules in shipping stacks (5 modules were oriented horizontally, 5 modules vertically) were exposed to different environmental tests after the transport simulation with test methods deriving from the IEC 61215 [IEC61215] and DIN EN 12210/12211 [DIN EN 12210, DIN EN 12211] test standards. The aim of these test sequences is to generate an intentionally induced stress which helps to predict failures from the pre-stress (transport) that potentially may also occur in the field. To determine the electrical and mechanical behavior of the modules in relation to the extended stress tests, thermal cycling- and dynamic wind loads were carried out. In combination with electrical measurements, such as the wet leakage and insulation test, EL images are taken as well as IV-measurements for the determination of the electrical power output.

The temperature cycles shall induce high thermo-mechanical stresses on the material compound, but also on the conducting materials and interconnections. In total, 100 cycles are carried out. To transfer single mechanical loads for the substitution of wind gusts, dynamic loads in the form of alternating impacts (0.04 Hz at ± 1000 Pa) are applied on the test samples.

After the transport simulation, single cell cracks could be detected at single modules [Reil11]. Although individual parts of the crystalline wafers are affected, the severity and impact on the generated power output at STC are marginal. Even the subsequently conducted environmental tests, as shown in Fig. 7.1.2, did not downgrade mechanical failures from the transport.

According to the development and results of the IV-measurements, the transport simulation of the two complete module stacks according to ASTM D4169/4728, resulted in changes of the electrical power at a maximum degradation of $\Delta p_{MAX} = 1.5\%$. The adjacent conducted environmental tests (thermal cycling, dynamic wind loads) induced after the transport tests a power degradation up to $\Delta p_{MAX} = 2.8\%$.

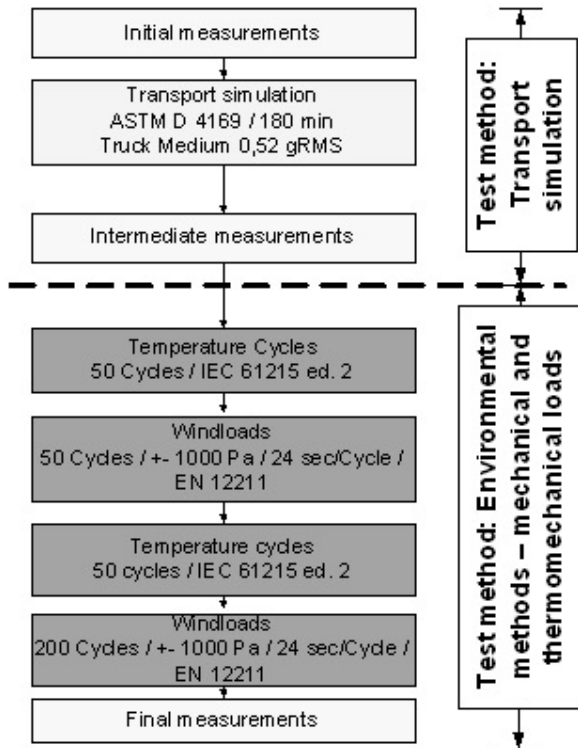


Fig. 7.1.2: Test pattern for combined transport and environmental simulation to determine the longtime behavior of the modules.

7.1.3 Transport testing of single silicon wafer-based PV modules

To assess the influence of transportation on the cracking behaviour and the module power of PV modules several PV module transports were attended. One general setup is used for the measurement of the vibrations and shocks. Figure 7.1.3 shows the positioning of the sensors during the transportation. For the logging of the acceleration of the modules two kinds of sensors are used. A calibrated standard conform acceleration logger is used to measure shocks at the pallet. However these loggers are quite heavy. To avoid an influence of the logger on the vibration of the PV modules lightweight uncalibrated data logger are used to log the vibration on the PV modules. The lightweight logger is calibrated on a shaker at 10 Hz with an effective 1g and 10g sine wave against the calibrated shaker sensors. For shock measurements the MSR 165 is used in a shock mode. In the shock mode both sensors are programmed to start logging after an acceleration of at least 3g. For vibration measurements the logger is connected to a self made remote control so that vibrations for 10 s can be measured. For that purpose the truck is followed with a car to document the route section and start the sensor by a remote control.

To assess the influence of vibrations on 60 cell multi crystalline PV modules a shaker system is used to simulate vibrations to PV modules. To measure the acceleration of the modules small calibrated acceleration sensors are used. These sensors are very lightweight so they do not influence the vibration of the PV module.

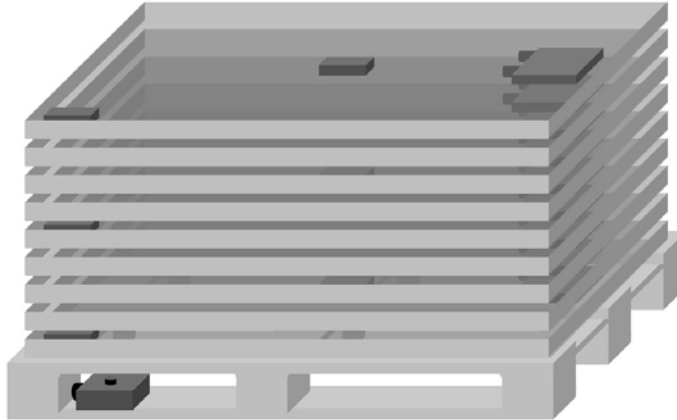


Fig. 7.1.3: The sketch shows the standard positions of the data logger for the acquisition of acceleration data in a PV module transport stack. The standard logger is screwed in the corner of the pallet. Each module in the bottom, in the middle, and in the top position is equipped with two lightweight loggers. They are taped with double sided carpet tape on the module back sheet. On the above-mentioned PV modules one logger is positioned in the module middle and one logger in the module corner. The logger in the module corner is located in the opposite corner of the junction box directly above the lightweight logger.

The shaker inclusive expander platform is free of resonance frequencies in the range of 3 Hz to 140 Hz. To test the cracking sensitivity of seven types of PV modules to transportation single PV modules are mounted on the shaker platform. The module is mounted on the shaker by rigidly fixing the PV module corners like it is in a module shipping stack.

For the counting of cell cracks the differential electroluminescence method is used which reveals even small cell cracks in multi crystalline solar cells. The EL images of the PV modules are measured in the initial state and after any test procedure at the nominal current of the module. Subsequently both EL images are compared. A high quality alignment of the two images is achieved by applying image registration techniques before comparison of both images. The method is already used in former crack analysis [Kajari11]. To characterize the direct impact of the crack on the PV module power the cracked cells are classified according to the cell crack classes A (no electrical loss over the crack), B (crack with electrical losses), and C (electrical isolating crack) as defined in Table 5.4.1.

The shock intensity and frequency for transport handling, a full loaded 40-ton truck and transport done by a shipping company with an unknown truck type are compared in Fig. 7.1.4. The results show that during the transport handling shocks with the highest intensity occur to the pallet, but not to the PV modules. The full loaded 40-ton truck transport shows as expected shocks with low intensity and low frequency. The transportation with the shipping company shows the highest shock intensity for the modules and the highest shock frequency. So we focus on that worst case transport (truck company). The maximum number of cell cracks per module after the transport of a module package is two if the manufacturer's packaging is used. There is still the uncertainty that it cannot be differentiate in the test between cell cracks caused by the transport handling and the transport itself.

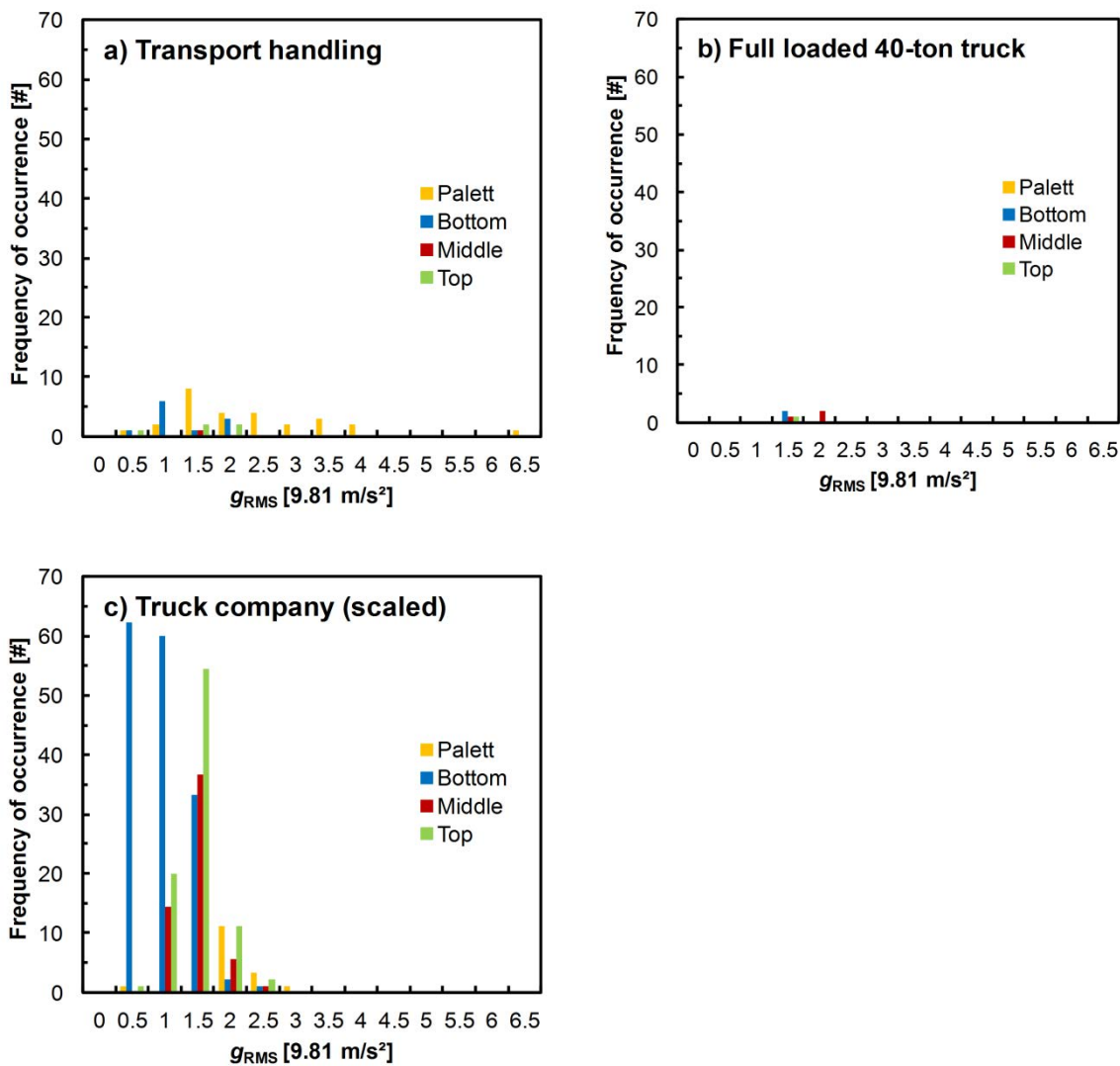


Fig. 7.1.4: Measured shock frequency for a) transport handling, b) transport in a fully loaded 40-ton truck, and c) transport with a truck company driving the same distance. Pallet, bottom, middle, and upper indicate the measurement at the module positions in the bottom, middle, and upper part of packaging unit.

To create a test PSD-spectrum for single PV modules the vibration of the PV modules is measured and a reduced PSD-spectrum is created in accordance to standard DIN EN 15433-5 [DIN EN 15433]. Figure 7.1.5 shows the reduced PSDs for the upper and bottom module in the transport stack. This analysis is done for city, country road and autobahn. The country road exhibits the highest reduced PSD-spectrum for the upper module. A comparison with existing standards shows a good agreement with the PSD-spectrum of the ASTM D4169-09 Truck Assurance Level II with $g_{RMS} = 0.52g$ [ASTM1]. The standard spectrum is used in the following to test single PV modules on a shaker.

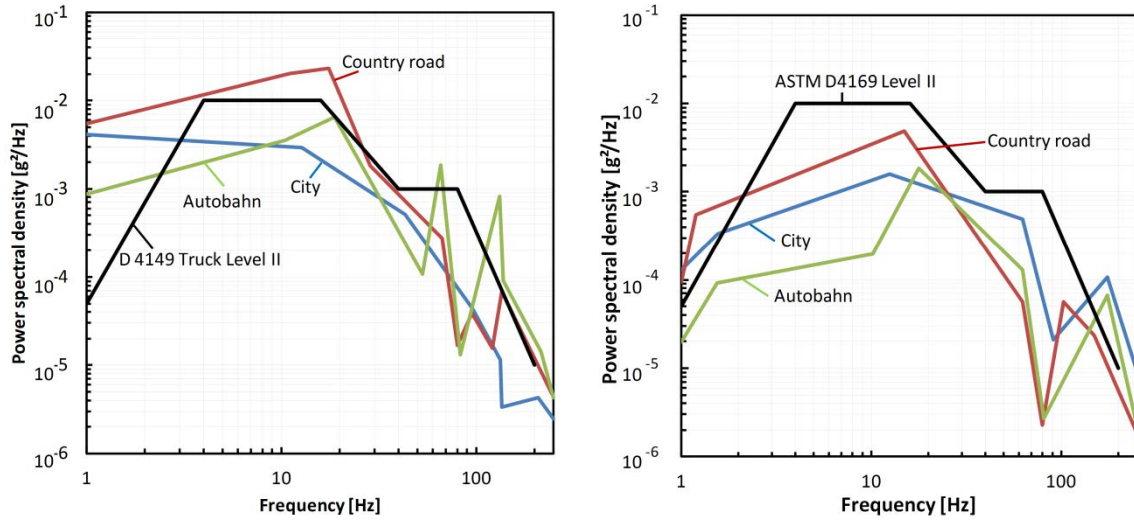


Fig. 7.1.5: Measured reduced PSDs in the corners of PV modules in a transport stack for sunny side down stacked PV modules. Left: Upper PV module in the stack, right: Bottom PV module in the stack. The reduced PSDs are created according to the standard DIN EN 154335 [DIN EN 15433]. The purple and black PSD spectra are similar standard spectra.

Seven different types of PV modules with the chosen PSD-spectrum are tested. With low mean acceleration intensity (a_{RMS}) the test is started for 15 min. For the same PV module the mean acceleration intensity for the chosen spectrum is increased by 0.98 m/s^2 again for 15 min and so on. In-between EL images are taken and the new cell cracks are counted and classified into the crack classes A, B and C. Figure 7.1.6 shows the mean cumulative cracks counted for all 7 module types.

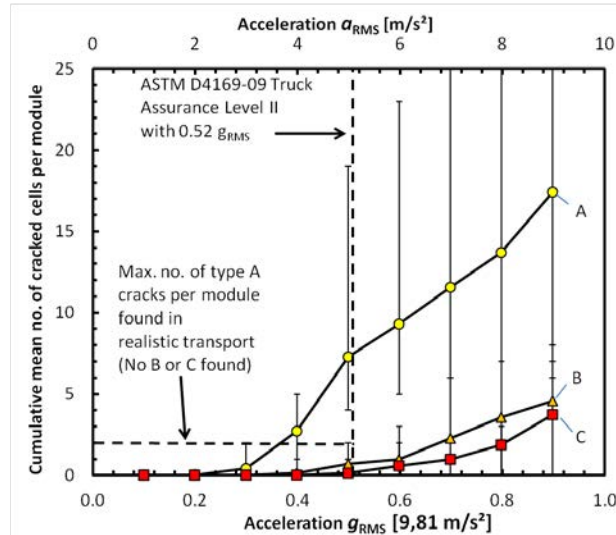


Fig. 7.1.6: The graph shows the cumulative mean number of solar cells with new cracks of type A, B, and C after a 15 min. noise test using the ASTM D4169-09 Truck PSD-spectrum [ASTM1]. The RMS acceleration amplitude a_{RMS} of the PSD-spectrum is varied in this experiment. The error bars show the maximal variance of the set of tested PV modules.

The ASTM D4169-09 Truck Assurance Level II [ASTM1] is a well fitting PSD-spectrum to simulate the vibration of PV-modules in a PV module stack during transportation. However if we look into Fig. 7.1.6 and compare the number of cell cracks found in this test at the level $g_{RMS} = 0.52g$ of the standard we find that even after 15 minutes there are many more cell cracks than found in the realistic tests. If we choose a level of maximum 2 cell cracks as found in the realistic transports we should choose a mean test acceleration intensity of 3-4 m/s² ($g_{RMS} = 0.32\text{-}0.41g$) for the test. Moreover we find a clear threshold of mean acceleration level for the first occurrence of a cell crack in all PV modules. Below 3 m/s² mean acceleration intensity no cell cracks occurs, below 4 m/s² no type B cell crack occurs, and below 5 m/s² no type C cell crack occurs. The time dependence of the cell cracking behaviour is still under investigation.

References

- [ASTM1] ASTM 4169 - Standard Practice for Performance Testing of Shipping Containers and Systems1 - 2008
- [ASTM2] ASTM 4728 - Standard Test Method for Random Vibration Testing of Shipping Containers1 - 2006[DIN EN 12210] DIN EN 12210, Windows and doors - Resistance to wind load - Classification (includes Corrigendum AC:2002), 2003-08
- [DIN EN 12211] Windows and doors - Resistance to wind load - Test method; German version EN 12211:2000, 2000-12
- [DIN EN 15433] DIN EN 15433-5, Transportation loads - Measurement and evaluation of dynamic mechanical loads - Part 5: Derivation of test specifications, Feb2008
- [IEC61215] International Electrotechnical Commission (IEC) 61215: 2nd edn, 2005. Crystalline silicon terrestrial photovoltaic modules - Design qualification and type approval
- [IEC62759-1] International Electrotechnical Commission (IEC) 62759: CDV, 26-07-2013. Transportation testing of photovoltaic (PV) modules – Part 1: Transportation and Shipping of Module Package Units
- [Kajari11] S. Kajari-Schröder, I. Kunze, U. Eitner, M. Köntges, *Solar Energy Materials and Solar Cells* **95** (2011), p. 3054-3059
- [Reil10] F. Reil, J. Althaus, W. Vaaßen, W. Herrmann, K. Strohkendl, The Effect of Transportation Impacts and Dynamic Load Tests on the Mechanical and Electrical Behaviour of Crystalline PV Modules, Proc. 25th EUPVSEC (WIP, Valencia, Spain, 2010), pp. 3989-3992
- [REIL11] F. Reil, K. Strohkendl, J. Althaus, M. Thiele, S. Raubach, G. Winkler, B. Heinzel, Development of a New Test Standard and Experiences of Transportation and 'Rough Handling' Testing on PV Modules, Proc. 26th EUPVSEC (WIP, Hamburg, Germany, 2011), pp. 3270-3274

7.2 Mechanical loads caused by snow

Several incidents in the field revealed various mechanisms of structural failure in installed PV modules under the impact of long-term snow loads as reported in chapter 6.1.4. Although IEC 61215 and IEC 61646 require mechanical load (ML) tests (10.6) at 2.4 kPa and 5.4 kPa, the qualification test sequences for modules do not yet represent potential mechanical failures in the field. The mechanical load test transfers homogeneously distributed loads such as weights in the form of simulated wind gusts or snow applications to the top and rear surfaces of the modules. As the PV modules are installed rather at a tilt angle than horizontally oriented, a completely different load characteristic arises when these products are subject to high snow loads.

Previous research and publications have already treated these aspects and lead to the introduction of these issues in the industry [Schletter08, Haeberlin07]. TÜV Rheinland has followed up by developing a testing apparatus for heavy snow load testing on PV modules subject to inhomogeneous distributed snow loads on inclined surfaces. The main goal of this research is to simulate similar snow load characteristics as to be found in several regions subject to longer-term snow loads and to define a test procedure for potentially qualifying PV modules as resistant to such environmental influences.

A test apparatus was therefore developed to transfer such factors from nature to the laboratory, where similar failures could be reproduced based on standardized load calculations from the Eurocode [EUROCODE10]. Figure 7.2.1 shows the newly developed test apparatus at TÜV Rheinland. Several test series are performed on a total of more than 20 PV modules. The apparatus allows free positioning and the application of different installation angles, along with expansions of individual loads up to 10 kPa [Reil12].

Under a load of only 15% of initial load and a two-point load application, modules already revealed weaknesses from lack of frame rigidity, with deformations of up to 5 mm. The slight deformation of the frame is also greatly influenced by the loosening of the adhesive bonds between the frame and the glass surface. With different frame designs we observed a single specimen with screws broken off from the corner clamps.



Figure 7.2.1: New test apparatus for snow load testing at TÜV Rheinland 2012: Application of load elements causing the bending of a PV module frame.

Following these initial observations, tests are carried out at a module inclination of 45° and 37° starting from an initial load of 2.37 kPa. The loads were intensified according to the calculations from EN 1991-1-3 [EUROCODE10]. Most of the damage described occurred during the first 60 minutes, either directly with deformation of the frame and breakage of the glass or with slow creepage of the adhesive over a longer period of time.

PV modules with longer frame lengths are more susceptible to easy bending and to the material contact of the back surface with supporting mounting constructions (mounting rails) compared with frames of reduced height. Electrical safety may then be affected should the insulation properties of the backsheets deteriorate due to scratches and contact of the frame with electrical conductors.

It was found that modules with silicone-based adhesives can resist loads of up to nearly 500 kg (~3 kPa) without any frame bending or permanent damage, while modules with the same dimensions and frame design but with tape-based adhesives allow frame bending and a glass breakage at lower loads between 230 kg – 360 kg (1.4-2.3 kPa). The loads were applied to 2/3 of the module length.

The work carried out at TÜV Rheinland clearly identifies the weaknesses of module types as a function of the frame and the adhesives under inhomogeneous applied snow loads. The test results will help to estimate design weaknesses (constructional dimensions, materials etc.) under such stress situations and qualify modules according to their mechanical resistance under snow loads when those modules are installed at inclined angles. The results and proposed test methodologies are being presented in future IEC standardization work.

References

[EUROCODE10] EN 1991-1-3: Eurocode 1: Eurocode 1 - Actions on structures - Part 1-3: General actions - Snow loads, 2010

[Haeberlin10] Heinrich Häberlin, Photovoltaik. Strom aus Sonnenlicht für Verbundnetz und Inselanlagen, VDE Verlag, 1st edition 2007 (in German), pp. 167-170

[Reil12] F. Reil, G. Mathiak, S. Raubach, C. Schloth, B.v.Wangenheim, K. Fotak, Experimental Testing of PV Modules under Inhomogeneous Snow Loads, 27th European PVSEC, Frankfurt, September 2012, pp. 3414 - 3417

[Schletter08] Schletter GmbH, Extended module testing procedure in accord. with RAL GZ 966,
http://www.schletter.de/files/addons/docman/solarmontage/allgemeineinformationen/Modultest_RAL_komplett_I113113GB.pdf (02.04.2013)

7.3 Testing for UV degradation of PV modules

Solar spectrum comprises different wavelength ranges. Normally, Ultra violet (UV) light (200 nm-400 nm), visible light (400 nm-750 nm) and infrared light (750 nm $\sim 1 \mu\text{m}$) cover the majority of solar spectral irradiation. The reference solar spectrum distribution AM1.5G is shown in Fig. 7.3.1. The UV light intensity in the solar irradiation varies with climate and altitude, which is about 3%-5% of the global irradiation. The UV effect on the material is very different with UV wavelength changing. The UV wavelength range is typically divided into three ranges, which are UVA (320 nm-400 nm), UVB (280 nm-320 nm) and UVC (200 nm-280 nm). Many materials can be easily influenced by long term UV irradiation such as human skin, eyes and some polymers. UV light only is a small fraction of the whole solar spectral irradiation. Nevertheless, the importance and impact of UV irradiation cannot be ignored. The annual UV irradiation dose reaches about 100 kWh/m² in lower altitude regions and more than 150 kWh/m² in plateau regions (3000 m above sea level).

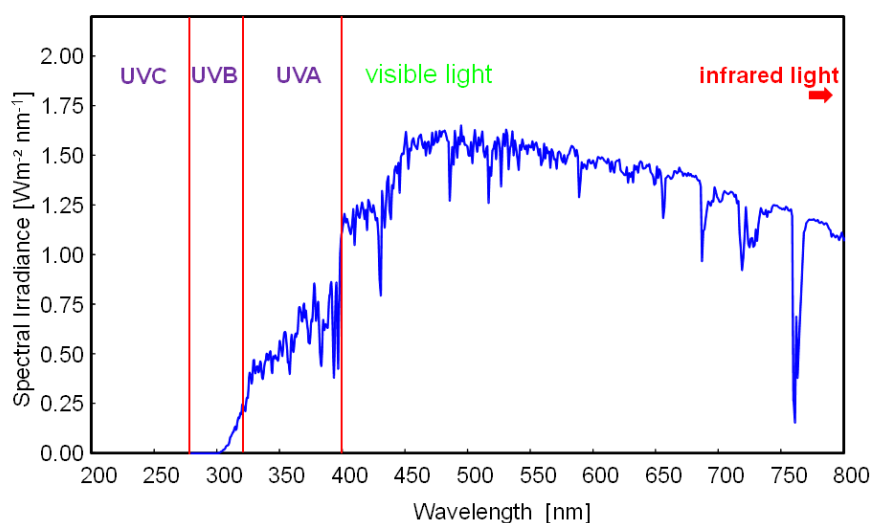


Figure 7.3.1: AM1.5 global reference spectral irradiance distribution. The solar spectrum comprises UV light, visible light, and infrared light.

7.3.1 UV preconditioning for PV modules

Photovoltaic modules operate under solar irradiation condition. Ultra violet (UV) light in the natural sunlight can cause degradation of polymeric materials that are used for encapsulation. As spectral responses of most PV devices cover the UVA and UVB wavelength ranges, it is important to confirm whether the performance of polymeric materials changes *I-V* characteristics after long-term UV irradiation.

Because outdoor UV pre-conditioning requires much more time to reflect the changing and impact on the electrical performance of modules, indoor UV light simulation methods are widely adopted by the majority of test laboratories. In order to clarify the degradation level of modules before and after UV light irradiation, presently, UV irradiation test is carried out according to standards of IEC 61215 and IEC 61646. The dose of only 15 kWh/m² comprising wavelength ranges from UVA to UVB is defined to simulate a low dose of UV light under natural sunlight condition. The peak power degradation of module should be limited to less than 5% after UV exposure.

To achieve indoor UV irradiation testing, the most important thing is the choice of the UV light source. To meet the requirement of module size and operation condition, a large area and high intensity UV light source is needed. Furthermore, the spectrum of a UV light source should be matched with the natural sunlight spectrum over the certain wavelength. A filtered Xenon light source having a spectrum as close as possible to the AM1.5G is not chosen for UV exposures, because the visible and infrared light intensity heat the modules unacceptably. It is difficult to maintain the module temperature around normal operation temperature range. Besides, the usage of xenon lamps is restricted by their high costs for consumables. Therefore, fluorescent lamps are adopted by many PV laboratories to be UV light sources. As the contribution in the visible and infrared wavelength range is small, and there is little temperature rising influence with the module, fluorescent lamps and other new type lamps are being developed to achieve accurate simulation of outdoor UV irradiation.

The PV module temperature is another important factor during outdoor long term UV light irradiation. The impact of UV irradiation not only relates to the UV dose over a certain time period, but also to the module temperature during operation. In order to obtain the worst case conditions of UV irradiation, the integral UV irradiation data in different regions should be monitored and verified around the world. The module temperature used under different environmental conditions must be combined with the UV irradiation dose. Since the module temperature accelerates the photo-degradation processes during operation, an appropriate UV acceleration level and module temperature are needed to simulate and to reflect the actual UV irradiation condition in laboratory tests. The relevant research and experiments are described by Koehl [Koehl01].

7.3.2 Performance degradation of PV modules

As the standards IEC 61215 and IEC 61646 require a total UV irradiation of 15 kWh/m^2 in the wavelength range between 280 nm and 400 nm, with 3% to 10% of the total energy within the wavelength band between 280 nm and 320 nm, the UV dose above does not reflect the actual UV irradiation condition. In order to clarify the correlation of UV dose and power degradation of a module, a typical experimental result of performance degradation of a PV module is shown in Fig. 7.3.2. Five single crystalline PV modules (different manufacturers) were chosen to be samples under test. The UV test is carried out under indoor fluorescent lamp irradiation. The UVA and UVB irradiation is adopted in accordance with IEC 61215 requirements. The UV intensity is five times that of natural sunlight and the spectral distribution is shown in Fig. 7.3.3.

The temperature in the UV chamber is in the range of 55°C to 70°C . The total UV dose of 160 kWh/m^2 simulates UV effects for different regions over a long time period. The UV irradiation dose is equivalent to one to two years outdoor weathering depending on the site.

It is clear that the output power degradation of five modules do not reach 5% after 15 kWh/m^2 UV irradiation according to the IEC 61215 standard. However, two samples of five modules show slight changes of power after 20 kWh/m^2 irradiation dose. The power degradation of one of the modules is more than 5% after 160 kWh/m^2 irradiation. This result illustrates failures of module electrical performance and polymeric materials. Two modules show an apparent trend of power degradation over long term UV irradiation.

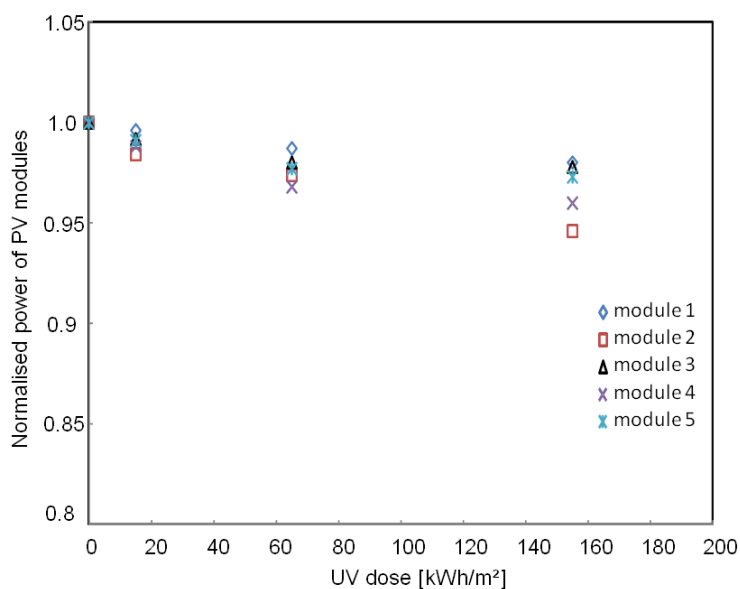


Fig. 7.3.2: The peak power degradation of monocrystalline PV modules after UV irradiation exposure under a simulated UV light source is shown. The module temperature is between 75°C and 85°C .

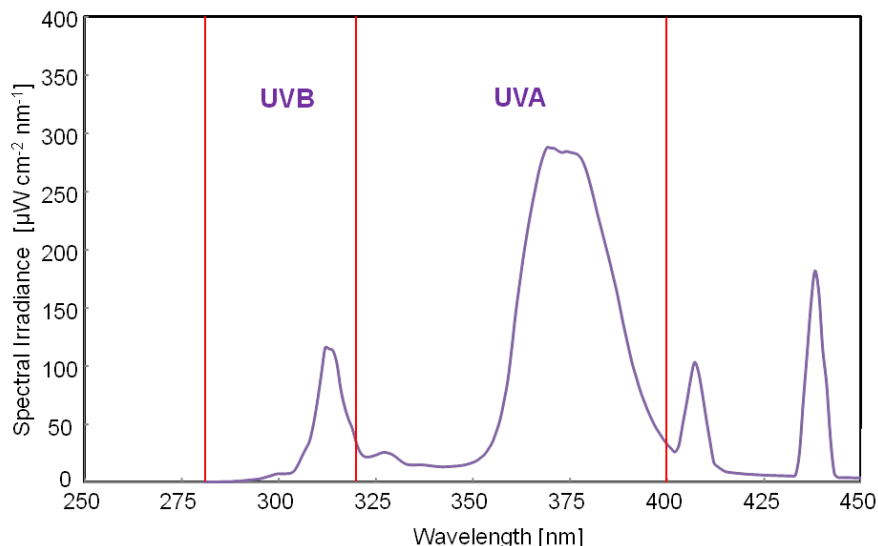


Fig. 7.3.3: The spectral irradiance distribution of a fluorescent lamp used in laboratory is shown. The UVB irradiation (wavelength range between 280 nm and 320 nm) share 9% of the total UV energy.

The IEC 61215 standard only requires total UV energy of 15 kWh/m^2 irradiation. The modules under test usually can meet the acceptance requirements under these conditions. However, some of these have the potential for power degradation of more than 5% after long term UV irradiation (150 kWh/m^2 or more). In addition, these modules often show browning of EVA materials with significant power loss. The UV testing method in a laboratory (fluorescent lamp or other artificial UV light source) provides an accelerated test to simulate long term UV irradiance under natural sunlight condition. Considering different UV irradiation and module temperature under outdoor condition, desired UV irradiation, and controlled temperature of module and environment can be set to adapt real outdoor conditions.

The polymeric materials (such as EVA) in the PV module are very sensitive to UV irradiation; the spectral response of these materials dominates the degradation speed and status. It must be noticed that the spectral irradiance distribution of a UV light source influences the effects of UV irradiation. Therefore, the UV testing results are affected not only by dose of UV irradiation, but also by spectral distribution over the wavelength range of UVA and UVB.

References

- [Koehl01] Michael Koehl, D. Philipp, N. Lenck, M. Zundel. Development and application of a UV light source for PV-module testing, Proc. Reliability of Photovoltaic Cells, Modules, Components, and Systems II 7412 (SPIE, San Diego, CA, USA, 2009) 741202; doi:10.1117/12.825939

7.4 Ammonia Testing

Quality tests of PV modules, e.g. the damp-heat test of IEC 61215 or IEC 61646 [IEC61215, IEC61646], often show corrosion at the cell connectors, soldering joints, and other metallic parts. The installation of PV modules on farm rooftops in an agricultural environment leads to extra environmental stress. Besides corroded mounting systems, power loss, and damaged seals have been found in the field [Mathiak12]. Corrosion of silicone-based adhesive sealing may result in loss of insulation effectiveness as well as adhesive strength and pose a risk to human beings and animals or to the infrastructure. Corrosive atmospheres can cause arcing possibly leading to fire. Failures found in the field must be analysed and simulated in environmental test chambers. TÜV Rheinland accordingly studied the corrosion effects on PV modules under special environmental stress. A test chamber accommodating full-size PV modules was developed and qualified for ammonia testing according to the standard IEC 62716 [IEC62716].

The relatively high corrosive effect of ammonia is well known in the case of copper alloys (brass) and polycarbonate. Both materials are used in photovoltaics: copper as a conductor in the cell interconnect ribbon and polycarbonate in polymeric blends for the plugs and the junction box.

As different test institutions have started developing their own methods of ammonia resistance testing [Petzold11], it is important to harmonize these efforts and provide a uniform scientific basis. The ammonia emission data from several pig pens was analysed. The data collected by a research project of the German institute INRES showed ammonia concentrations of up to 46 ppm [INRES06]. In a roof-integrated system such concentration levels seem realistic on the rear sides of installed PV modules. The data in this project was limited to pig pens. However chicken coops generally have an even higher ammonia concentration.

TÜV Rheinland employs a test procedure according to IEC 62716 [IEC62716] “Ammonia corrosion testing of photovoltaic (PV) modules”, which is based on the Kesternich test. Table 7.4.1 shows the test parameters of the Ammonia corrosion test procedure.

Tab. 7.4.1: Test parameters according to IEC 62716 [IEC62716]. The NH₃ concentration level is chosen based on ISO 6988 [ISO6988] using ammonia gas instead of sulfur dioxide. This standard suggests two litres of gas and two litres of water for a chamber volume of 300 litres, resulting in 6667 ppm.

Standard	IEC 62716 (draft)
NH ₃ concentration (initial)	6667 ppm
Temperature	60°C / 23°C
Relative humidity	100% / 75%
Test duration	20 days (20 cycles)
Cycles	8 h @ 60°C, 100%

The moist/humid sulphur dioxide test was developed by Kesternich (1951) to simulate the effects of acid rain. The test method is described in DIN 50018: "Testing in a saturated atmosphere in the presence of sulphur dioxide" [DIN50018]. The test has been used extensively in the automotive and construction industries and initially was performed not only with sulphur dioxide as in the present days, but also with ammonia gas, for example. In its original form metal parts are exposed in a cabinet to an elevated temperature and high humidity in the presence of sulphur dioxide. The exposure conditions may be varied to suit particular requirements set down in various standards, as for corrosion protection films, for example. The method described in DIN 50018 [DIN50018] calls for cycles of alternate exposure to a sulphur dioxide atmosphere and an ambient atmosphere. The sealed test cabinet contains a water basin placed underneath the sample. While the chamber is being filled with gas, the water basin is heated to the saturation level of 100% relative humidity. The gas mixes with the water and forms the corrosive ammonia solution. The water solution will condense on the surface of the test specimen, initiating the corrosion process. Pairs of slightly tilted modules, one sunny side up, the other sunny side down, are tested. The specimens are left in the cabinet with the mixed atmosphere of corrosive gas and water for eight hours, followed by exposure to ambient atmosphere for 16 hours. The water at the bottom of the cabinet and the gas is changed daily. The test can be performed on fully assembled products, for better simulating actual conditions.

The module performance and insulation properties are assessed before and after the exposure to ammonia atmosphere. Table 7.4.2 shows the full test sequence with visual inspection, insulation tests and power measurements which are performed in accordance with IEC 61215 Ed. 2 [IEC61215].

Tab. 7.4.2: Test paths of IEC 62716: Two modules run through the complete path. The reference module undergoes preconditioning and initial measurement only. The flowchart is analogous to that for the salt mist corrosion test according to IEC 61701 Ed.2 [IEC61701].

* Numbers correspond to test numbers in standard IEC 61215 [IEC61215].

** Code numbers correspond to module safety test (MST) numbers in standard IEC 61730-2 [IEC61730].

Ammonia Corrosion Test steps	Description
Preconditioning	Sunlight exposure for 5 kWh/m ² @ open-circuit conditions
Initial measurements	10.1* Visual inspection 10.2* Determination of maximum power MST16** Dielectric withstand test 10.15* Wet leakage test MST13** Ground continuity test
Corrosion test	Ammonia resistance test based on ISO 6988 using ammonia gas instead of sulphur dioxide
Recovery	Cleaning and recovery
Final measurements	10.1* Visual inspection 10.2* Determination of maximum power MST16** Dielectric withstand test 10.15* Wet leakage test MST13** Ground continuity test
Final measurements	Bypass diode functionality test

7.4.1 Tests performed on crystalline Si glass/foil PV modules

A series of tests are performed with 30 different small-sized PV module samples in a small chamber and with more than 20 full-size PV modules in the new chamber. Visual inspection, insulation measurements and power determination are performed before and after submitting the samples to a Kesternich-based test of varying duration. All samples pass the suggested pass criteria of a maximum power degradation of <5%. None of the samples failed the minimum requirements of the insulation or wet leakage current test. A subsequent bypass diode functionality test shows no failed diodes.

However, visual inspections do reveal corrosion and erosion effects similar to the ones found on samples taken from the field. The seal, the surfaces of the anodised aluminium frame and the anti-reflective coatings of the glass are slightly affected. Potentially critical findings are small, 10 µm pores in the backsheet (see Fig. 7.4.1 and Fig. 7.4.2), resulting from the chemical reaction of the outer layer of the backsheet with ammonia.

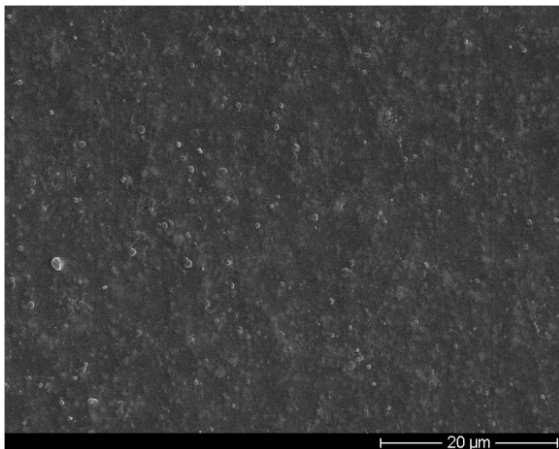


Fig. 7.4.1: Scanning electron microscopic image of a backsheet before ammonia test.

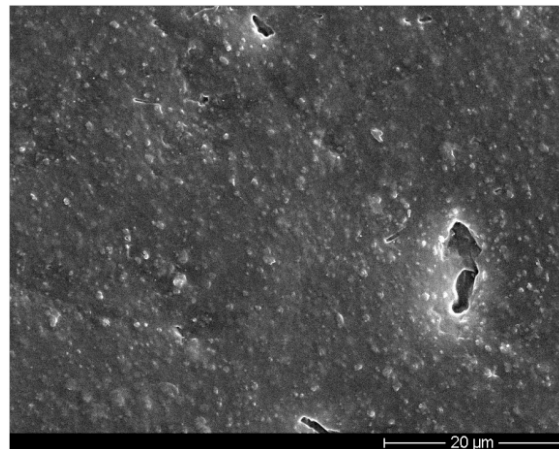


Fig. 7.4.2: Scanning electron microscopic image of a backsheet after the ammonia test. Small pores (10 µm in diameter) can be seen.

7.4.2 Tests performed on non-glass modules

The ammonia test IEC 62716 applies only to flat-plate panels. The test procedure had to be adapted for flexible non-glass PV modules, which are more than 3 metres long, with solar cells consisting of amorphous silicon glued onto a metal sheet of 1 millimetre thickness. Due to the lengths of the PV modules, performance measurements by pulsed sun simulator are not possible. Before and after the ammonia exposure the modules are exposed to light for 43 kWh/m² and maximum power is recorded continuously under light-soaking conditions. In addition, one module is wrapped in polyethylene foil during the ammonia exposure, to inhibit the effects of the aqueous ammonia solution and to allow action of the gaseous ammonia.

The difference in the effect on the corrosion of the metal sheet as described above is evident. The metal sheet of the wrapped module is less corroded. The electrical performance of the two modules is similar: During the first light-soaking phase the modules become degraded as expected. After the ammonia exposure, the maximum power decrease to 70% of the value after the first light-soaking. During the second light-soaking phase the modules recovered to 80% of the value after the initial light-soaking. These measurements suggest a negative effect of gaseous ammonia on the a-Si or TCO layer, although the error of power determination of flexible PV modules lies in the order of 10%.

In the ammonia test chamber, a serial examination on current quality modules shows no major failures inside the junction box (bypass diode test) or in insulation and performance. However, visual inspections revealed minor corrosion and erosion effects similar to the ones found on samples taken from the field. Potentially critical findings of the ammonia corrosion test were small pores 10 µm in diameter in the backsheet and the power loss of non-glass PV modules. In particular, roof-integrated PV systems on such buildings will be continuously exposed to an ammonia

atmosphere and condensation on the modules is likely. The water and gas mixture has corrosive properties and hence forms a potential risk to the durability of the PV modules and components.

Investigations are continued to benchmark ammonia concentration and test duration relative to real life effects. Studies using reference samples of polycarbonate and brass for exposure in the ammonia test chamber and on agricultural roofs are performed to determine the accelerating factor.

References

- [DIN50018] Deutsches Institut für Normung e.V. (DIN) 50018: 2013-05 Prüfung im Kondenswasser-Wechselklima mit schwefeldioxidhaltiger Atmosphäre (Testing in saturated atmosphere in the presence of sulphur dioxide)
- [ISO6988] Deutsches Institut für Normung e.V. (DIN) Europäische Norm (EN) ISO 6988:1997-03 Metallische und andere anorganische Überzüge (Metallic and other non-organic coatings - Sulfur dioxide test with general condensation of moisture), Edition March 1997
- [IEC61215] International Electrotechnical Commission (IEC) 61215: 2nd ed. 2005, Crystalline silicon terrestrial photovoltaic modules - Design qualification and type approval
- [IEC61646] International Electrotechnical Commission (IEC) 61646: 2nd ed. 2008. Thin-film terrestrial photovoltaic modules - Design qualification and type approval
- [IEC61701] International Electrotechnical Commission (IEC) 61701: 2nd ed. 2011. Salt mist corrosion testing of photovoltaic (PV) modules, Edition 2.0 2011-12
- [IEC61730] International Electrotechnical Commission (IEC) 61730-2: Photovoltaic (PV) module safety qualification – Part 2: Requirements for testing, ed. 1.0 2004-10
- [IEC62716] International Electrotechnical Commission (IEC) 62716: 2013 Photovoltaic (PV) modules - Ammonia corrosion testing, Edition 1.0 2013-06-27
- [INRES06] Institut für Nutzpflanzenwissenschaften und Ressourcenschutz (INRES), Bonn University, 2006: Forschungsbericht Nr. 138-"Biofilters in livestock farming as a relevant source of nitrous oxide and ammonia"
- [Mathiak12] G. Mathiak, J. Althaus, S. Menzler, L. Lichtschläger, W. Herrmann, PV Module Corrosion from Ammonia and Salt Mist - Experimental Study with Full-Size Modules, 27th EUPVSEC, WIP, Frankfurt, Germany, 2012, pp. 3536 - 3540.
- [Petzold11] K. Petzold, Ammonium hydroxide attacks panels, *PV Magazine 09* (2011), pp. 220-223.

7.5 Testing for potential induced degradation of crystalline silicon PV modules

Measurement for durability to system voltage stress effects in the laboratory is generally carried out by applying a high voltage, such as the module's rated system

voltage written on the nameplate, to the shorted modules leads and grounding the module exterior surfaces in any number of ways. The Jet Propulsion Laboratory [Mon84, Mon85a, Mon85b] first studied effects of system voltage in various module technologies and in crystalline silicon mini modules built for the purpose. They also studied coulombs transferred as a function of degradation and found extreme degradation in all cases after around 1 C/cm of module frame edge transferred. Significant degradation could also be seen before this threshold in some cases. Leakage current was shown to vary with module materials and increase with the temperature and humidity within these materials. Despite it being understood that ionic current is fundamental to the PID mechanism, leakage current is now considered a weak indicator of the degradation extent because of many extraneous factors that also enter into the relationship in crystalline silicon cell technology [Hattendorf12].

Stressing of modules under system voltage for the testing of PID has been carried out in the literature in the range of 25°C up to 85°C. An example of the circuit for application of the voltage stress is given in Fig. 7.5.1. Grounding has been carried out in the damp heat chamber using humidity itself adsorbed on the module surface, with wet condensed water or wet towels, with conductive mediums (pastes, jells), and with metal foils wrapped on the module faces. Leakage current may be monitored for verifying stability and reproducibility. Major considerations in the choice of testing include representation of the stresses that exist in the natural environment, reproducibility, and expediency.

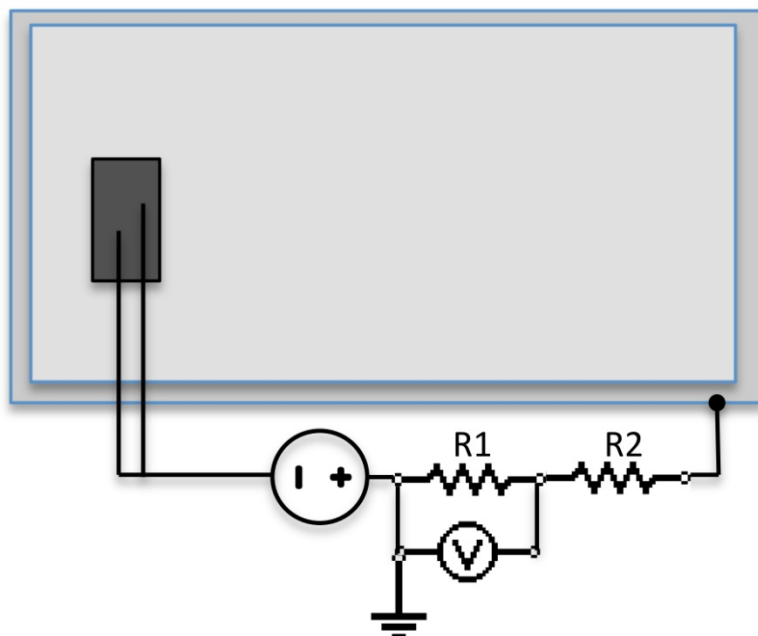


Figure 7.5.1: Application of voltage to the active layer of a PV module via the shorted leads. The leakage current in this example is monitored by a voltmeter across a resistor R1 connected to ground. The voltmeter may be protected from overvoltage by a second resistor R2 [Hacke11]. High voltage power supplies that meter the leakage current may alternatively be used.

Use of foil films to ground the module faces has been preferred by some organizations. A significant number of companies have been performing such testing for 168 h at 25°C [Schütze11]. Some have modified the test with this grounding method to higher temperatures (50°C, 60°C, 70°C) and reduced the duration of the test [Hattendorf12, Dietrich13]. There is however no systematic long term testing performed outdoors to show the equivalency to real world conditions, to understand the meaning of these various stress levels, nor information showing the lab-to-lab repeatability of these foil tests published at this time. While not a concern for testing of a given module design comparatively, use of a solid conductor film bypasses any components of the module frame design such as small edge clamps or use of rear rails, that can increase the resistive path from the active cell circuit to ground and slow the through-glass ionic current associated with PID [Hacke13a]. More work is therefore required to understand the optimum test conditions to get meaningful results and to understand any limitations of the tests by grounding with film conductors such as metal foil.

Damp heat chambers without use of any applied conductor other than the adsorbed humidity itself are also used to test for system voltage stress. Tests originating from the IEC 61215 ed. 2 condition of 85°C 85% relative humidity with application of system voltage bias exist [Koch12]; however, extended tests in this regime may lead to alternate degradation mechanisms such as silicon nitride degradation and dissolution of metal–silicon interface that contains glass frit [Hacke13b].

A module design surviving with around 5% degradation in 96h at the reduced temperature of 60°C and 85% relative humidity and -600 V system voltage was also tested in an outdoor test with -600 V applied to the cell circuit during daylight hours in Florida USA, which displays stable power for 28 months. Modules that degrade more than 5% in the 60°C stress test fail by PID in the outdoor tests [Hacke12]. Since then, other modules that fail this stress test are also found to fail by PID in the natural environment [Hacke13c].

Repeatability of the 60°C and 85% relative humidity test with two module designs was examined among five test labs. Using a sample of two modules per polarity, it was found that the test could differentiate modules with PID problems at the 5% pass/fail criterion with satisfactory consistency. Still, maintaining uniform and accurate temperature and relative humidity in the chamber, and the non-equilibrium water on the cooler module surfaces during ramp up were found to be issues that need attention [Hacke13c]. Additional testing and inter-laboratory round robin comparisons are being performed to further refine these test methods.

To simulate the diurnal stressing of the natural environment, a multiple sequence test called the Spain test was devised [Nagel12]. The procedure has an initial short-duration accelerated test phase with high voltage, temperature, and humidity applied, followed by a 24 h harsh cyclic climate with constant 85% relative humidity, a night time of low temperature, without voltage applied, and a “day time” with a bell shaped temperature curve up to 75°C, with bias voltage applied. In some cases, continued degradation is found to occur, while recovery of power is seen in other PID susceptible modules.

A worldwide recognized standard for the determination of PID does not yet exist. The above developing results are being considered to define such a common test to discern if a module is durable to stresses that the combination of system voltage, humidity, and temperature exert in bulk of the marketplace for photovoltaic modules today. IEC 62804 Ed. 1. System Voltage Durability Qualification Test for Crystalline Silicon Modules is a standard presently under development to meet this need.

References

- [Dietrich13] S. Dietrich, J. Froebel, M. Ebert, J. Bagdahn, Experiences on PID Testing of PV Modules in 2012, Proc. Photovoltaic Module Reliability Workshop (NREL, Golden, Colorado, USA, Feb. 26–27, 2013), http://www1.eere.energy.gov/solar/sunshot/pvmrw_2013.html
- [Hacke11] P. Hacke K. Terwilliger, R. Smith, S. Glick, J. Pankow, M. Kempe, S. Kurtz, I. Bennett, M. Kloos, "System voltage potential-induced degradation mechanisms in PV modules and methods for test," 37th PVSC, (IEEE, Seattle, USA, 2011), pp. 814-820
- [Hacke12] P. Hacke, Considerations for a Standardized Test for Potential Induced Degradation of Crystalline Silicon PV Modules, Proc. Photovoltaic Module Reliability Workshop (NREL, Golden, Colorado, USA, Feb. 28–Mar. 1, 2012), http://www1.eere.energy.gov/solar/sunshot/pvmrw_2013.html
- [Hacke13a] P. Hacke, R. Smith, K. Terwilliger, G. Perrin, B. Sekulic, and S Kurtz, Development of an IEC test for crystalline silicon modules to qualify their resistance to system voltage stress, submitted 28th EU PVSEC (WIP, Paris, France, 2013), 4DO.1.5
- [Hacke13b] P. Hacke, R. Smith, R., K., Terwilliger, S. Glick, D. Jordan, S. Johnston, M. Kempe, S. Kurtz, Testing and Analysis for Lifetime Prediction of Crystalline Silicon PV Modules Undergoing Degradation by System Voltage Stress, *IEEE Journal of Photovoltaics* 3 (1) (2013), pp. 246-253, doi: 10.1109/JPHOTOV.2012.2222351
- [Hacke13c] P. Hacke K. Terwilliger, S. Koch, T. Weber J. Berghold PI-Berlin, S Hoffmann, M. Koehl, Initial Round Robin Results of the IEC 62804 (draft) System Voltage Durability Qualification Test for Crystalline Silicon Modules, Proc. Photovoltaic Module Reliability Workshop (NREL, Golden, Colorado, USA, Feb., 26-27, 2013), http://www1.eere.energy.gov/solar/pdfs/pvmrw13_ps4_nrel_hacke.pdf
- [Hattendorf12] J. Hattendorf, R. Loew, W.-M. Gnehr, L. Wulff, M. C. Koekten, D. Koshnicharov, A. Blauaermel, J. A. Esquivel, Potential Induced Degradation in Mono-Crystalline Silicon Based Modules: an Acceleration Model, 27th EUPVSEC (WIP, Frankfurt, Germany, 2012), pp. 3405-3410, DOI: 10.4229/27thEUPVSEC2012-4BV.2.51
- [Koch12] S. Koch, J. Berghold, D. Nieschalk, C. Seidel, O. Okoroafor, S. Lehmann, S. Wendlandt, Potential Induced Degradation Effects and Tests for Crystalline Silicon Cells, Photovoltaic Module Reliability Workshop (NREL, Golden, Colorado, USA, Feb. 28–Mar. 1, 2012), http://www1.eere.energy.gov/solar/sunshot/pvmrw_2012.html

[Mon84] G. R. Mon, J. Orehotsky, R. G. Ross, G. Whitla, Predicting Electrochemical Corrosion in Terrestrial Photovoltaic Modules, Proc. 17th PVSC (IEEE, Kissimmee, FL, USA, 1984), pp. 682-692

[Mon85a] G. R. Mon, R. G. Ross, Electrochemical Degradation Of Amorphous-Silicon Photovoltaic Modules, Proc. 18th PVSC, (IEEE, Las Vegas, NV, USA, 1985), pp. 1142-1149

[Mon85b] G. R. Mon, L. Wen, R.G. Ross, Jr., D. Adent, Effects of temperature and moisture on module leakage currents, Proc. 18th PVSC (IEEE, Las Vegas, NV, USA, 1985), pp. 1179-1185

[Nagel12] H. Nagel, R. Pfeiffer, A. Raykov, K. Wangemann, Lifetime warranty testing of crystalline silicon modules for potential-induced degradation, 27th EUPVSEC, (WIP, Frankfurt, Germany, 2012), pp. 3163-3166, doi:10.4229/27thEUPVSEC2012-4DO.6.4

[Schütze11] M. Schütze, M. Junghänel, O. Friedrichs, R. Wichtendahl, M. Scherff, J. Müller, P. Wawer, Investigations Of Potential Induced Degradation Of Silicon Photovoltaic Modules, Proc. 26th EUPVSEC (WIP, Hamburg, Germany, 2011), pp. 3097-3102, DOI: 10.4229/26thEUPVSEC2011-4CO.5.4

7.6 Extended IEC testing in the lab

The product qualification of c-Si PV modules refers to the IEC 61215 test standard. The stress tests defined in the test programmes are short-duration accelerated tests performed at stress levels higher than the operating stress level in order to facilitate the occurrences of failure in a timely manner. The qualification tests constitute a minimum requirement on reliability testing and demonstrate (within reasonable constraints of cost and time) the ability of the module to withstand prolonged exposure in so-called general, open-air climates.

The general view is that the primary goal of IEC qualification testing is to identify the initial short-term reliability issues in the field. As a consequence, mainly early product failures are detected. The IEC standards allow no conclusions to be made concerning the actual lifetime expectancy for qualified products, however. It is merely noted that the lifetime depends on the design, the environment, and the conditions under which the product is operated.

However it is useful to know whether an expanded test leads to realistic failures or just to failures that are never found under realistic conditions. Therefore, we show test results of extended standard tests and relate these to field experience in the following chapters.

7.6.1 Test results from extended testing

With qualification testing, the tests showing the largest impact on PV module performance are temperature cycle tests and tests in which the temperature and humidity act on the modules. Figure 7.6.1 shows the change of output power of 8 modules of the same type after 1000 h, 1500 h, and 2000 h of damp heat. Obviously

the degradation of these modules does not proceed similarly. This is an important issue when it comes to correlate degradation by theoretical models as, for example, using the Arrhenius equation. The differences in the degradation behaviour of different types of modules impede the prediction of PV module degradation from qualification test results.

However, even after exposure to 2000 h of damp-heat, which is twice the time required by IEC 61215, seven out of eight modules showed less than 5% power degradation. The degradation though was clearly measurable and could serve the comparison with the degradation outdoors.

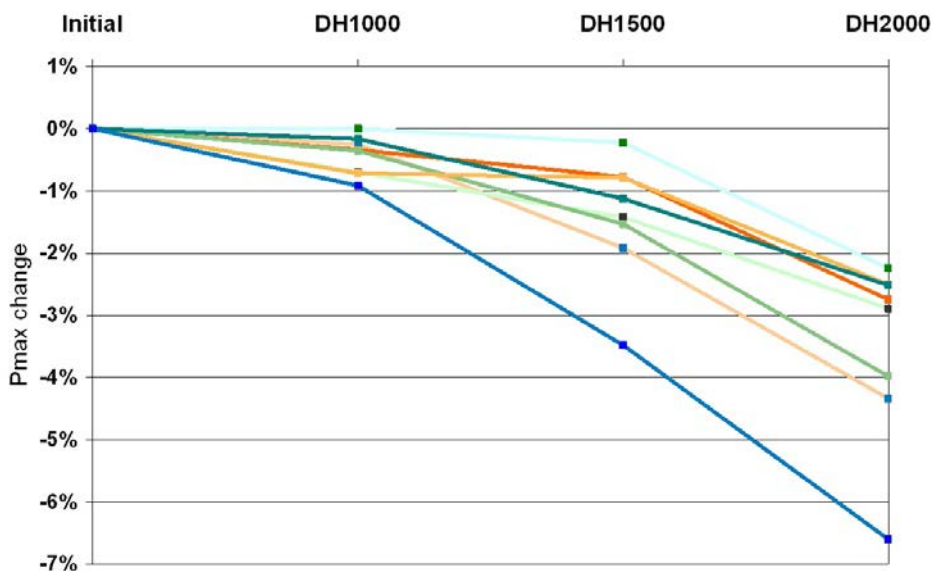


Fig. 7.6.1: Change of output power of 8 PV modules of same type after 1000 h, 1500 h, and 2000 h damp-heat test at 85°C/85%RH [Herrmann11].

After 2000 h of damp heat the power degradation of another module amounted to 4%, as is also visible in the EL image in Fig.7.6.2. A further extension of the damp heat test to 3000 h causes severe cell degradation. The output power of the module drops by 28%. In the EL image the outer parts of the cell are completely dark. Evidently the moisture diffused through the rear side of the module in the gaps between the cells caused cell corrosion on the front side of the cell. Comparing such results with outdoor degradation behaviour, we find the module obviously overstressed after 3000 h since modules featuring such intense degradation by water vapour ingress can hardly be found in the field even after decades of exposure. Nevertheless, despite one single module which showed some browning (compare 5.3.1) neither delamination as described in chapter 5.3.5 and 5.3.6 nor loss of adhesion strength could be observed.

An extension of the thermo-cycling (TC) test leads, with respect to loss of output power, to comparable results, although the type of stress is different. Figure 7.6.3 shows the results of 7 crystalline modules manufactured by different companies and undergoing TC tests for 200, 400, 600, and 800 cycles, with re-measurement after each subtest. Again, at twice the stress, the power loss for all modules remained within the margins set by IEC 61215. Another 200 cycles were needed in order to

observe significant degradation with one of the modules. Three modules showed less than 5% power degradation even after 800 cycles.

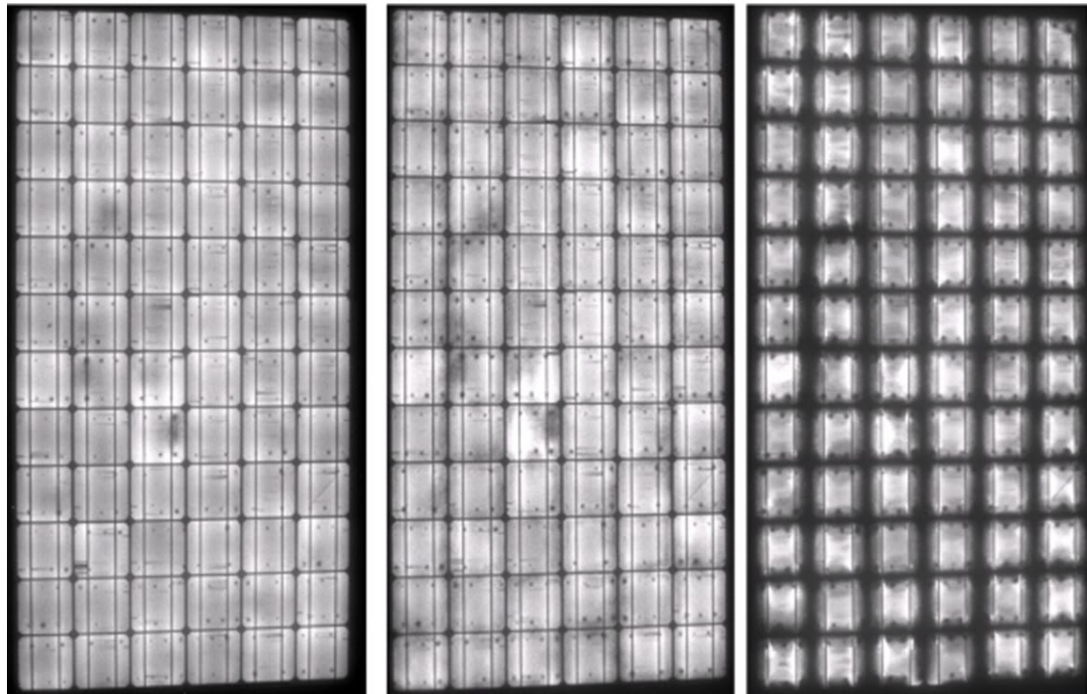


Fig. 7.6.2: Electroluminescence images of a module after 1000 h, 2000 h, 3000 h of damp heat (from left to right) at 85°C/85%RH, featuring -1%, -4%, and -28% degradation of output power, respectively [Herrmann11].

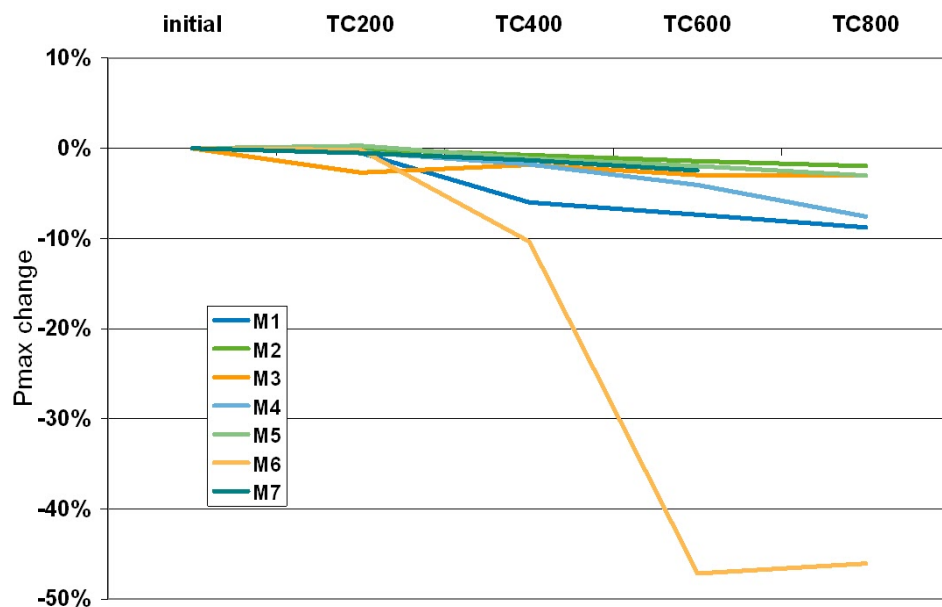


Fig. 7.6.3: Change of power of 7 modules of different types after 200, 400, 600, and 800 temperature cycles [Herrmann11].

Frequent changes in temperature are known to wear out the cell interconnections. Temperature cycle tests reveal weak connections within modules. Figure 7.6.4 shows EL images of modules after 200, 400, and 600 cycles, respectively. With an

increasing number of cycles and after 200 cycles, an increasing number of busbars become disconnected, as is evident from the dark areas. While some of these disconnections may not last permanently (see red markers), in general the output power will decrease as the number of cycles increases. The result is further degradation. Due to the inhomogeneous current distribution between cells with broken busbars, high temperatures or even hot spots can occur. Loose contacts can also cause arcing.

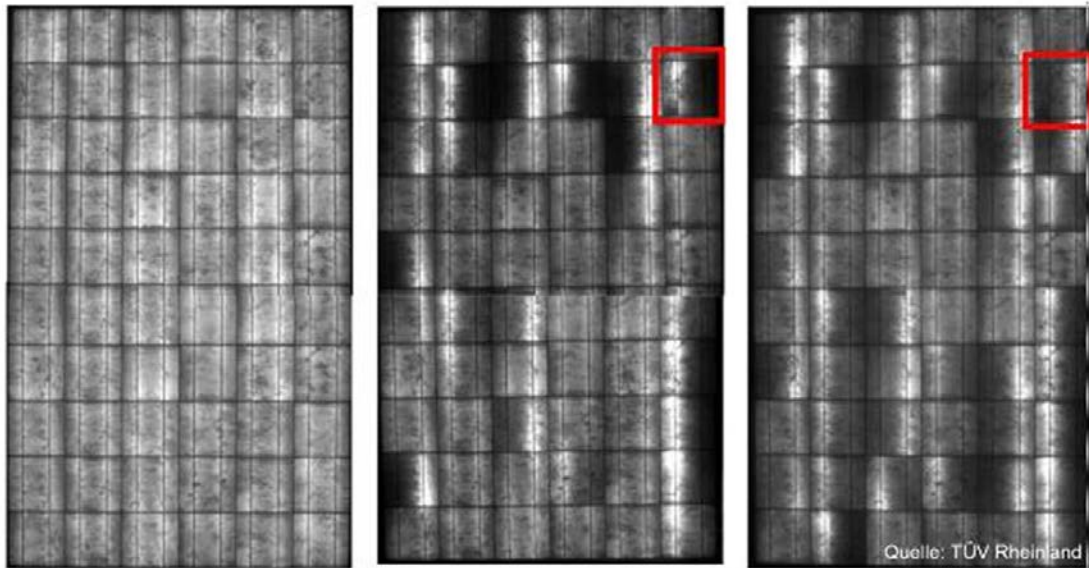


Fig. 7.6.4: Electroluminescence images after 200, 400, and 600 temperature cycles, as described in IEC 61215. Dark areas indicate disconnection of busbars that may not always be permanent, see red markers [Herrmann11].

7.6.2 Accelerated testing and field experience

The expressiveness of such extended stress tests however is impaired by the questionable correlation to the real impact occurring in the field. As a result, extended stress tests might overstress the modules generating degradation that would not occur in that particular manner in the field.

Numerous studies have shown that failures of cell interconnect ribbons and/or solder bonds can cause failures of silicon modules [Degraaff11, Kato02, Munoz08, Wohlgemuth93]. Thermal cycling with injected current has been demonstrated to identify design flaws leading to early failure of the modules, but the 200 cycles typically used in qualification testing have been reported to be inadequate for giving confidence in the warranty of ~ 20 years [Wohlgemuth05, Bosco10]. While there is evidence that longer thermal cycling would be useful toward reducing field failures within the warranty period, it is not clear how many cycles are needed and/or whether the damage caused by thermal cycling has a significant variation with climate. The addition of hundreds more thermal cycles adds substantial test time, so other strategies for increasing the damage rate are useful to explore. As noted above, it is possible to fabricate modules that can survive > 800 cycles, see Fig. 7.6.3.

When attempting to demonstrate that a module design has greater durability, a common practice has been to increase the damp heat test to 2000 h, 3000 h or more. However, 3000 h has been reported to cause failures that have not been reported in the field. E.g. Fig. 7.6.2 shows a detachment of the silver front side fingers of the solar cell which has not yet been reported from the field. Thus, it is unclear whether the application of 3000 h of damp heat to a module with a breathable back sheet has any value toward predicting life in the field. However, modules that attempt to keep all moisture out by using two sheets of glass with an edge seal age in a very different way and a recent paper estimates that 3000 h may be appropriate for quantifying the movement of moisture through the edge seal to simulate close to a 20-year in-field exposure [Kempe12]. Nevertheless, the value of 3000 h of damp heat testing as a predictor of field performance has not yet been reported.

In addition to the exploration of the effects of longer thermal cycling and damp heat, there has been substantial discussion of the need for longer UV exposure. The UV exposure used in the qualification tests represents only a small fraction of the expected UV dose for a module throughout its lifetime. Historically, EVA manufacturers have optimized their formulations by applying longer UV exposures, but these types of tests have not been adopted into the standard qualification tests. According to one review, encapsulant discolouration is seen to some extent in the majority of long-term silicon installations [Jordan12]. Nevertheless, it can be difficult to correlate accelerated test results on encapsulant materials with outdoor test results because of the complexity of some of the degradation mechanisms.

References

- [Bosco10] Nick Bosco, Sarah Kurtz, “Quantifying the Weather: an analysis for thermal fatigue”, Proc. PV Module Reliability Workshop (NREL, Golden, CO, US, May 23, 2011), http://www1.eere.energy.gov/solar/pv_module_reliability_workshop_2010.html.
- [DeGraaff11] D. DeGraaff, R. Lacerda, Z. Campeau, Degradation Mechanisms in Si Module Technologies Observed in the Field; Their Analysis and Statistics, Proc. PV Module Reliability Workshop (NREL, Golden, Golden, USA, 2011) http://www1.eere.energy.gov/solar/pdfs/pvmrw2011_01_plen_degraaff.pdf
- [Herrmann11] W. Herrmann, N. Bogdanski, Outdoor weathering of PV modules — Effects of various climates and comparison with accelerated laboratory testing, 37th PVSC, (IEEE, Seattle, USA, 2011), pp. 2305 - 2311, doi: 10.1109/PVSC.2011.6186415
- [Kato02] K. Kato, “PVResQ!”: A Research Activity on Reliability of PV System from an user’s viewpoint in Japan, Proc. Optics + Photonics 8112 (SPIE, San Diego, California, USA, 2011), 811219
- [Kempe12] M.D. Kempe, M.O. Reese, A.A. Dameron, D. Panchagade, Long term performance of edge seal materials for PV applications, Proc. SPIE Optics + Photonics, Reliability of photovoltaic cell, modules and systems V, OP206 (San Diego, CA, USA, August 12-16, 2012)

[Munoz08] J. Munoz, E. Lorenzo, F. Martinez-Moreno, L. Marroyo and M. Garcia, An Investigation into Hot-Spots in Two Large Grid-Connected PV Plants, *Prog. Photovolt: Res. Appl.* **16** (8) (2008), p. 693–701

[Wohlgemuth05] J.H. Wohlgemuth, D. W. Cunningham, A.M. Nguyen and J. Miller, Long Term Reliability of PV Modules, 20th EU PVSEC, (WIP, Barcelona, Spain, 2005), p. 1942

[Wohlgemuth93] J.H. Wohlgemuth, R.C. Petersen, in Reliability of EVA modules, Proc. 23rd PVSC (IEEE, Louisville, KY, USA, 1993), p. 1090-1094

8 Conclusions

PV modules may degrade or fail in many ways. While the types of failures are highly dependent on the design (or failure of the design) of the PV module and on the environment in which the module is deployed, statistical evaluation of what has been reported can help understand some of the most common failures. Hasselbrink recently summarized data for returns from a fleet of >3 million modules, from ~20 manufacturers [Hasselbrink13]. The study found that 0.44% of the modules were returned after an average deployment of 5 years, with the majority (~66%) of these returned because of problems with interconnections in the laminate (e.g. breaks in the ribbons and solder bonds). The second most common reason (~20%) for a return was because of problems with the backsheet or encapsulant (e.g. delamination). Thus, the vast majority of the returns were associated with failures that can usually be identified visually, though there could be bias in this data since modules with no visual defects would be harder to identify by the customer.

Modules that have failed and been returned to the manufacturer are not the only thing to be considered; modules are usually observed to degrade slowly in the field. Figure 8.1 summarizes ~400 reports in the literature of degradation rates for silicon modules [Jordan13]. The degradation is dominated by a loss of short-circuit current. In most cases, the researchers observed that this decrease in short-circuit current is associated with discolouration and/or delamination of the encapsulant material. Thus, both statistics on returns of modules and statistics on slow degradation appear to be correlated with mechanisms that can be observed visually. Although there is much value in more sophisticated investigations, the simplicity of collecting visual observations allows collection for a very large set of modules, enabling us to correlate the environment with the types of changes that are occurring. We propose to collect the data in a systematic format, greatly simplifying the analysis.

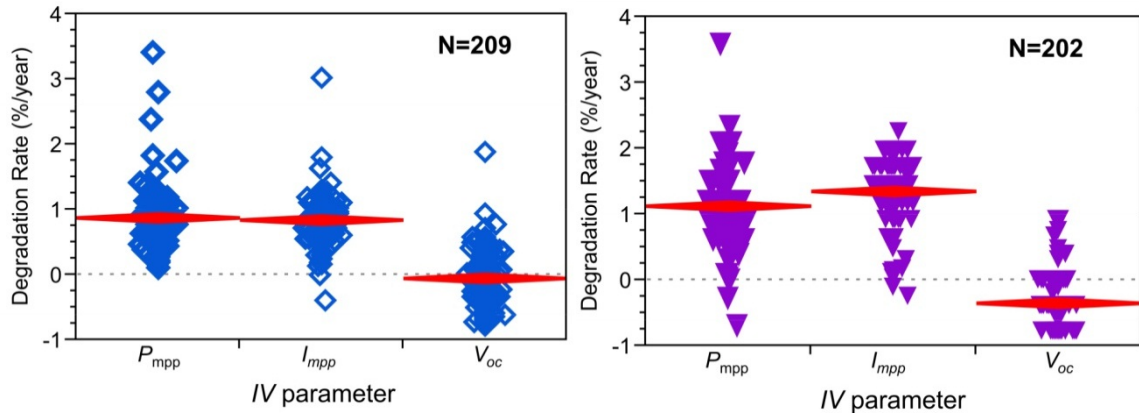


Fig. 8.1: Degradation rates of the maximum-power-point values for power, current and voltage for monocrystallineSi (left), multicrystalline-Si (right). As a guide for the eye, dashed lines indicate no degradation. A negative degradation implies improvement. The symbol N represents the number of PV modules of the statistic [Jordan13].

A standardized method and format for collecting the data are developed and multiple sets of data were contributed by IEA Task 13 members. Refinements were made to the standardized format to clarify ambiguities in definitions. Analysis of the data sets that were shared found that an additional field is needed to define how the sample set was obtained. For example, Tab. 8.1 shows highly variable results depending on the module selection process. The data from Tab. 8.1 is populated based on the top five most commonly observed defects within each data set.

Tab. 8.1: Summary of data sets obtained from Task 13 members using a variety of selection methods.

	I S F H 1	I S F H 2	T U V	I N E S	N R E L 1	N R E L 2	N R E L 3	N R E L 4	A I T 1	A I T 2
# modules	33	10	4	3	32	18	18	16	38	5
BACKSHEET										
Backsheet- dented/cracked/ scratched/delaminated	58%	100%	75%						24%	
Backsheet- delamination								100%		
Backsheet- discolouration				50%						
Backsheet chalking								100%		
WIRES/CONNECTORS/J-BOX/FRAME										
Wires degraded	45%	80%								
Connectors- degraded				33%						

J-box weathered	30%				100%				
Frame damage		100%	25%	33%				11%	
Frame adhesive issues									40%
Frame ground corrosion							100%		
GLASS/EDGE SEAL									
Scratches/chips in glass					81%				
Glass cracks							6%		
Glass-milky discolouration								8%	40%
Frameless edge seal degraded					100%				
Soiling	94%							21%	
METALLIZATION									
Gridline issues							78%		40%
Busbars misaligned				33%					
Cell interconnect- discolouration							100%	100%	
String interconnect-discolouration					100%			100%	
SILICON									
Silicon-discolouration	30%							39%	100%
Silicon- embedded foreign body		30%							
Silicon- delamination							100%		60%
Silicon- damage burns							6%		
THIN FILM									
Thin-film- cracking				33%					
Thin-film- delamination				33%					

If the proposed visual inspection tool becomes widely adopted, a variety of data mining and analysis techniques may prove useful for understanding module degradation and failure. Basic analyses will include identification of the most frequently observed defects among a set of identical modules in a single location. An extension of this type of study will seek to identify which defects are more likely to be associated with decreased performance ratio and which defects are more likely to be benign, similar to the approach of Sanchez-Friera et al. [Sanchez-Friera11]. More comprehensive studies will compare data from similar module types in a single location over time [Dunlop06, Ishii11] or over multiple locations for the same amount of field exposure time. Comparison within and between these kinds of studies will be greatly simplified by using the data collection method developed here. Degradation issues that arise from environmental exposure may be correlated with climate zone through the linkage of defect frequency with latitude and longitude data. Statistical

analysis of very large sets of data may reveal more subtle connections between specific defects or groups of defects and their correlation with the electrical performance characteristics of modules. This type of data is currently in limited supply, though analytical frameworks for assessing reliability based on field degradation studies are in development [Vazquez08]. If visually observable defects can be correlated or conclusively linked with the measured electrical performance degradation rates, visual inspection may provide a relatively low impact method for assessing which PV installations may be more likely to see accelerated degradation based on the frequency and types of defects that develop.

During the past Task 13 project phase we recognise that the topic “Characterising and Classifying Failures of PV Modules” is an important ongoing topic in the field of PV research. The current review of failure mechanisms shows that the origin and the power loss assessment of some important PV module failures is not yet clear (snail tracks, cell cracks) or the community is stuck in the question of how to test for a specific failure (potential induced degradation, tests for the assessment of cell cracks). Furthermore, despite the fact that a defective bypass diode or a defective cell interconnect ribbon in the PV module might lead to a fire, there is very little work done to detect these defects in an easy and reliable way in the system. But, there are currently groups working on those topics to overcome these challenges. Therefore, we suggest to continue the review on failures of photovoltaic modules in an extention of the TASK 13 project.

References

- [Dunlop06] E. D. Dunlop and D. Halton, The performance of crystalline silicon photovoltaic solar modules after 22 years of continuous outdoor exposure, *Progress in Photovoltaics* **14** (2006), pp. 53-64, doi 10.1002/Pip.627
- [Hasselbrink2013] E. Hasselbrink, M. Anderson, Z. Defreitas, M. Mikofski, Y.-C. Shen, S. Caldwell, A. Terao, D. Kavulak, Z. Campeau, D. DeGraaff, Site Data Validation of the PVLife Model Using 3 Million Module-Years of Live, Proc. 39th PVSC (IEEE, Tampa, FL, USA, 2013) in press
- [Ishii11] T. Ishii, T. Takashima, and K. Otani, Long-term performance degradation of various kinds of photovoltaic modules under moderate climatic conditions, *Progress in Photovoltaics* **19** (2011), pp. 170-179, doi 10.1002/Pip.1005
- [Jordan13] D. C. Jordan, J. H. Wohlgemuth, and S. R. Kurtz, Technology and Climate Trends in PV Module Degradation, Proc. 27th EUPVSEC (WIP, Frankfurt, Germany, 2013), to be published
- [Sanchez-Friera11] P. Sanchez-Friera, M. Piliougine, J. Pelaez, J. Carretero, and M. S. de Cardona, Analysis of degradation mechanisms of crystalline silicon PV modules after 12 years of operation in Southern Europe, *Progress in Photovoltaics* **19** (2011), pp. 658-666, doi 10.1002/Pip.1083
- [Vazquez08] M. Vazquez and I. Rey-Stolle, Photovoltaic module reliability model based on field degradation studies, *Progress in Photovoltaics* **16** (2008), pp. 419-433, Doi 10.1002/Pip.825

ANNEX A: Module condition checklist

Documentation of module condition for field exposed modules

Date _____ Name of data recorder _____
Location _____
Latitude _____ Longitude _____ Altitude _____

1. SYSTEM DATA

System design: single module multiple modules (a.) unknown

(a.) Multiple module system: not applicable

Module location/number in a series string (from negative): _____

of modules in series (string) _____ # of strings in parallel (array) _____

of bypass diodes _____ # of modules per bypass diode _____

System Bias: open circuit resistive load max. power tracked
short-circuit unknown

System Grounding: grounded (a.) not grounded unknown
(a.): negative positive centre of string unknown

BEGIN INSPECTION AT BACK SIDE OF MODULE

2. MODULE DATA

Technology: mono Si multi Si a-Si CdTe CIGS/CIS
other: _____

Certified: unknown UL 1703 UL 61730 IEC 61215 IEC 61646
IEC 61730 other: _____

Estimated deployment date: _____

Photo taken of nameplate: yes no

Manufacturer _____

Model # _____

Serial # _____

Installation Site/Facility Serial # _____

Width _____ cm Length _____ cm

Nameplate: nameplate missing

P_{max} _____ V_{oc} _____ J_{sc} _____

System voltage _____ V_{max} _____ I_{max} _____

Bypass diode, If _____

Series fuse _____

3. Rear-side Glass: not applicable applicable

Damage: no damage small, localized extensive

Damage type (mark all that apply):

- crazing or other non-crack damage shattered (tempered)
shattered (non-tempered) cracked (a.) chipped (b.)

(a.) Cracks (#): 1 2 3 4-10 >10

Crack(s) start from: module corner module edge cell junction box
foreign body impact location

(b.) Chips (#): 1 2 3 4-10 >10

Chipping location: module corner module edge

4. Backsheet: not applicable applicable

Appearance: like new minor discolouration major discolouration

Texture: like new wavy (not delaminated) wavy (delaminated) dented

Material quality chalking: none slight substantial

Damage: no damage small, localized extensive

Damage Type (mark all that apply):

- burn marks (a.) bubbles (b.) delamination (c.) cracks/scratches(d.)

(a.) Burn marks (#): 1 2 3 4-10 >10

Fraction of area burned:

- <5% 5-25% 50% 75%-100% (consistent overall)

(b.) Bubbles (#): 1 2 3 4-10 >10

Average bubble dimension:

- <5 mm 5-30 mm >30 mm

Fraction of area with bubbles > 5 mm:

- <5% 5-25% 50% 75%-100% (consistent overall)

(c.) Fraction of area delaminated:

- <5% 5-25% 50% 75%-100% (consistent overall)

Fraction of delamination that exposes circuit or cell(s):

- <5% 5-25% 50% 75%-100% (consistent overall)

(d.) Cracks/scratches (#): 1 2 3 4-10 >10

Cracks/scratches location: random/no pattern over cells between cells

Fraction of area affected by cracks/scratches (approx.):

- <5% 5-25% 50% 75% - 100% (consistent overall)

Fraction of cracks/scratches that expose circuit (approx.):

- 0% 25% 50% 75% 100%

5. Wires/Connectors:

Wires: not applicable like new pliable, but degraded embrittled
(mark all that apply): cracked/disintegrated insulation burnt
corroded animal bites/marks

Connectors: not applicable like new pliable, but degraded embrittled
Type: unsure MC3 or MC4 Tyco Solarlok other
(mark all that apply): cracked/disintegrated insulation burnt corroded

6. Junction Box:

Junction box itself:	<input type="checkbox"/> not applicable/observable	<input type="checkbox"/> applicable
<u>Physical state:</u>	<input type="checkbox"/> intact	<input type="checkbox"/> unsound structure
<u>(mark all that apply):</u>	<input type="checkbox"/> weathered	<input type="checkbox"/> cracked
<u>Lid:</u>	<input type="checkbox"/> intact/potted	<input type="checkbox"/> loose
	<input type="checkbox"/> fell off	<input type="checkbox"/> warped
	<input type="checkbox"/> cracked	
Junction box adhesive:	<input type="checkbox"/> not applicable/observable	<input type="checkbox"/> applicable
<u>Attachment:</u>	<input type="checkbox"/> well attached	<input type="checkbox"/> loose/brittle
<u>Pliability:</u>	<input type="checkbox"/> like new	<input type="checkbox"/> pliable, but degraded
		<input type="checkbox"/> fell off
		<input type="checkbox"/> embrittled
Junction box wire attachments:	<input type="checkbox"/> not applicable/observable	<input type="checkbox"/> applicable
<u>Attachment:</u>	<input type="checkbox"/> well attached	<input type="checkbox"/> loose
<u>Seal:</u>	<input type="checkbox"/> good seal	<input type="checkbox"/> seal will leak
<u>other:</u>	<input type="checkbox"/> arced/started a fire	

7. Frame Grounding:

Original state: Wired ground Resistive ground No ground Unknown

Appearance: Not applicable Like new Some corrosion Major corrosion

Function: Well grounded No connection

Photos taken of back, label, and junction box

CONTINUE INSPECTION ON FRONT SIDE OF MODULE

8. Frame:	<input type="checkbox"/> not applicable	<input type="checkbox"/> applicable
Appearance:	<input type="checkbox"/> like new	<input type="checkbox"/> damaged (a.)
<u>(a.)(mark all that apply):</u>	<input type="checkbox"/> minor corrosion	<input type="checkbox"/> missing
	<input type="checkbox"/> frame cracking	<input type="checkbox"/> major corrosion
		<input type="checkbox"/> frame joint separation
		<input type="checkbox"/> bent frame
		<input type="checkbox"/> discolouration
Frame Adhesive:	<input type="checkbox"/> like new/not visible	<input type="checkbox"/> degraded (a.)
<u>(a.) (mark all that apply):</u>	<input type="checkbox"/> adhesive oozed out	<input type="checkbox"/> adhesive missing in areas
9. Frameless Edge Seal:	<input type="checkbox"/> not applicable	<input type="checkbox"/> applicable
Appearance:	<input type="checkbox"/> like new	<input type="checkbox"/> discolouration (a.)
		<input type="checkbox"/> visibly degraded
<u>(a.) Fraction affected by discolouration:</u>		
	<input type="checkbox"/> <5%	<input type="checkbox"/> 5-25%
	<input type="checkbox"/> 50%	<input type="checkbox"/> 75%-100% (consistent overall)
Material problems:	<input type="checkbox"/> squeezed/pinched out	<input type="checkbox"/> shows signs of moisture penetration
Delamination:	<input type="checkbox"/> none	<input type="checkbox"/> areas(s) delaminated (a.)
<u>(a.) Fraction Delaminated:</u>	<input type="checkbox"/> <5%	<input type="checkbox"/> 5-25%
	<input type="checkbox"/> 50%	<input type="checkbox"/> 75%-100% (consistent overall)

10. Glass/Polymer (front):

Material: glass polymer glass/polymer composite unknown

Features: smooth slightly textured pyramid/wave texture
 antireflection coating

Appearance: clean lightly soiled heavily soiled

Location of soiling: locally soiled near frame:
 left right top bottom all sides
 locally soiled on glass /bird droppings

Damage: no damage small, localized extensive

Damage Type (mark all that apply):

crazing or other non-crack damage shattered (tempered) shattered (non-tempered)

	<input type="checkbox"/> Cracked (a.)	<input type="checkbox"/> Chipped (b.)	<input type="checkbox"/> Milky discolouration (c.)
(a.) Cracks (#):	<input type="checkbox"/> 1 <input type="checkbox"/> 2 <input type="checkbox"/> 3	<input type="checkbox"/> 4-10 <input type="checkbox"/> >10	
Crack(s) start from:	<input type="checkbox"/> module corner	<input type="checkbox"/> module edge	<input type="checkbox"/> cell <input type="checkbox"/> junction box
	<input type="checkbox"/> somewhere else	<input type="checkbox"/> foreign body impact location	
(b.) Chips (#):	<input type="checkbox"/> 1 <input type="checkbox"/> 2 <input type="checkbox"/> 3	<input type="checkbox"/> 4-10 <input type="checkbox"/> >10	
Chipping location:	<input type="checkbox"/> module corner	<input type="checkbox"/> module edge	
(c.) Fraction of area:	<input type="checkbox"/> <5% <input type="checkbox"/> 5-25%	<input type="checkbox"/> 50% <input type="checkbox"/> 75%-100% (consistent overall)	

11. Metallization:

Gridlines/Fingers: not applicable/barely observable applicable

Appearance: like new light discolouration(a.) dark discolouration(a.)

(a.) Fraction of discolouration:

<5% 5-25% 50% 75% -100% (consistent overall)

Busbars: not applicable/not observable applicable

Appearance: like new light discolouration (a.) dark discolouration(a.)

(a.) Fraction of discolouration:

<5% 5-25% 50% 75% -100% (consistent overall)

(mark all that apply:) obvious corrosion diffuse burn mark(s)

discernibly misaligned

Cell Interconnect Ribbon: not applicable/not observable applicable

Appearance: like new light discolouration(a.) dark discolouration(a.)

(a.) Fraction of discolouration:

<5% 5-25% 50% 75% 100% (consistent overall)

(mark all that apply:) obvious corrosion burn marks breaks

Appearance: like new light discolouration(a.) dark disco

(a.) Fraction of discolouration: bright discolouration(%) faint discolouration(%)

(d) Fraction of dissociation

0% 25% 50% 75% 100% (select one or more)

arc tracks (thin, small burns)

■ **THE WORKS (ART, CULTURAL SERVICES)**

12. Silicon (mono or multi) module: not applicable applicable

Number of:

Cells in module _____

Cells in series per string _____

Number of Bypass diodes per string _____

Strings in parallel _____

Cell size: Width _____ cm Length _____ cm

Distance between frame and cell: >10 mm <10 mm

Distance between cells in a string: >1 mm <1 mm

Discolouration: none/like new light discolouration dark discolouration

Number of cells with any discolouration: _____

of those, average % discolored area: _____

<5% 5-25% 50%

75%-100% (consistent overall)

Discolouration location(s) (mark all that apply):

module center

module edges

cell centers

cell edges

over gridlines

over busbars

over tabbing

between cells

individual cell(s) darker than others

partial cell discolouration

Junction box area:

same as elsewhere

more affected

less affected

Damage: none

(mark all that apply):

burn mark (a.) cracking (b.)

moisture

worm marks/snail tracks (c.)

foreign particle embedded

(a.) Burns (#): 1 2 3 4-10 >10

(b.) Number of cells cracked: _____

(c.) Number of cells with worm marks/snail tracks: _____

Delamination: none from edges uniform corner(s) near junction box
 between cells (a.) over cells (b.) near cell or string interconnect

(a.) Fraction delamination between cells:

<5% 5-25% 50% 75% -100% (consistent overall)

(b.) Fraction delaminated over cells:

<5% 5-25% 50% 75% -100% (consistent overall)

Likely interface (choose 2):

glass semiconductor

encapsulant back sheet busbar

13. Thin-film module: not applicable applicable

Number of cells:

Number of cells in module _____

Number of cells in series/string _____

Number of strings in parallel _____

Cell size: Width _____ cm Length _____ cm

Distance between frame and cell: >10 mm <10 mm

Appearance: like new minor/light discolouration major/dark discolouration

Discolouration type (mark all that apply):

spotted degradation haze(encapsulant browning) other

Discolouration location (mark all that apply):

overall/no location pattern module centre module edge(s)
cell centre cell edges near crack(s)

Damage: no damage small, localized extensive

Damage type (mark all that apply): burn mark(s) cracking

possible moisture foreign particle embedded

Delamination: no delamination small, localized extensive

Location: from edges uniform corner(s)
near junction box near busbar along scribe lines

Likely interface (choose 2): glass semiconductor encapsulant
busbar

Delamination type: absorber delamination AR coating delamination

other

Photos taken of front and defects

14. Electronic Records applicable not applicable

Photographs and I-V curves recorded electronically-list file names in blanks

Photo files _____

I-V curve _____

Connector function: functions no longer mates exposed

Irradiance _____ Sensor _____

Temperature _____ Sensor _____

EL picture _____

IR picture _____

Bypass Diode Test: applicable not applicable

Number of diodes: _____

In total _____, shorted _____, open _____

OTHER

For further information about the IEA – Photovoltaic Power Systems Programme and Task 13 publications, please visit www.iea-pvps.org.



ISBN 978-3-906042-16-9

A standard linear barcode representing the ISBN number 978-3-906042-16-9.

9 783906 042169 >